ULTRASOUND-MEDIATED PRECISION STIMULATION OF PANCREATIC β-CELLS FOR NON-INVASIVE GLYCEMIC CONTROL IN TYPE 2 DIABETES

ZHAO XINYI

PhD

The Hong Kong Polytechnic University

2026

The Hong Kong Polytechnic University

Department of Biomedical Engineering

Ultrasound-Mediated Precision Stimulation of Pancreatic β-Cells for Non-Invasive Glycemic Control in Type 2 Diabetes

ZHAO Xinyi

A thesis submitted in partial fulfillment of the requirements for the degree of Doctor of Philosophy

August 2025

CERTIFICATE OF ORIGINALITY

I hereby declare that this thesis is my own work and that, to the best of my knowledge and belief, it reproduces no material previously published or written, nor material that has been accepted for the award of any other degree or diploma, except where due acknowledgment has been made in the text.

_____ (Signed)

_____ZHAO Xinyi_____ (Name of student)

Abstract

Diabetes mellitus is a chronic metabolic disorder of widespread concern, with type 2 diabetes (T2D) constituting the majority of cases. While insulin therapy is central to T2D management, its limitations—including rapid degradation and the need for frequent injections—highlight the demand for non-invasive alternatives. This research advances non-invasive alternatives through the development of ultrasound (US)-mediated precision stimulation technologies targeting pancreatic β-cells. Central to this endeavor is achieving cell-type-specific insulin release while circumventing unintended activation of glucagon-secreting α-cells—a critical prerequisite for effective glycemic regulation.

Microbubbles (MBs) are one of the most widely used ultrasound amplifiers. The first strategy established the critical importance of spatially confined energy delivery specifically to β-cells for effective ultrasound-mediated glycemic control. Utilizing MBs as ultrasound amplifiers, in vitro studies with RINm5F β-cells demonstrated that MB-conjugated ultrasound exposure induces rapid calcium influx via mechanosensitive ion channel activation, triggering insulin exocytosis. Validation in a murine transplantation model confirmed that MB-mediated ultrasound stimulation significantly attenuated acute hyperglycemia following glucose challenge. Systematic parameter optimization ensured biosafety with no evidence of cellular damage. This work provided essential proof-of-principle for β-cell-specific ultrasound modulation as a viable therapeutic concept. Nevertheless, the instability of MBs and challenges in their systemic delivery challenged their validation and therapeutic application in the T2D mice model.

Sonogenetics, another innovative methodology also capable of achieving localized ultrasound energy amplification, more importantly, offers superior cell-type specificity and convenient *in vivo* targeting through systemic delivery. This strategy employed a

pancreatic-tropic adeno-associated virus (AAV) carrying the large-conductance mechanosensitive channel (MscL) gene under the insulin promoter (AAV-INS-MscL). A single intraperitoneal injection achieved specific genetic modification of endogenous pancreatic β-cells in T2D mice. Subsequent non-invasive ultrasound stimulation elicited robust calcium influx and significant insulin release from these sonogenetically engineered cells, leading to rapid reductions in both random and postprandial hyperglycemia. Comprehensive assessments confirmed a favorable safety profile. This approach successfully demonstrated truly non-invasive, ultrasound-regulated glycemic control using endogenous β-cells in a T2D model, offering a clinically attractive paradigm requiring only a single injection for durable sensitization followed by repeated non-invasive treatments.

In summary, this thesis established ultrasound-mediated precision activation of pancreatic β-cells as an effective and non-invasive approach for glycemic regulation in type 2 diabetes. The MBs-based approach validates the principle of spatially confined energy delivery, and the subsequent sonogenetic system pioneers truly non-invasive, ultrasound-regulated glycemic control in T2D models. Together, this sequential innovation provides a strong foundation for the development of novel, non-invasive stimulation-based therapeutic options for T2D patients who retain functional β-cells.

Publication list

1. **Xinyi Zhao**, Yong Wu, Quanxiang Xian, Jianing Jing, Yizhou Jiang, Jinghui Guo, Lei Sun. “Harnessing Sonogenetics for Non-Invasive Treatment of Type 2 Diabetes.” Submitted.
2. Yong Wu, **Xinyi Zhao**, Yizhou Jiang, Congmin Chen, Langzhou Liu, Xuandi Hou, Quanxiang Xian, Jinghui Guo, Lei Sun. “β-cell-specific Non-invasive Ultrasound Stimulation to Enhance Insulin Release and Glucose Control in Mice.” Journal of Nanobiotechnology, accepted, DOI:10.1186/s12951-025-03926-6. (**co-first author**)
3. Quanxiang Xian, Danni Li, **Xinyi Zhao**, Dongshuai Zhao, Yizhou Jiang, Jianing Jing, Xuandi Hou, Xiaohui Huang, Kin Fung Wong, Suresh Murugappan, Zhihai Qiu, Lei Sun. “Impact of endogenous sonosensation on in vivo sonogenetics.” iScience (2025) 28(12):114030.
4. Xuandi Hou, Jianing Jing, Yizhou Jiang, Xiaohui Huang, Quanxiang Xian, Ting Lei, Jiejun Zhu, Kin Fung Wong, **Xinyi Zhao**, Min Su, Danni Li, Langzhou Liu, Zhihai Qiu and Lei Sun. "Nanobubble-actuated ultrasound neuromodulation for selectively shaping behavior in mice." Nature communications 15.1 (2024): 2253.
5. Mengzhu Sun, Yong Wu, Chun Yuan, Jingya Lyu, **Xinyi Zhao**, Ye Chun Ruan, Jinghui Guo, Hui Chen & Wen Qing Huang. "Androgen-induced upregulation of CFTR in pancreatic β-cell contributes to hyperinsulinemia in PCOS model." Endocrine 83.1 (2024): 242-250.
6. Yizhou Jiang, Xuandi Hou, **Xinyi Zhao**, Jianing Jing, Lei Sun. "Tracking adoptive natural killer cells via ultrasound imaging assisted with nanobubbles." Acta biomaterialia 169 (2023): 542-555.
7. Jiejun Zhu, Quanxiang Xian, Xuandi Hou, Kin Fung Wong, Tingting Zhu, Zihao Chen, Dongming He, Shashwati Kala, Suresh Murugappan, Jianing Jing, Yong Wu, **Xinyi Zhao**, Danni Li, Jinghui Guo, Zhihai Qiu, and Lei Sun. "The mechanosensitive ion channel Piezo1 contributes to ultrasound neuromodulation." Proceedings of the National Academy of Sciences 120.18 (2023): e2300291120.

8. Ting Zhu, Jinghui Guo, Yong Wu, Ting Lei, Jiejun Zhu, Hui Chen, Shashwati Kala, Kin Fung Wong, Chi Pong Cheung, Xiaohui Huang, **Xinyi Zhao**, Minyi Yang, Lei Sun. "The mechanosensitive ion channel Piezo1 modulates the migration and immune response of microglia." Iscience 26.2 (2023).
9. Jinghui Guo, Yong Wu, Zhiyong Gong, Xixi Chen, Fei Cao, Shashwati Kala, Zhihai Qiu, **Xinyi Zhao**, Jun-jiang Chen, Dongming He, Taiheng Chen, Rui Zeng, Jiejun Zhu, Kin Fung Wong, Suresh Murugappan, Ting Zhu, Quanxiang Xian, Xuandi Hou, Ye Chun Ruan, Baojun Li, Yu Chao Li, Yao Zhang, and Lei Sun. "Photonic Nanojet‐Mediated Optogenetics." Advanced Science 9.12 (2022): 2104140.

Acknowledgment

As I stand at the culmination of this challenging and enriching doctoral journey, a profound sense of gratitude washes over me. This thesis could not have been completed without the indispensable contributions of numerous individuals and institutions whose support, expertise, and resources were fundamental to my work. To each of you, I owe an immense debt of thanks.

My deepest and most sincere appreciation flows first to my supervisor, Prof. Lei SUN. Your brilliant guidance, insightful critiques, and steadfast belief in my potential were the bedrock of this endeavor. Thank you for challenging me intellectually and nurturing my growth as a researcher.

I am immensely grateful to several key supporters: Prof. Sharon RUAN for generously providing access to essential experimental equipment and sharing her invaluable expertise; Prof. Jinghui GUO for her dedicated guidance on my research and, crucially, for her genuine care and support extending well beyond academics.

My sincere thanks also go to the Department of Biomedical Engineering, the University Research Facility in Life Sciences (ULS), and Centralised Animal Facilities (CAF) at the Hong Kong Polytechnic University and the staff, whose platforms and technical assistance were vital to the experimental success of this thesis.

I am deeply thankful to my colleagues within the SUN LAB for their camaraderie and support: Quanxiang XIAN, Xuandi HOU, Yizhou JIANG, Xiaohui HUANG, Jianing JING, Langzhou LIU, Dongshuai ZHAO, Congmin CHEN, Danni LI, Zhuohan SHI, Pengwei JU, etc. In particular, I wish to specially acknowledge Yong WU, whose collaborative partnership was instrumental in conducting the majority of the experimental work central to this thesis. Furthermore, I also want to acknowledge Junjiang CHEN, Yanting QUE, Ruiyao XU, Wanting DU etc., members of Sharon's Lab for their helpful discussions and occasional resource sharing.

Finally, my deepest roots of gratitude extend to my family – your boundless love,

unwavering belief, and quiet sacrifices formed the bedrock that sustained me through storms. Alongside them, I thank my boyfriend and colleague – Bing HU, whose intellectual synergy and unwavering care illuminated both my research and daily life. Equally vital were my friends, whose steadfast presence, listening ears, and timely reminders that joy exists beyond data and deadlines became my sanctuary. Finally, I would like to express my gratitude to my cats – neinei and xixi. They have been a light in the darkness on this journey, and a source of emotional solace for me.

This dissertation stands as a testament to your collective support. With deepest appreciation, I close this chapter grateful for each of you.

Table of contents

List of figures

List of tables

List of abbreviations

T2D(M)	**type 2 diabetes (mellitus)**
MB	**microbubble**
AAV	**adeno-associated virus**
MscL	**large-conductance mechanosensitive channel**
US	**ultrasound**
DM	**diabetes mellitus**
T1D(M)	**type 1 diabetes (mellitus)**
GAD65	**glutamate decarboxylase 65**
IA-2	**islet antigen 2**
ZnT8A	**zinc transporter 8 autoantibody**
IAA	**insulin autoantibodies**
HLA	**human leukocyte antigen**
IRS	**insulin receptor substrates**
PKC	**protein kinase C**
MODY	**maturity onset diabetes of the young**
HNF	**hepatocyte nuclear factor**
GDM	**gestational diabetes mellitus**
GLP-1	**glucagon-like peptide-1**
SGLT2	**sodium-glucose co-transporter 2 inhibitor**
RAs	**receptor agonists**
ESCs	**embryonic stem cells**
iPSCs	**induced pluripotent stem cells**
MSCs	**mesenchymal stem cells**
HbA1c	**hemoglobinA1c, glycated hemoglobin**
AAVs	**adeno-associated viruses**
PDX1	**pancreatic and duodenal homeobox 1**
NeuroD1	**neuronal differentiation 1**

L-PK	**L-type pyruvate kinase**
GSIS	**glucose-stimulated insulin secretion**
GLUT	**glucose transporter**
NADH	**nicotinamide adenine dinucleotide, reduced**
ATP	**adenosine triphosphate**
ADP	**adenosine diphosphate**
ES	**electrical stimulation**
DBS	**deep brain stimulation**
SCS	**spinal cord stimulation**
tDCS	**transcranial direct current stimulation**
FES	**functional electrical stimulation**
NMES	**neuromuscular electrical stimulation**
GES	**gastric electrical stimulation**
IES	**intestinal electrical stimulation**
VNS	**vagus nerve stimulation**
tVNS	**transcutaneous VNS**
PNES	**pancreatic nerve electrostimulation**
MENS	**microcurrent electrical nerve stimulation**
NIR	**near-infrared**
TBI	**traumatic brain injury**
ChR2	**channelrhodopsin-2**
cAMP	**cyclic adenosine monophosphate**
GLP-1	**glucagon-like peptide-1**
TMS	**transcranial magnetic stimulation**
SMF	**static magnetic fields**
rTMS	**repetitive transcranial magnetic stimulation**
MES	**mild electrical stimulation**
HS	**heat shock**
HSP	**heat shock protein**

kHz	**kilohertz**
MHz	**megahertz**
HIFU	**high-intensity focused ultrasound**
MRI	**magnetic resonance imaging**
ESWL	**extracorporeal shock wave lithotripsy**
BBB	**blood-brain barrier**
CNS	**central nervous system**
LIPUS	**low-intensity pulsed ultrasound**
UTMD	**ultrasound-triggered microbubble destruction**
LV	**lentivirus**
LNPs	**lipid nanoparticles**
AAVR	**AAV receptor**
AIP	**acute intermittent porphyria**
EGFR	**pidermal growth factor receptor**
FGFR	**fibroblast growth factor receptor**
HGFR	**hepatocyte growth factor receptor**
LamR	**laminin receptor 1**
PDGFR	**platelet-derived growth factor receptor**
PEG	**polyethylene glycol**
RMS	**root mean square**
MTS	**3-(4,5-dimethylthiazol-2-yl)-5-(3-carboxymethoxyphenyl)-2-(4-sulfophenyl)-2H-tetrazolium, inner salt**
FBS	**fetal bovine serum**
NaCl	**sodium chloride**
KCl	**potassium chloride**
$MgCl_2$	**magnesium chloride**
$CaCl_2$	**calcium chloride**
HEPES	**N- (2-Hydroxyethyl)piperazine-N-2-ethanesulfonic acid**
$GdCl_3$	**gadolinium chloride**

ELISA	**enzyme-linked immunosorbent assay**
PBS	**phosphate buffer saline**
PCR	**polymerase chain reaction**
qPCR	**quantitative real-time PCR**
DNA	**deoxyribonucleic acid**
cDNA	**complementary DNA**
RNA	**ribonucleic acid**
H&E	**hematoxylin and eosin staining**
BSA	**bovine serum albumin**
PI	**propidium iodide**
DMSO	**dimethyl sulfoxide**
HFD	**high-fat diet**
STZ	**streptozocin**
DAPI	**4',6-diamidino-2'-phenylindole**
NC	**Negative control**
IPGTT	**intraperitoneal glucose tolerance test**
AUC	**area under the curve**
TRP	**transient receptor potential**
SEM	**standard error of the mean**
PFA	**paraformaldehyde**

Chapter 1: Introduction

Diabetes mellitus, a chronic metabolic disorder characterized by persistent hyperglycemia, represents a critical and escalating global health challenge, imposing substantial morbidity, mortality, and socioeconomic burdens [1-3]. Type 2 diabetes (T2D), accounting for the vast majority (90-95%) of cases, arises from a complex interplay of insulin resistance and progressive dysfunction of pancreatic β-cells, leading to impaired glucose-dependent insulin secretion [4]. While lifestyle modifications and pharmacological interventions, including insulin secretagogues, sensitizers, and ultimately exogenous insulin therapy, form the cornerstone of management [5], significant limitations persist. Conventional therapies often suffer from waning efficacy, systemic side effects, and the inherent challenges of peptide-based treatments. Insulin therapy, despite its efficacy in advanced disease, is particularly burdened by rapid degradation, instability, the necessity for frequent injections, associated risks of hypoglycemia, injection-site complications, and substantial logistical demands [6, 7]. These drawbacks underscore an urgent and unmet clinical need for safe, effective, and truly non-invasive alternatives capable of restoring physiological insulin release patterns.

The quest for non-invasive modalities to regulate insulin secretion has recently focused on harnessing physical energy sources, such as light, magnetic fields, and electrical stimulation [8-10]. Among these, therapeutic ultrasound has emerged as a particularly promising candidate, offering unique advantages of deep tissue penetration, high spatiotemporal precision, non-invasiveness, and an excellent safety profile [11]. Pioneering work demonstrated the potential of ultrasound to stimulate insulin release from pancreatic β-cells in vitro [12]. However, translating this potential into a viable in vivo therapy faces a critical barrier: the inherent lack of cellular specificity within the complex pancreatic microenvironment [13]. The close anatomical proximity of insulin-secreting β-cells to glucagon-producing α-cells and other exocrine cells means that non-

specific ultrasound application risks unintended activation of counter-regulatory hormones (e.g., glucagon), potentially negating the desired glucose-lowering effect [14]. Consequently, achieving cell-type-specific targeting of ultrasound energy to β-cells is paramount for realizing effective and reliable ultrasound-mediated glycemic control.

This imperative for precision targeting drives the development of innovative strategies to confine and amplify the ultrasonic stimulus specifically within β-cells. Microbubbles, widely employed as ultrasound contrast agents and energy amplifiers, offer one such pathway. By conjugating MBs to β-cells, ultrasound energy can be locally concentrated at the target site. Our work utilizing this approach demonstrated a critical proof-of-principle: MBs-mediated, spatially confined ultrasound stimulation selectively activates mechanosensitive ion channels on RINm5F β-cells *in vitro*, triggering rapid calcium influx and subsequent insulin exocytosis [Ref to Chapter 3]. Crucially, this targeted strategy effectively attenuated acute hyperglycemia in a murine model, providing the first direct evidence that β-cell-specific ultrasound stimulation can indeed regulate blood glucose *in vivo* [Ref to Chapter 3]. Systematic optimization ensured the biosafety of the parameters employed. This MBs-based strategy thus established the fundamental importance of cellular specificity and validated the core therapeutic concept of ultrasound-mediated, β-cell-targeted insulin release for glycemic regulation. While this approach provides a robust experimental foundation and demonstrates significant potential, the inherent instability of MBs and challenges in their systemic delivery *in vivo* limit the therapeutic approach to a proof-of-concept demonstration, without achieving genuine therapeutic application in a T2D model.

Sonogenetics—a technique utilizing ultrasound to control genetically engineered cells—offers a more precise cellular specificity method through genetic targeting while circumventing the limitations of MBs [15, 16]. By genetically engineering cells to overexpress mechanosensitive ion channels, followed by enhancing the ultrasound sensitivity of specific cell types, sonogentics enables cell-type-specific activation while sparing neighboring cells [16, 17]. —For example, the islets contain both α cells and β

cells, which are located in the pancreas, where the most widespread type is the acinar cells; thus, β cells cannot be distinguished in terms of their spatial positions when ultrasound stimulation in the pancreas area, even confined to the islet area. Therefore, we hypothesize that sonogenetics could localize ultrasound effects only on pancreatic β-cells to achieve glycemic control through specifically triggered insulin release.

This strategy circumvents the need for exogenous agents like MBs by genetically modifying endogenous cells to express ultrasound-sensitive mechanotransducers. Here, we selected the bacterial large-conductance mechanosensitive channel (MscL) as the overexpressed mechanotransducer, based on its well-characterized biophysical properties, small gene size, and exogenous origin, which minimizes potential interactions with mammalian ligands or proteins, thereby avoiding interference with endogenous cellular functions [18, 19]. MscL expression has been shown to potentiate ultrasound-mediated cellular stimulation [20], and our previous work has demonstrated ultrasound sensitivity in MscL-expressing neurons, enabling precise neuromodulation in targeted populations [21, 22]. In this study, we developed an adeno-associated virus (AAV) -mediated gene delivery system for β-cell-specific MscL overexpression. Specifically, a pancreatic-tropic AAV serotype coupled with an insulin promoter (AAV-INS-MscL) was engineered. Following intraperitoneal administration, this system achieved precise pancreatic targeting and β-cell-specific MscL expression in diabetic mice. Subsequent ultrasound stimulation of the pancreas enabled effective blood glucose regulation. Through systematic validation in mouse models of type 2 diabetes, we demonstrated a truly non-invasive diabetes management approach [Ref to Chapter 4]. Comprehensive safety assessments supported the favorable profile of this approach. The sonogenetic strategy, requiring only a single injection for durable sensitization followed by repeated non-invasive ultrasound treatments, establishes a highly attractive and clinically viable therapeutic paradigm for T2D management.

Collectively, this thesis demonstrates the feasibility and therapeutic promise of ultrasound-mediated precision stimulation of pancreatic β-cells as a non-invasive

strategy for glycemic control in type 2 diabetes. The MBs-based approach provides essential proof-of-concept, unequivocally demonstrating the criticality of spatial confinement and cellular specificity for effective ultrasound-driven glycemic regulation *in vivo*. Building on a microbubble-based proof-of-concept, we further established a sonogenetic-based approach that has the capability of cell-specific *in vivo* delivery, pioneering a novel, minimally invasive, and clinically promising method for achieving non-invasive diabetes therapy in a relevant T2D model by harnessing endogenous β-cells. Together, these explorations establish a robust foundation for the development of next-generation, stimulation-based therapeutic options aimed at restoring physiological insulin release for the majority of T2D patients who retain functional β-cell mass. This manuscript details the rationale, methodology, key findings, and implications of these integrated research endeavors.

Chapter 2: Literature review

2.1 Diabetes mellitus (DM)

2.1.1 Definition, global Status, and complications

Diabetes mellitus (abbreviation, diabetes) constitutes a heterogeneous cluster of metabolic disorders unified by the defining feature of chronic hyperglycemia. This pathological state arises from compromised insulin secretion, impaired insulin action (insulin resistance) at target tissues (primarily skeletal muscle, adipose tissue, and liver), or a combination of both defects [1, 23, 24]. The fundamental metabolic derangements in carbohydrate, lipid, and protein metabolism stem from insufficient insulin action, attributable to deficient hormone secretion and/or diminished cellular responsiveness involving disruptions at insulin receptor, post-receptor signaling, or effector molecule levels [1, 23]. Clinical manifestations vary significantly; individuals, particularly with type 2 diabetes in its initial phases, may remain asymptomatic. Conversely, pronounced hyperglycemia, especially in cases of absolute insulin deficiency, presents with classic symptoms including polyuria, polydipsia, polyphagia, unintentional weight loss, and visual disturbances [1, 23]. Acute, life-threatening metabolic decompensations encompass diabetic ketoacidosis and hyperosmolar hyperglycemic state [1, 23]. Chronic persistent hyperglycemia inflicts progressive damage leading to organ dysfunction and failure. Major long-term sequelae involve microvascular complications: retinopathy potentially culminating in blindness, nephropathy progressing to end-stage renal disease, and peripheral/autonomic neuropathy, increasing risks of foot ulceration, amputations, and diverse systemic dysfunctions. Additionally, there is a significantly elevated incidence of macrovascular complications, including atherosclerotic cardiovascular disease, peripheral arterial disease, and cerebrovascular events. Hypertension and dyslipidemia are frequently comorbid conditions [1]. The severity of both symptoms and chronic complications correlates

with the specific diabetes type and the duration of exposure to hyperglycemia [23].

2.1.2 Classification and pathogenesis

Diabetes classification remains challenging due to overlapping features, particularly in younger adults, with potential diagnostic revisions required. The American Diabetes Association (ADA) classification system (type 1, type 2, other specific types, gestational diabetes mellitus) is widely accepted [25]. The accelerator hypothesis proposes that Type 1 and Type 2 represent the same insulin resistance disorder manifesting differently based on genetic background and tempo [26].

- Type 1 diabetes mellitus (T1DM):

T1DM (5-10% of cases) results from autoimmune destruction of pancreatic β-cells, leading to absolute insulin deficiency [1, 23]. Autoantibodies (GAD65, IA-2, ZnT8A, IAA) and HLA associations (DR/DQ) are hallmarks [27]. Environmental triggers (e.g., viruses) may initiate disease in genetically susceptible individuals. Presentation is typically acute with symptoms and ketoacidosis, requiring lifelong insulin. Subtypes include rare Idiopathic T1DM (non-autoimmune, episodic ketoacidosis) and Fulminant T1DM (rapid β-cell destruction, prevalent in East Asia) [1, 23].

- Type 2 diabetes mellitus (T2DM):

T2DM (>90% of cases) arises from insulin resistance combined with progressive β-cell dysfunction failing to compensate. Obesity is the primary driver of insulin resistance. Molecular defects involve impaired insulin signaling pathways (e.g., IRS proteins, AKT/PKC kinases). Presentation is often insidious. Latent Autoimmune Diabetes in Adults (LADA) presents with T2DM features but positive autoantibodies. [1, 23, 24].

- Other specific types:
  - Monogenic diabetes: Caused by single gene defects (e.g., MODY: HNF1α, HNF4α; Neonatal diabetes: K_{ATP} channel genes; Mitochondrial diabetes).
  - Exocrine pancreatic disease: Diabetes due to pancreatic damage (pancreatitis,

cystic fibrosis, pancreatectomy).

- Endocrinopathies: Hormone excess (Cushing's, acromegaly), antagonizing insulin.
- Drug-induced: Agents like glucocorticoids or certain antipsychotics impair insulin secretion/action.
- Genetic syndromes: Increased diabetes risk (e.g., Down, Turner, Wolfram syndromes). [1, 23, 24].

- Gestational diabetes mellitus (GDM):

GDM is glucose intolerance first diagnosed during pregnancy, driven by pregnancy-induced insulin resistance overwhelming β-cell capacity. It increases maternal and offspring diabetes risk. Diagnosis typically occurs at 24-28 weeks using defined criteria. Overt diabetes diagnosed during pregnancy is distinct. [1, 23, 24].

2.1.3 Management strategies

- Lifestyle interventions

Lifestyle modification remains the cornerstone of diabetes management, particularly for type 2 diabetes and prediabetes. The American Diabetes Association (ADA) emphasizes medical nutrition therapy promoting balanced dietary patterns like the Mediterranean or DASH diets, coupled with regular physical activity of at least 150 minutes per week of moderate intensity. Achieving weight loss of 5-15% in overweight or obese individuals with T2DM significantly enhances insulin sensitivity and glycemic control. These interventions work by reducing glucotoxicity, improving insulin action in peripheral tissues, and ameliorating cardiovascular risk factors, often serving effectively as first-line therapy or as a crucial adjunct to pharmacotherapy [28, 29].

- Pharmacological therapies and combination approaches

Pharmacotherapy targets diverse pathophysiological defects. Metformin remains the first-line oral agent, reducing hepatic glucose output through AMPK activation and mitochondrial complex I inhibition, offering efficacy with minimal hypoglycemia risk

[30]. Sulfonylureas stimulate insulin secretion but carry risks of hypoglycemia and weight gain [30]. GLP-1 receptor agonists (e.g., semaglutide) enhance glucose-dependent insulin secretion, suppress glucagon, promote weight loss, and demonstrate significant cardiovascular/renal benefits [31]. SGLT2 inhibitors (e.g., empagliflozin) promote urinary glucose excretion, providing robust cardiorenal protection [32]. Insulin is essential for type 1 diabetes and advanced T2DM. Given the progressive nature of T2DM, combination therapy is frequently required. Common strategies include metformin combined with SGLT2 inhibitors for synergistic glycemic control and cardiorenal protection, basal insulin paired with GLP-1 RAs to enhance efficacy while mitigating weight gain and hypoglycemia risk, and triple therapy (e.g., metformin + SGLT2i + GLP-1 RA) for refractory hyperglycemia. Early combination therapy (e.g., metformin + pioglitazone) can delay disease progression in high-risk individuals [33].

- Stem cell therapy

Stem cell therapy aims to restore functional insulin production or modulate the diabetic microenvironment. Pluripotent stem cells (ESCs/iPSCs) can be differentiated into glucose-responsive β-like cells, with transplantation restoring normoglycemia in animal models; however, challenges include complex differentiation protocols, tumorigenicity risks, and immune rejection [34]. Mesenchymal stem cells (MSCs) from adipose tissue, bone marrow, or umbilical cord exert therapeutic effects primarily through immunomodulation (suppressing destructive T-cells) and paracrine signaling, creating a microenvironment supportive of β-cell survival and improved insulin sensitivity [35, 36]. Clinical trials using MSCs report improved HbA1c and C-peptide with good safety, though evidence for direct in vivo transdifferentiation into functional β-cells remains limited [37].

- Gene therapy

Gene therapy strategies seek to restore physiological insulin production and glucose sensing. Adeno-associated viruses (AAVs) are favored vectors due to low immunogenicity. A key approach involves co-expressing insulin and glucokinase genes

in skeletal muscle via AAV vectors, creating "synthetic" glucose-sensing units that achieved long-term normoglycemia in diabetic animal models without exogenous insulin [38, 39]. Delivery of pancreatic transcription factors (e.g., PDX1, NeuroD1) to the liver induces ectopic insulin production, reducing hyperglycemia in studies. Liver-specific promoters (e.g., L-PK, Albumin) aim for glucose-responsive secretion, though their activity is often weaker than viral promoters [40]. Non-viral methods (e.g., plasmid DNA) and ex vivo approaches show efficacy but face challenges like transient expression [41].

2.2 Pancreatic β-cells

2.2.1 Overview of pancreatic β-cells

The pancreas, a retroperitoneal organ extending from the duodenum (head) to the spleen (tail), consists of two functionally distinct compartments. The exocrine pancreas, comprising approximately 98% of its mass, is organized into clusters of pyramidal acinar cells. These cells synthesize and store inactive digestive enzymes within specialized granules, releasing them into a ductal network that drains into the duodenum to facilitate nutrient breakdown. Embedded within this exocrine tissue are scattered endocrine islets (of Langerhans), constituting the remaining 2% of pancreatic mass. These highly vascularized micro-organs house several critical hormone-secreting cell types: Beta cells (β-cells), the most abundant islet cell type, centrally located and responsible for secreting insulin to lower blood glucose by promoting cellular uptake; Alpha cells (α-cells), typically found at the islet periphery, secrete glucagon to elevate blood glucose by stimulating hepatic glucose release; Delta cells (δ-cells), scattered throughout the islet, secrete somatostatin to paracrinally inhibit the secretion of both insulin and glucagon; PP cells (or Gamma cells), which release pancreatic polypeptide to modulate exocrine secretion and gut motility; and rare Epsilon cells (ε-cells) that secrete ghrelin to stimulate appetite. Through antagonistic, synergistic, and inhibitory interactions—particularly the insulin-glucagon counterregulation—these islet cells

work in concert to ensure strict physiological blood glucose homeostasis. This integrated exocrine-endocrine architecture enables the pancreas to concurrently manage digestive processes and systemic metabolic equilibrium. [42-44]

2.2.2 Mechanism of insulin release from pancreatic β-cells

β-Cells are central to glucose homeostasis, secreting insulin in response to hyperglycemia. Glucose enters β-cells via transporters and undergoes mitochondrial metabolism, elevating ATP/ADP ratios. This triggers closure of ATP-sensitive potassium channels, membrane depolarization, and calcium influx, culminating in insulin granule exocytosis. Precise regulation prevents hypoglycemia; conversely, β-cell dysfunction—manifested as impaired glucose-stimulated insulin secretion (GSIS)—underlies diabetes pathogenesis and its complications. [42]

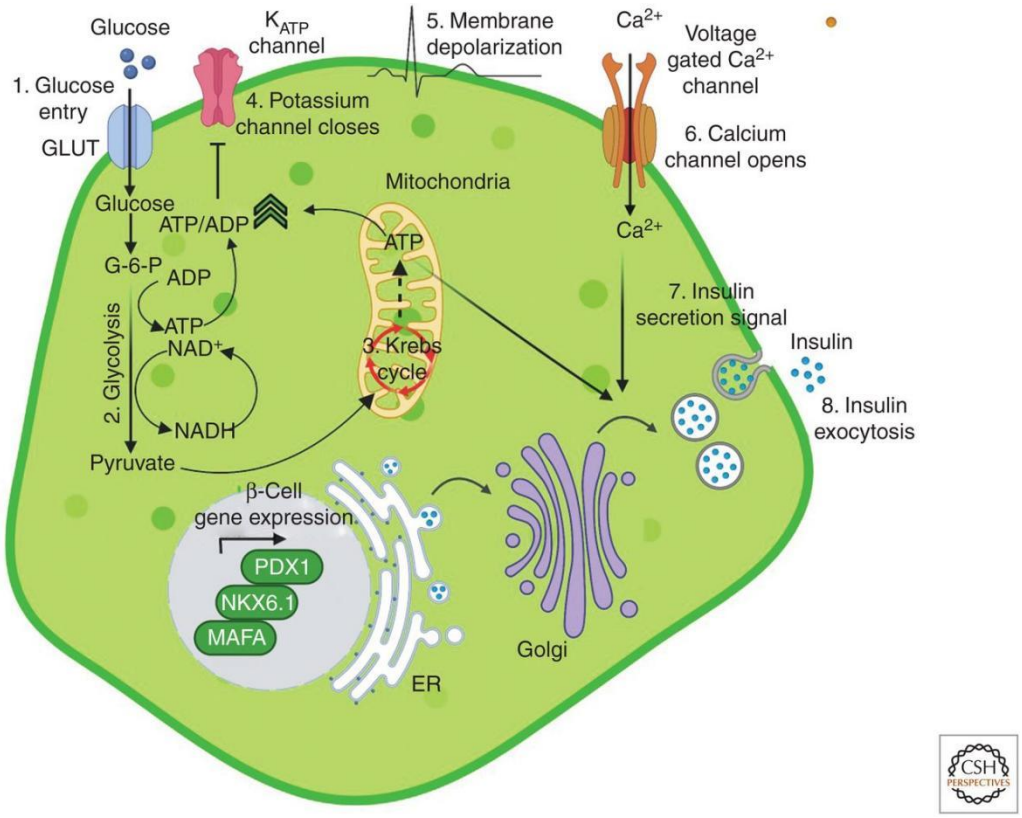

Figure 2.2. A schematic illustrates the principal stages of insulin secretion in β-cells.

Elevated extracellular glucose is transported into β-cells via GLUT2 (GLUT1 in humans) and phosphorylated by glucokinase, forming glucose-6-phosphate, which enters glycolysis to produce

pyruvate, ATP, and NADH. Pyruvate is metabolized in mitochondria through the Krebs cycle, generating additional ATP and increasing the ATP/ADP ratio. This rise closes ATP-sensitive K+ (K_{ATP}) channels, causing membrane depolarization and opening voltage-gated Ca^{2+} channels. The resulting Ca^{2+} influx elevates cytosolic Ca^{2+}, triggering insulin exocytosis. Elevated ATP also promotes insulin granule trafficking and fusion with the plasma membrane for secretion. [42]

2.3 Physical stimulation in diabetes therapy

2.3.1 Electrical stimulation

Electrical stimulation (ES) is a therapeutic technique that applies controlled electrical currents to nerves, muscles, or specific brain regions to modulate their activity and function [45, 46]. Its key advantages include being minimally invasive or non-invasive, highly targeted to specific neural circuits, adjustable, and often reversible, offering an alternative or adjunct to pharmaceuticals or surgery. Historically, ES has evolved significantly, finding established applications in diverse areas: cardiac pacing via pacemakers for arrhythmias, deep brain stimulation (DBS) for movement disorders like Parkinson's disease [47], spinal cord stimulation (SCS) for chronic pain [48], transcranial stimulation (e.g., tDCS) for depression and neurorehabilitation [49], and functional electrical stimulation (FES) to restore movement in paralysis [50]. Its therapeutic scope continues to expand through ongoing research.

Electrical stimulation offers diverse non-pharmacological strategies targeting core metabolic dysregulation in diabetes. Neuromuscular electrical stimulation (NMES) effectively improves glycemic control. Percutaneous EMS attenuates postprandial hyperglycemia and reduces C-peptide in T2D, suggesting enhanced glucose disposal and reduced insulin demand [51]. Meta-analyses confirm NMES lowers fasting glucose and improves overall glycemic control in T2D [52], with benefits extending to immobile patients, improving HbA1c and lipids [53]. Gastrointestinal neuromodulation also shows promise. Gastric electrical stimulation (GES) devices like Maestro® improve T2D parameters alongside weight loss [54], while chronic intestinal electrical

stimulation (IES) in obese rats ameliorates fasting hyperglycemia, glucose intolerance, and insulin resistance via metabolic and motility effects [55]. Direct neural targeting is actively explored. Vagus nerve stimulation (VNS) demonstrates contrasting effects: preclinical studies show afferent and efferent VNS can modulate insulin secretion and glucose regulation [56, 57], though clinical transcutaneous VNS (tVNS) trials in T2D patients have shown variable results, including no significant metabolic effect [58], highlighting the need for further optimization. Pancreatic nerve electrostimulation (PNES) inhibited autoimmune diabetes in mice by modulating pancreatic lymph node immunity [59]. Furthermore, microcurrent electrical nerve stimulation (MENS) improved biochemical indices in diabetic mice and influenced critical pathways (e.g., PPAR, insulin signaling) comparably to drugs [60]. These ES approaches represent a growing frontier in bioelectronic diabetes therapy.

2.3.2 Photostimulation

Photostimulation therapy utilizes specific wavelengths of light to modulate biological processes. A key modality is photobiomodulation (PBM), which employs non-thermal red or near-infrared (NIR) light (typically 600-1000 nm) to stimulate cellular chromophores, primarily mitochondrial cytochrome c oxidase, enhancing cellular energy metabolism and reducing inflammation [61]. Optogenetics represents a distinct, highly targeted approach, using genetic engineering to confer light sensitivity to specific cells, enabling precise spatiotemporal control over cellular activity (e.g., hormone secretion) with specific wavelengths. Valued for their non-invasiveness (PBM), tissue-penetrating capabilities (NIR light), safety, and precision (optogenetics), these light-based approaches are finding established or investigational roles in diverse medical fields. These include neurology (e.g., addressing depression, TBI, restoring vision), dermatology, pain management, and metabolic health.

Photostimulation strategies, particularly PBM and optogenetics, are actively investigated for directly targeting diabetes pathophysiology. PBM using transcutaneous NIR light demonstrates preclinical efficacy in improving glucose tolerance and insulin

sensitivity, likely through enhanced mitochondrial function and reduced oxidative stress [62]. Clinically, while a randomized trial in comorbid depression and type 2 diabetes found bright light therapy (10,000 lux) did not significantly improve depressive symptoms or insulin sensitivity overall, subgroup analyses suggested potential benefits for depression in highly insulin-resistant patients and insulin users [63]. Whole-body NIR therapy has also shown reductions in fasting glucose and HbA1c in T2D patients [64]. Optogenetics offers a revolutionary approach by genetically engineering cells for light-controlled hormone secretion. This includes modifying pancreatic β-cells to express light-sensitive proteins like Channelrhodopsin-2 (ChR2) or photoactivated adenylate cyclase (bPAC), enabling controlled insulin secretion via calcium influx or cAMP production in diabetic models [65-67]. Alternatively, synthetic approaches engineer non-β cells (e.g., HEK-293, stem cells) to produce insulin or glucagon-like peptide-1 (GLP-1) using diverse optogenetic tools (melanopsin/NFAT, BphS/c-di-GMP, TtCBD, GAVPO) activated by various light wavelengths, demonstrating glycemic improvement in vivo [65, 66, 68, 69]. Optogenetic neuromodulation of specific hypothalamic circuits or vagal nerves also influences glucose homeostasis [65, 66]. Critical translational efforts focus on integrating these approaches with smart devices like wireless micro-LED implants and a closed-loop system.

2.3.3 Magnetic stimulation

Magnetic stimulation encompasses various non-invasive methods, such as transcranial magnetic/electric stimulation (TMS/tDCS) and static magnetic/electric fields (sBE/SMF). These techniques modulate neural activity or systemic redox/metabolic pathways through electromagnetic induction [70, 71]. They offer the benefits of minimal invasiveness, avoidance of pharmacological side effects, and the capacity to produce sustained physiological changes. Initially deployed in neurology (e.g., for depression, chronic pain) [72], emerging investigations are extending its scope to metabolic disorders. This expansion capitalizes on its ability to influence both central

and peripheral pathways.

Magnetic stimulation shows significant promise as a non-pharmacological intervention for the core pathophysiology of diabetes mellitus itself. Transcranial approaches, such as repeated tDCS, have been shown to reduce blood glucose through insulin-independent mechanisms by enhancing cerebral energy metabolism. Human studies demonstrate that daily anodal tDCS persistently lowers blood glucose levels without altering insulin, correlating with increased brain ATP and phosphocreatine levels [73, 74]. Static electromagnetic fields (sBE/SMF) target systemic redox and metabolic dysregulation: sBE rapidly improves glucose intolerance in diabetic mice by modulating mitochondrial superoxide to rebalance the glutathione redox couple [70], while specifically oriented static magnetic fields reduce pancreatic iron deposition, oxidative stress, and hyperglycemia, also improving gut microbiota profiles [75]. Repetitive transcranial magnetic stimulation (rTMS) further enhances metabolic control, promoting weight loss and improving insulin sensitivity in diabetic rats. This effect involves modulation of hypothalamic appetite regulation, altered hepatic lipid metabolism gene expression, and reduced circulating lipids [76]. Collectively, these diverse magnetic stimulation modalities demonstrate efficacy in improving core diabetic features—glycemic control, insulin sensitivity, and metabolic dysregulation—through central neuromodulation and peripheral effects on redox/iron homeostasis.

2.3.4 Thermal stimulation

Thermal stimulation (thermotherapy) entails the regulated delivery of heat to biological systems, spanning targeted hyperthermia to systemic warming, to trigger advantageous physiological effects. These encompass augmented blood flow in tissues, regulation of cellular stress responses (including heat shock protein upregulation), and optimized metabolic performance. Primary benefits feature non-invasive application, reduced adverse effects relative to drug-based treatments, and the prospect of lasting metabolic enhancements. Conventionally employed in domains such as oncology (for tumor treatment sensitization), musculoskeletal recovery (alleviating pain and inflammation),

and tissue repair, this approach capitalizes on its capacity to modulate vascular functions, inflammatory processes, and cellular regeneration pathways [77].

Thermal stimulation effectively targets core type 2 diabetes pathophysiology, enhancing insulin sensitivity and glucose control. The combined approach of mild electrical stimulation with heat shock (MES+HS) potently induces heat shock protein 72 (HSP72). Studies show MES+HS improves insulin signaling, reduces fasting glucose/insulin, decreases visceral adiposity and fatty liver in diabetic rodents, and protects pancreatic β-cells by reducing cellular stress [8, 78, 79]. Critically, human trials confirm MES+HS (2-7 sessions/week for 12 weeks) significantly lowers visceral fat, fasting glucose, insulin, HbA1c (dose-dependent), and improves insulin resistance and inflammation in metabolic syndrome and T2DM patients [80, 81]. Alternative thermal strategies are also effective. Passive whole-body heat therapy (e.g., hot tub immersion ~40°C) reduces fasting glucose and HbA1c [82], while repeated hot water immersion improves fasting insulin sensitivity [83]. Lower-body heat therapy specifically enhances postprandial leg blood flow in T2DM, indicating improved vascular insulin responsiveness, though not primarily via endothelial HSP72 [84]. Heat preconditioning also attenuates hepatic metabolic disturbances in diabetic models [85]. Key mechanisms involve HSP72 induction, which inhibits stress kinases, improves insulin signaling cascades, reduces inflammation/oxidative stress, and enhances vascular function, establishing thermal stimulation as a promising non-pharmacological adjunct for T2DM management.

2.4 Ultrasound and therapeutic ultrasound

2.4.1 Overview of ultrasound

Ultrasound refers to acoustic energy with frequencies beyond the range of human hearing, typically above 20 kHz. Medical applications utilize frequencies spanning kilohertz (kHz) to megahertz (MHz), classified as low-frequency (<1 MHz) or high-frequency (≥1 MHz) [3,5]. Intensity is categorized as low (≤3 W/cm², promoting

biological processes) or high (>5 W/cm², enabling tissue disruption) [86, 87]. Key advantages include non-invasiveness, deep tissue penetration, high spatial-temporal resolution, absence of ionizing radiation, and real-time monitoring capabilities [88, 89]. Due to its safety, cost-effectiveness, and excellent spatiotemporal resolution, ultrasound has been a mainstay imaging modality for a long time. Increasingly, evidence suggests that low-intensity ultrasound produces diverse biological effects. Its capacity to deliver controlled energy into tissues now positions it as a versatile platform for therapeutic interventions, marking a significant expansion from its diagnostic origins [86-88, 90].

2.4.2 Mechanisms of therapeutic ultrasound

Therapeutic effects arise from three bio-physical interactions:

- Thermal effects

Thermal effects occur when tissue absorbs acoustic energy, generating heat. This elevates local temperatures, inducing protein denaturation, coagulation, or ablation at hyperthermic thresholds (>56°C). Temperature rise depends on intensity, exposure duration, and tissue absorption properties [87-90].

- Mechanical effects

Mechanical effects involve non-thermal forces. Radiation pressure displaces tissue or fluids, while acoustic streaming enhances fluid movement, facilitating molecular transport and cellular stimulation [87, 88, 90].

- Cavitation effects

Cavitation effects entail microbubble dynamics within tissues. Stable cavitation features rhythmic bubble oscillations generating localized shear stresses. Inertial cavitation involves violent bubble collapse, producing shockwaves and high localized pressures capable of mechanical disruption. Microbubble agents can amplify these effects for targeted therapy [87-91].

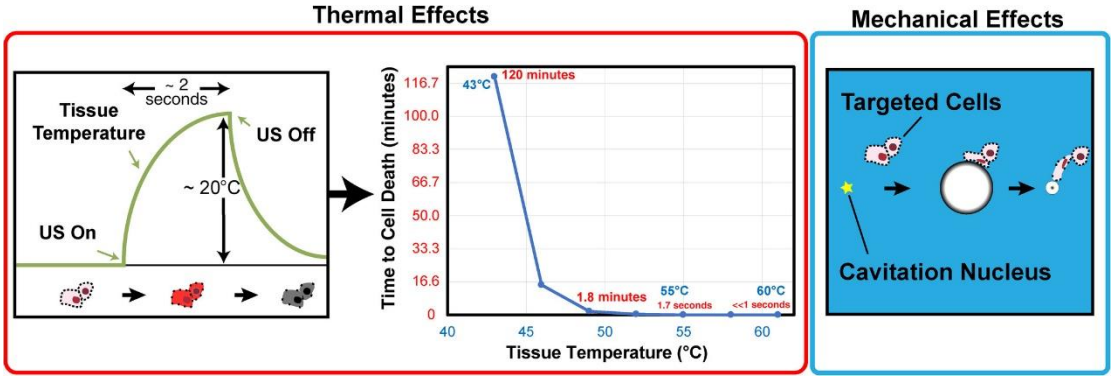

Figure 2.4. Bio-physical effect of ultrasound.

(Left) Focal tissue heating via ultrasound absorption, causing effects from hyperthermia to thermal necrosis or boiling. (Middle) Temperature-time relationship for irreversible thermal cell death. Cavitation and heating interact: cavitation modifies heating rates, while heating lowers cavitation thresholds. (Right) Bubble oscillation dynamics under ultrasound generating mechanical bioeffects (cavitation ablation, sonoporation, streaming). Bubble expansion and collapse cycles inflict damage on surrounding cells. [90]

2.4.3 Application of therapeutic ultrasound

The diverse bioeffects of therapeutic ultrasound underpin a rapidly expanding range of clinical applications. High-intensity focused ultrasound (HIFU) exploits thermal and cavitational effects for precise, non-invasive ablation of pathological tissues. It is clinically approved for treating uterine fibroids, prostate cancer, essential tremor, metastatic bone lesions (for pain palliation), and soft-tissue tumors, often guided by MRI for accuracy [88-90]. Extracorporeal shock wave lithotripsy (ESWL) utilizes focused mechanical shockwaves, primarily relying on cavitation and direct stress waves, to fragment renal and biliary calculi, offering a non-surgical alternative [87, 90]. Ultrasound significantly enhances drug delivery: low-frequency energy permeabilizes the stratum corneum for transdermal transport (sonophoresis), while microbubble-assisted focused ultrasound transiently opens the blood-brain barrier (BBB) for targeted CNS drug delivery (sonoporation) [87, 89, 91]. Low-intensity pulsed ultrasound (LIPUS), operating via primarily non-thermal mechanisms, accelerates bone fracture healing and soft tissue regeneration (e.g., tendons, ligaments), with FDA approval for

non-union fractures [87, 92]. Emerging applications include sonothrombolysis for clot dissolution (enhanced by microbubbles) [89, 90], histotripsy for mechanical tissue fractionation [87], and neuromodulation for influencing neural activity [91]. This breadth demonstrates ultrasound's transformative role in interventional medicine.

Modality	Key advantages	Limitations/risks
Electrical stimulation (ES: NMES, GES/IES, VNS/tVNS, PNES, MENS)	Adjustable, targeted, reversible; minimally/non-invasive options; complements drugs; mature device ecosystem	Heterogeneous protocols/outcomes; implant/lead placement complexity; nerve-specific side effects; variable durability; many approaches still preclinical
Photostimulation (PBM, optogenetics)	Non-invasive (PBM), safe, repeatable; high precision (optogenetics); potential for closed-loop integration	PBM effect sizes vary with parameters; limited large RCTs; optogenetics requires gene modification and implants; light penetration constraints
Magnetic stimulation (tDCS/rTMS, static magnetic/electric fields)	Non-invasive; session-based with durable effects; avoids drug side effects	Parameter sensitivity; inter-individual variability; mechanistic heterogeneity; long-term safety/maintenance protocols not fully defined
Thermal stimulation (heat therapy; MES+HS)	Non-invasive; low systemic toxicity; potential lasting metabolic benefits; feasible in home/clinic settings	Dose standardization (temperature, duration, frequency) challenging; adherence/logistics; contraindications (cardiovascular disease, skin conditions, neuropathy)
Ultrasound (low-intensity therapeutic ultrasound)	Non-invasive; deep penetration; high spatiotemporal precision; no ionizing radiation; cost-effective	Parameter optimization (frequency, intensity, duty cycle); tissue-specific safety; off-target effects at higher intensities

Table 2.4. Conclusion of the pros and cons of the strategies described above.

2.5 MBs-mediated ultrasound therapy

Microbubbles (MBs) represent one of the most established and widely utilized

ultrasound contrast agents in clinical practice. Commonly employed to enhance ultrasonography, MBs leverage their inherent hyperechogenic properties—resulting from a significant acoustic impedance mismatch with blood and tissues—to substantially improve real-time imaging quality [89]. Their non-linear oscillations under acoustic energy emission generate harmonic signals that enhance diagnostic sensitivity, making them ideal contrast agents for clinical imaging [93]. MBs demonstrate high stability in circulation and relatively low manufacturing expenses, facilitating large-scale production and clinical accessibility [94]. Structurally, these gas-filled microspheres (1–10 μm diameter) feature a stabilized core (perfluorocarbons or sulfur hexafluoride) encapsulated within biocompatible shells of lipids, proteins, or polymers [89, 93, 94]. Beyond diagnostics role, their unique dual functionality enables simultaneous use as imaging enhancers and therapeutic vehicles, allowing precise spatiotemporal delivery of bioactive agents to target sites [93, 95]. Clinically approved agents, including Lumason® (sulfur hexafluoride lipid), Optison® (albumin-coated perfluoropropane), and Definity® (phospholipid-shelled perfluoropropane), exemplify their successful translation [89, 94].

The therapeutic efficacy of microbubble-ultrasound systems arises from synergistic physical interactions: cavitation dynamics (including stable oscillations and inertial collapse), acoustic radiation forces that directionally propel microbubbles toward target sites, microstreaming generating localized fluid shear stresses (12–3,000 Pa), sonoporation inducing transient membrane permeability, and associated thermal effects from energy dissipation [95-97]. These mechanisms collectively enable microbubbles to significantly improve tissue penetration by non-invasively disrupting endothelial tight junctions—facilitating controlled blood-brain barrier opening for CNS therapeutics and enhancing transdermal transport efficiency through cavitation-mediated bioeffects [93, 97]. Precise cargo release is achieved when ultrasound-triggered microbubble destruction (UTMD) exploits inertial cavitation to violently rupture vesicles at designated anatomical sites, deploying encapsulated chemotherapeutics or genetic payloads with sub-millimeter spatial precision while

minimizing systemic toxicity [93, 95, 96]. Concurrently, microstreaming-induced shear stresses combined with sonoporation critically augment cellular uptake by creating transient membrane pores (0.5–5 μm diameter) and stimulating clathrin-mediated endocytosis, dramatically increasing intracellular internalization of co-administered macromolecules [96, 97]. The violent collapse during inertial cavitation further generates high-energy reactive oxygen species through sonoluminescence and thermal decomposition, enabling free radical-mediated oxidative damage in sonodynamic tumor therapy when combined with porphyrin-based sonosensitizers [93, 96]. Finally, microbubbles amplify high-intensity focused ultrasound bioeffects by lowering cavitation thresholds up to 50%, permitting mechanical tissue fractionation via histotripsy—a non-thermal ablation modality generating precise lesions through controlled bubble cloud formation and collapse [89, 93, 96].

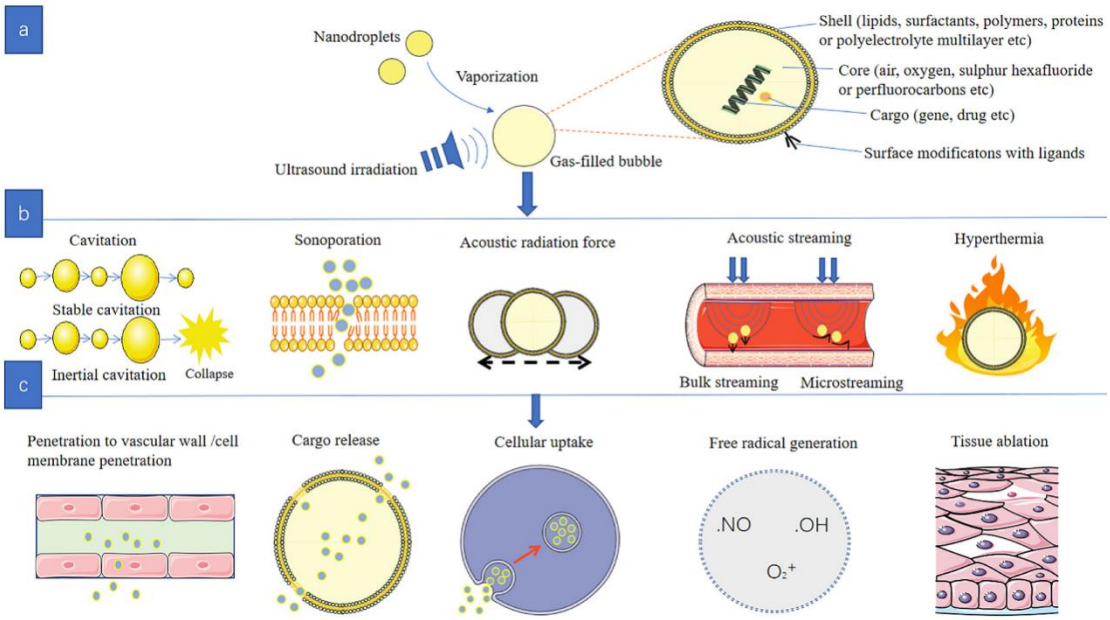

Figure 2.5. MBs-mediated ultrasound therapy

(a) Structural configuration schematic of a microbubble. (b) Mechanism underlying bubble-mediated ultrasound therapy. (c) Biological outcomes induced by bubble-facilitated ultrasound exposure. [95]

2.6 Sonogenetics

Sonogenetics represents a distinct approach to ultrasound sensitization, diverging from material-based strategies like MBs by leveraging genetic engineering. It involves the targeted expression of ultrasound-sensitive mediators (e.g., mechanosensitive ion channels like Piezo, TRP channels, MscL variants) within specific cell populations. This genetic targeting allows ultrasound waves to selectively modulate the activity of only those engineered cells, translating the mechanical (and sometimes thermal) energy of ultrasound into precise cellular responses such as ion flux or gene expression changes [16, 17, 98-101]. The primary advantage of sonogenetics lies in its exceptional cell-type specificity [17, 98-101]. Unlike MBs, which broadly amplify ultrasound effects in their vicinity and can cause collateral tissue damage or inflammation [17, 98], sonogenetics confines sensitivity to genetically defined cells [16, 17, 98-101]. Compared to optogenetics, it offers vastly superior tissue penetration depth (reaching deep brain structures non-invasively) without requiring implanted light guides [17, 98-101]. Against magnetogenetics, sonogenetics provides higher spatiotemporal precision and avoids the need for magnetic nanoparticles and complex field-generating equipment [99-101]. This unique combination of non-invasiveness, deep penetration, and precise cellular targeting makes sonogenetics a powerful tool for interrogating and manipulating biological systems [16, 17, 98-101].

Sonogenetics is rapidly expanding into diverse therapeutic and research domains, demonstrating significant potential. In neuromodulation and neurological disorders, it enables non-invasive activation or inhibition of specific neuronal populations deep within the brain with high spatiotemporal resolution. For instance, expression of ultrasound-sensitive channels like MscL-G22S in dopaminergic neurons of the ventral tegmental area allows ultrasound to alleviate motor symptoms in Parkinson's disease mouse models through enhanced dopamine release and targeted modulation of dyskinetic pathways [102]. It also holds promise for controlling seizures or chronic pain by precisely modulating specific neural circuits and provides a powerful tool for

fundamental neuroscience research by mapping neural connectivity and function [103].

In oncological therapies, sonogenetics offers strategies for more targeted cancer treatment. Ultrasound activation of mechanosensitive channels like Piezo1 or MscL variants in tumor cells can trigger lethal calcium (Ca^{2+}) influx, leading to selective tumor cell death, as demonstrated in models like pancreatic cancer, sometimes enhanced by MBs for initial plasmid delivery [104-106]. Furthermore, engineering T-cells (e.g., CAR-T cells) to express ultrasound-sensitive elements allows precise spatiotemporal control over their activation or therapeutic payload expression only at the tumor site. This can be achieved via ultrasound-triggered mechanical activation (e.g., via Piezo1) or thermal activation using heat-shock promoters (HSPs) induced by mild ultrasound heating, minimizing off-target effects on healthy tissues [107, 108].

For ophthalmic therapy, sonogenetics presents a potential alternative to optogenetics for vision restoration in degenerative diseases like retinitis pigmentosa and glaucoma. Ultrasound can effectively stimulate retinal ganglion cells or neurons in the visual cortex engineered to express mechanosensitive channels such as MscL-G22S, achieving millisecond temporal resolution and spatial resolution sufficient for visual perception in animal models [109, 110].

Finally, the field of stem cell research and regenerative medicine presents a promising frontier for sonogenetics. While low-intensity pulsed ultrasound is known to influence stem cell behavior (proliferation, differentiation, migration) via mechanosensitive pathways [111-116], sonogenetics offers the potential strategy to enhance this interaction. By genetically engineering stem cells to overexpress specific mechanosensors (e.g., Piezo1), their ultrasound sensitivity could be increased, potentially enabling more precise spatiotemporal control over stem cell fate and activity for applications in tissue repair and regeneration.

While challenges remain, such as optimizing delivery vectors, identifying/engineering more sensitive and specific ultrasound-responsive proteins, and translating findings to larger animals and humans, the breadth of current applications underscores the

immense potential of sonogenetics as a transformative, non-invasive tool for precision medicine [17, 98, 100, 101].

2.7 Sonogenetic delivery systems

2.7.1 Gene delivery systems in sonogenetics

Effective expression of mechanosensitive channels in target cells is essential for sonogenetic applications, relying heavily on gene delivery systems to transport genetic constructs. These systems are broadly categorized into viral and non-viral vectors, each with distinct advantages and limitations [117].

Adeno-associated virus (AAV) is widely utilized in sonogenetics research due to its excellent safety profile, low immunogenicity, and capacity for long-term transgene expression – crucial for chronic disease management. Its small size (~25 nm) facilitates tissue penetration. However, AAV suffers from a severely limited cargo capacity (~4.7 kb), restricting the size of deliverable genetic constructs, and carries a persistent, albeit low, risk of insertional mutagenesis and potential immunogenicity related to its capsid proteins [118-120]. Despite these drawbacks, AAV remains a dominant vector in sonogenetics. Studies consistently demonstrate its effectiveness, using it to deliver genes for mechanosensitive channels like MscL-G22S, TRPV1, and Prestin variants, alongside fluorescent reporters (e.g., EYFP, dTomato), achieving significant transfection rates (e.g., 24-50% in neuronal cells) both in vitro and in vivo [21, 22, 102, 110, 121, 122].

Lentivirus (LV), another viral vector, offers key advantages over AAV: a larger cargo capacity (~10 kb) enabling delivery of larger or multiple genes, and the ability to infect both dividing and non-dividing cells with high efficiency. Its genomic integration ensures stable, long-term expression. However, LV's major disadvantage lies in its propensity for random genomic integration, which poses a significant risk of insertional mutagenesis, potentially activating oncogenes or inactivating tumor suppressor genes, leading to tumorigenesis. Furthermore, persistent expression of gene editors can

increase off-target effects, and LV can also elicit immune responses [123-127]. While used in sonogenetics (e.g., for MscL delivery in neurons validated by immunostaining [20]), these safety concerns necessitate careful risk-benefit analysis compared to AAV.

Lipid Nanoparticles (LNPs) represent the leading non-viral approach, prized for their superior safety profile: they lack immunogenicity, avoid genomic integration entirely, and have a theoretically unlimited cargo capacity. Their modular composition (ionizable lipids, PEG lipids, phospholipids, cholesterol) allows engineering for specific needs, and the pH-dependent release mechanism of ionizable lipids minimizes systemic toxicity [128-132]. The primary drawbacks of LNPs are their significantly lower transfection efficiency compared to viral vectors and poor extrahepatic targeting. LNPs readily bind apolipoproteins in the bloodstream, leading to predominant accumulation in the liver, making precise delivery to other tissues like the brain a major challenge [133, 134]. In sonogenetics, LNPs have been used (e.g., for MscL I92L and pPrestin delivery), achieving modest transfection rates (~24%) under optimized ultrasound parameters (e.g., 0.5 MPa) [106, 135], but often require repeated administrations due to transient expression and face cytotoxicity concerns with certain formulations [128, 136, 137].

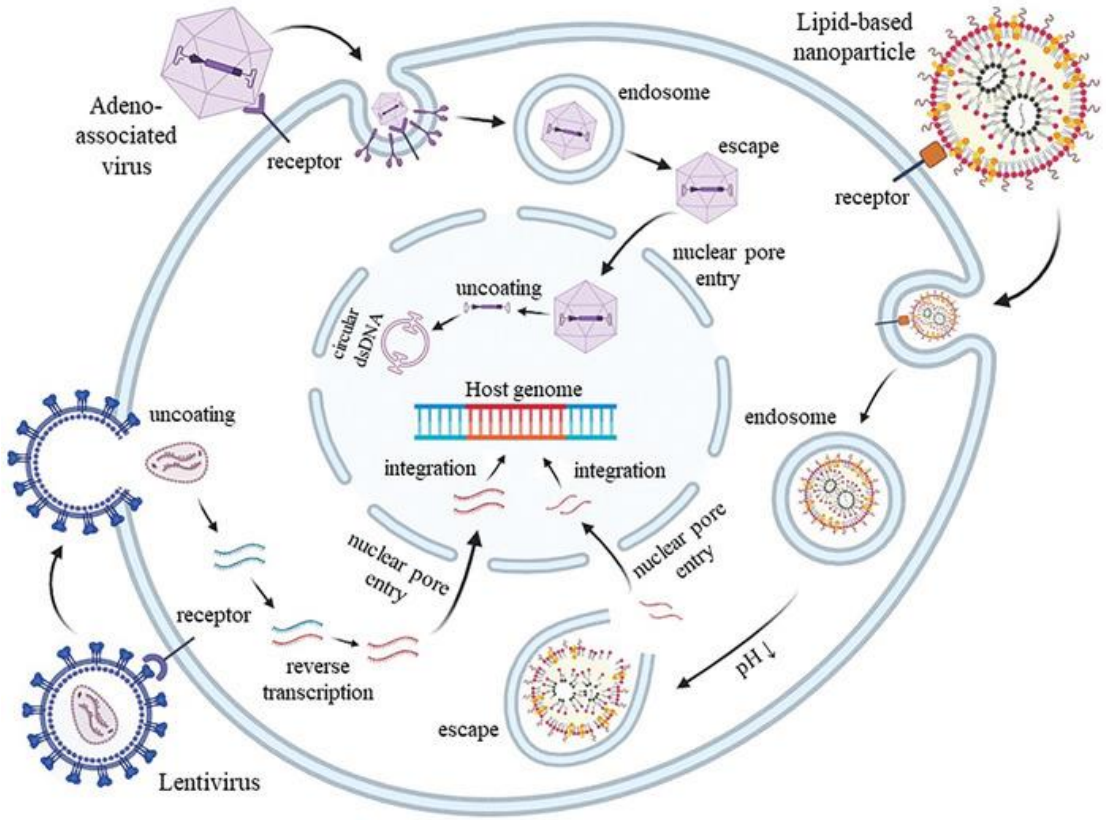

Figure 2.7. Sonogenetic gene carriers.

Current sonogenetic research primarily employs two transduction platforms: viral vectors (e.g., AAV, LVs) and non-viral systems (e.g., lipid nanoparticles, LNPs). This schematic illustrates their distinct intracellular delivery pathways. [98]

2.7.2 AAV targeted delivery

The distinct tissue tropism of AAV serotypes arises from structural variations in their capsid proteins, which govern differential interactions with host cell receptors and glycans. These molecular determinants critically influence cellular entry efficiency and organ-specific transduction patterns [138-140].

Established serotypes exhibit characteristic targeting profiles: AAV1 transduces muscle, CNS, and heart tissue; AAV2 targets liver, CNS, and muscle; AAV3 shows affinity for muscle and stem cells; AAV4 preferentially transduces ocular and CNS tissues; AAV5 efficiently targets CNS, lung, and retina; AAV6 demonstrates broad activity in muscle,

CNS, heart, and lung; AAV7 exhibits tropism for muscle and CNS; AAV8 achieves robust transduction in liver, muscle, pancreas, and CNS; while AAV9 demonstrates near-ubiquitous tissue penetration. [118]

AAV serotype	Origin of isolation	Primary receptor	Co-receptor	Tissue tropism	Condition (ClinicalTrials.gov identifier)	Approved drug
AAV1	Monkey	Sialic acid	AAVR	Muscle, CNS, heart	Muscle diseases (NCT01519349) Heart failure (NCT01643330) AAT deficiency (NCT01054339, NCT00430768)	None
AAV2	Human	Heparin	Integrin, FGFR, HGFR, LamR, AAVR	Liver, CNS, muscle	Eye diseases (NCT00643747) Haemophilia (NCT00515710) CNS diseases (NCT00400634) AAT deficiency (NCT00377416)	Luxturna for Leber congenital amaurosis
AAV3	Human	Heparin	FGFR, HGFR LamR, AAVR	Muscle, stem cells	No trials underway	None
AAV4	Monkey	Sialic acid	Unknown	Eye, CNS	Eye diseases (NCT01496040)	None
AAV5	Human	Sialic acid	PDGFR, AAVR	CNS, lung, eye	Haemophilia (NCT03520712) Eye diseases (NCT02781480) AIP (NCT02082860)	None
AAV6	Human	Heparin, sialic acid	EGFR, AAVR	Muscle, CNS, heart, lung	Haemophilia (NCT03061201) CNS diseases (NCT02702115)	None
AAV7	Monkey	Unknown	Unknown	Muscle, CNS	No trials underway	None
AAV8	Monkey	Unknown	LamR, AAVR	Liver, muscle, pancreas, CNS	Eye diseases (NCT03066258) Haemophilia (NCT00979238) Muscle diseases (NCT03199469)	None
AAV9	Human	Galactose	LamR, AAVR	Every tissue	CNS diseases (NCT02122952) Muscle diseases (NCT03362502)	Zolgensma for spinal muscular atrophy
AAV10	Monkey	Unknown	Unknown	Muscle	No trials underway	None
AAV11	Monkey	Unknown	Unknown	Unknown	No trials underway	None
AAV12	Human	Unknown	Unknown	Nasal	No trials underway	None

Table 2.7. Properties and clinical use of AAV serotypes. [118]

Among these, AAV8 has become the principal vector for pancreatic transduction due to its superior tropism for both endocrine and exocrine compartments. Systemic administration in mice achieves high β-cell transduction efficiency, significantly outperforming AAV serotypes 1, 2, and 6 [141, 142]. This capability stems from enhanced binding to laminin receptors and integrins [143], enabling robust transgene expression for diabetes research and therapeutic applications [144-146].

Chapter 3 MBs-Mediated Ultrasound Stimulation to Enhance Insulin Release and Glucose Control in Mice

3.1 Brief background and introduction

Diabetes remains a global health challenge, with insufficient β-cell insulin secretion being one of the key pathophysiological drivers. Ultrasound, with its non-invasiveness, deep tissue penetration capability, and spatiotemporal precision, may provide a promising alternative to conventional insulin injection therapies. While previous studies have established ultrasound's ability to stimulate insulin release, none have successfully translated this effect into functional blood glucose regulation. We hypothesize that non-selective activation of multiple pancreatic cell types (particularly insulin-antagonizing α-cells) under conventional ultrasound protocols masks therapeutic potential.

By confining ultrasound's mechanical effects to β-cells through microbubble-mediated targeting, we achieved significantly higher insulin levels than non-targeted ultrasound, and provided the first evidence of ultrasound-mediated glycemic control in mice. The cellular-level spatial specificity in our methodology prevents interference from non-target hormones while substantially reducing off-target side effects. Furthermore, this approach showed high biocompatibility and biosafety through systematic ultrasound parameter optimization and comprehensive evaluation.

This study demonstrated that β-cell-specific ultrasound stimulation can achieve meaningful glycemic control, making a critical advancement in developing non-invasive diabetes therapies. It shifts the paradigm from "ultrasound can trigger insulin release" to "targeted ultrasound can control glycemia. Though using an idealized model, our findings conclusively prove that cellular specificity determines therapeutic efficacy principle guiding future strategies' development.

3.2 Method

3.2.1 Cell culture

Rat beta-insulinoma cells (RINm5F) were obtained from the American Type Culture Collection (ATCC, Manassas, VA, USA) and routinely cultured in RPMI 1640 medium (Gibco, #11875093) supplemented with 10% (v/v) fetal bovine serum (FBS) (Gibco, #A5209401) and 1% penicillin-streptomycin (10,000 U/mL penicillin and 10,000 µg/mL streptomycin) (Gibco, #15140122). The cells were maintained in a humidified incubator at 37°C with 5% CO2. Cells were passaged upon reaching approximately 80-90% confluence using a standard trypsinization protocol (trypsin-EDTA solution, Gibco, #25200072). For experiments, cells were seeded at optimized densities including, 8×10^3 cells/well in 96-well plates for viability assays, 1×10^6 cells in a 35mm confocal dish for imaging studies, followed by 24-hour adhesion prior to treatments.

3.2.2 MTS assay

Cell viability was quantitatively assessed using the colorimetric MTS (3-(4,5-dimethylthiazol-2-yl)-5-(3-carboxymethoxyphenyl)-2-(4-sulfophenyl)-2H-tetrazolium) assay kit (Abcam, #ab197010), strictly adhering to the manufacturer's detailed protocol. Briefly, RINm5F cells in logarithmic growth phase were seeded into 96-well plates at a density of 8,000 cells per well. Cells were then either maintained under standard culture conditions (Control Group) or co-cultured with microbubbles under identical conditions (MBs Group). At the designated time points (12h, 36h, 60h), the MTS reagent was added directly to the culture medium in each well. Following an 3 hours incubation period to allow formazan formation, the absorbance at 490 nm was measured using a microplate reader (Labexim LEDETECT 96), with background subtraction using a reference wavelength (630 nm). The relative cell viability (%) for the MBs Group at each time point was calculated as: (Absorbance of MBs Group / Absorbance of Control Group) *100%.

3.2.3 Ultrasound stimulation system and protocol

The ultrasound stimulation system consisted of a function generator and a commercial transducer (I7-0012-P-SU, Olympus) to produce 200 tone burst pulses at a center frequency of 500 kHz and a repetition frequency of 1 kHz with a duty cycle of 50%. The peak negative pressure (PNP) output intensity was calibrated and maintained within the range of 0.1 to 0.5 MPa, with a 3-second interval between pulses. During Ca^{2+} imaging, the transducer was positioned with its acoustic axis perpendicular to the plane of the confocal dish (90° tilt). Temperature was monitored following ultrasound treatment using the same parameters as in our previous studies, with no significant temperature increase observed (data not shown).

3.2.4 Calcium imaging

Prior to imaging, RINm5F cells seeded in 35-mm confocal dishes were gently rinsed twice with a physiological bath solution. This solution contained (in mM): 130 NaCl, 5 KCl, 1 $MgCl_2$, 2.5 $CaCl_2$, 10 Glucose, and 20 HEPES, adjusted to pH 7.4 with NaOH. Cells were then loaded with the ratiometric Ca^{2+} indicator Fura-2 AM (#F1200, Thermo Fisher Scientific) by incubation in the dark at 37°C for 30 minutes. The loading solution consisted of 3 μM Fura-2 AM dissolved in the same bath solution, prepared from a 1 mM stock solution in anhydrous dimethyl sulfoxide (DMSO). Following loading, cells were washed twice with fresh bath solution to remove excess extracellular dye and allowed to de-esterify for an additional 15-20 minutes at room temperature in the dark. The dish was then mounted on the stage of an inverted fluorescence microscope (Eclipse Ti-E, Nikon Instruments, Tokyo, Japan). For ratiometric Ca^{2+} measurement, cells were alternately excited at wavelengths of 340 nm and 380 nm using a high-speed wavelength switcher, with an excitation interval of 3 seconds between image pairs. The emitted fluorescence was collected through a 510 ± 20 nm bandpass filter. The ratio of fluorescence intensity (F340/F380) was calculated and used as an indicator of intracellular free Ca^{2+} concentration ($[Ca^{2+}]i$). In specific experiments designed to investigate the role of mechanosensitive channels, cells were pre-incubated for 10

minutes with 20 μM gadolinium chloride ($GdCl_3$). The $GdCl_3$, dissolved in ultrapure water, was maintained in the bath solution throughout the subsequent Ca^{2+} imaging procedure.

3.2.5 Cell insulin ELISA

RINm5F cells were seeded in 24-well plates and allowed to reach approximately 70-80% confluence. Prior to the secretion assay, cells were washed once with phosphate-buffered saline (PBS) and then incubated for 2 hours in serum-free and glucose-free RPMI 1640 medium (Gibco, #11879020) to induce a basal state. After starvation, fresh full culture medium containing 10 mM glucose was replaced, and microbubbles (MBs), prepared and suspended in sterile PBS, were added to the designated wells at the specified concentration. Cells were then stimulated with or without ultrasound for 15 mins. Then, the culture supernatants were carefully collected, centrifuged (200 g, 4°C, 5 min) to remove any cellular debris, for the following insulin enzyme-linked immunosorbent assay (ELISA). Insulin content in the supernatants was quantified using a commercial Rat Insulin ELISA kit (#33100, ImmunoDiagnostics), strictly adhering to the manufacturer's instructions, including the generation of a standard curve.

3.2.6 Animals

Male nude mice were utilized in this study. Animals were sourced from the Centralized Animal Facilities (CAF) at The Hong Kong Polytechnic University or the Laboratory Animal Services Centre at The Chinese University of Hong Kong. All animals were housed at CAF under standard housing conditions: controlled temperature (22 ± 1°C), humidity (55 ± 10%), and a 12-hour light/dark cycle, with *ad libitum* access to standard rodent diet and autoclaved water. All animal procedures complied with ARRIVE guidelines and were approved by the Animal Subjects Ethics Sub-Committee (ASESC) of the Hong Kong Polytechnic University. Animal use and care were performed following the guidelines of the Department of Health – Animals (Control of Experiments) of the Hong Kong S.A.R. government (Approval No. (22-344) in

DH/HT&A/8/2/4 Pt.12).

3.2.7 Mice blood glucose and insulin measurement

Mice were fasted for 6 h prior to intraperitoneal glucose injection (2 g/kg body weight). Blood was collected via the tail vein nick at two critical time points: immediately prior to glucose administration (baseline, 0) and 15 minutes post-injection. Blood glucose concentration was measured immediately after collection using a handheld glucometer with compatible test strips (Bayer HealthCare LLC). Plasma insulin levels were quantified from the same blood samples. Plasma was separated by centrifugation (4°C, 2000 g, 15 min) and analyzed using a mouse insulin ELISA kit (#32380, ImmunoDiagnostics), strictly following the manufacturer's protocol. Ultrasound stimulation was delivered to the cell-transplant region for 15 min following glucose injection.

3.2.8 Quantitative real-time PCR (qPCR) analysis

Total RNA was isolated from RINm5F cells using a commercial RNA extraction kit (Takara, #9767), following the manufacturer's protocol. RNA concentration and purity were assessed spectrophotometrically (NanoDrop). Reverse transcription (RT) was performed on 1 μg of total RNA per sample using a cDNA reverse transcription kit (Takara, #RR036A). For real-time qPCR, each reaction contained 1 μL of diluted cDNA, gene-specific forward and reverse primers (0.2 μM each), and a master mix containing DNA polymerase, dNTPs, and a fluorescent DNA-binding dye (Takara, #RR420A), in a final volume of 10 μL. Reactions were run in technical triplicate on a real-time PCR detection system (Applied Biosystems QuantStudio). Gene expression levels were normalized to the geometric mean of endogenous reference genes (Gapdh). Relative quantification was performed using the comparative ΔΔCq method. Results are presented as fold changes relative to the designated control group, expressed as mean ± standard error of the mean (SEM) from three independent biological replicate experiments. Primer sequences used are listed below:

	Forward (5’-3’)	Reverse (5’-3’)
Rat TRPA1	AGGAATTTGCGGCCTGAGTT	TGGAGAGGCGTACATCCATC
Rat TRPC1	CTGAAGGATGTGCGAGAGGT	TCCATCGTTGTTGAGTATTCCG
Rat TRPC3	GAAGGATCTGGAACTGGGCAT	TCTGCTGATATCGTGTTGGCT
Rat TRPC4	GCAGTGACTACGGAAACCC	TCAGGCCATGCTAGTCCATC
Rat TRPC6	ATACTGGTGTGCTCCTTGCAG	AGGAGCTTGGTGCCTTCAAAT
Rat TRPM2	AACACGGACAATGCCTGGAT	GGCCGACTCCTTTGGATCAT
Rat TRPM3	ACATTGGCCTGGTGATCGAG	TTCCCAGCAGTTTCAAGGCT
Rat TRPM4	GTTCTTTGCCCAGGATGGAGT	ACAGTGCAGAGAGATAAGGGAGT
Rat TRPM5	AATCCAGATGCCCGGAGTTC	TCCGAAGTTGACCTCTCCCT
Rat TRPM7	GACGCTTTCCGATAGATGGCT	TCCACCTTTACCCAAGGAACC
Rat TRPV1	CCTGTGCCGGTTTATGTTCG	GCACTTGTGTGGTGTGGACT
Rat TRPV4	ACCTCTCCTCCCTGG	ACTTGTCCCTCAGCA

	ATACG	GTTCG
Rat TRPV6	TCGTTTGCTCTGGTGT TGGG	ATCAGCCAGCAGAAT CGCAT
Rat PIEZO1	TTGGAGCATACACGC TACCC	TTCACGAACTGACGC AGGAG
Rat PIEZO2	CCAAGTAGCCCATGC AAAAT	GCATAACCCTGTGCC AGATT

Table 3.2. List of primers.

3.2.9 Immunofluorescence staining

Freshly excised tumor tissues were immediately fixed by immersion in 4% (w/v) paraformaldehyde (PFA) in PBS for 24 hours at 4°C. Following fixation, tissues were washed thoroughly with PBS. For IF staining, tissues were cryoprotected in 30% sucrose/PBS overnight at 4°C, embedded in optimal cutting temperature (O.C.T.) compound, and sectioned at 6-8 μm thickness using a cryostat. Alternatively, fixed tissues could be processed for paraffin embedding (see H&E below). Tissue sections were permeabilized and blocked for 1 hour at room temperature in a solution containing PBS, 0.1% (v/v) Triton X-100, 5% (v/v) normal goat serum, and 1% (w/v) bovine serum albumin (BSA) to reduce non-specific binding. After removing the blocking solution, sections were incubated overnight at 4°C with primary antibodies diluted in the same blocking buffer. The primary antibody used was rabbit monoclonal anti-cleaved caspase-3 (#9661T, Cell Signaling Technology; dilution 1:500). The following day, sections were washed three times (5 min each) with PBS. Sections were then incubated for 1 hour at room temperature in the dark with fluorophore-conjugated secondary antibodies diluted in blocking buffer. The secondary antibody used was goat anti-rabbit IgG (H+L) highly cross-adsorbed, conjugated to Alexa Fluor 488 (#A-11008, Invitrogen, Thermo Fisher Scientific; dilution 1:1000). After three additional PBS

washes, sections were mounted using ProLong™ Diamond Antifade Mountant with DAPI (#P36966, Thermo Fisher Scientific), covered with #1.5 glass coverslips, sealed, and stored at 4°C in the dark until imaging. Images were acquired using a confocal laser scanning microscope (TCS SP8, Leica Microsystems).

3.2.10 Hematoxylin & Eosin (H&E) staining

For H&E staining, the 4% PFA-fixed tumor tissues were processed through a graded series of ethanol solutions (70%, 80%, 90%, 95%, 100%) for dehydration, followed by clearing in xylene. Tissues were then infiltrated and embedded in molten paraffin wax at 60°C. Embedded tissue blocks were sectioned at 4-6 µm thickness using a rotary microtome. Sections were mounted onto glass slides, deparaffinized in xylene, and rehydrated through a descending ethanol series to distilled water. Rehydrated sections were stained with hematoxylin and eosin solution (#SBT10001, Sunteambio Biotechnology) following the manufacturer's protocol. Finally, sections were dehydrated through ascending ethanol concentrations, cleared in xylene, and mounted under glass coverslips using a permanent mounting medium, Permount. Stained sections were examined and imaged using a standard brightfield light microscope.

3.2.11 Statistical analysis

A minimum of 3 independent experiments were performed for all experiments shown. By this, we mean at least 3 separate 'rounds' of cell preparations, transfections, or RINm5F cell harvests used for various experiments. Wherever possible, multiple plates from each round were evaluated. The data were collected into GraphPad Prism sheets for statistical analysis and graph preparation. The normality of the data was assessed using the Shapiro-Wilk normality test. Next, the homogeneity of variances was evaluated using either the Brown-Forsythe test or Bartlett's test. For data that were normally distributed and had homogeneous variances, ordinary one-way ANOVA was performed, followed by Tukey's post-hoc test for multiple comparisons. If the data exhibited heterogeneity of variance, Welch's ANOVA was used, followed by Dunnett's

T3 post-hoc test for multiple comparisons. Nonparametric data were analyzed using the Kruskal-Wallis test, followed by Dunn's post-hoc test for multiple comparisons. A significance level of p values below 0.05 was considered statistically significant.

3.3 Results

3.3.1 Microbubble characterization and biosafety evaluation

To specifically stimulate islet β cells, we first utilized microbubbles (MBs) as the ultrasonic amplifier. MBs were synthesized via agitation of a heated lipid solution in the presence of air, followed by PEGylation to enhance stability and biocompatibility. Size isolation yielded MBs with a uniform diameter distribution (average: 2.01 ± 0.31 μm; Fig.3.1 A, B), ensuring minimal risk of uncontrolled collapse or cell-damaging inertial cavitation during experiments. Zeta potential measurements confirmed colloidal stability (-18.1 ± 5.43 mV), consistent with PEG-coated MBs under physiological conditions.

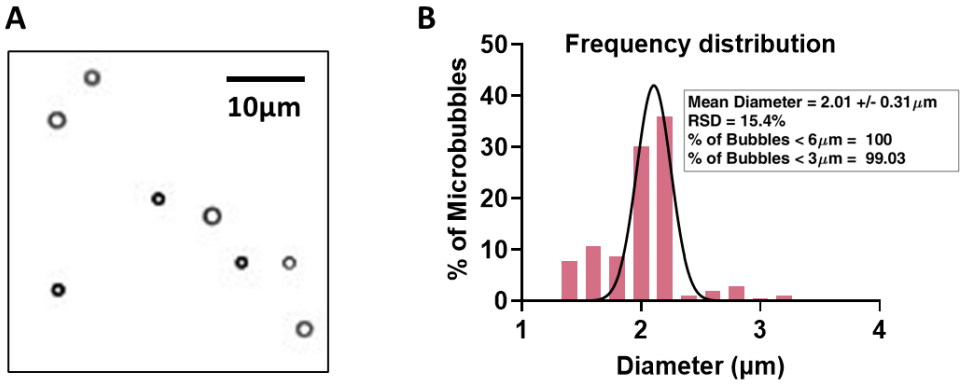

Figure 3.1. Characterization of microbubbles (MBs).

(A) Bright-field microscopy image of synthesized MBs (scale bar: 10 μm). (B) Size distribution of MBs (mean diameter: 2.01 ± 0.31 μm), analyzed from (A) using MATLAB.

To quantify MBs-mediated ultrasound amplification, we analyzed acoustic signals using a passive cavitation detector. Nonlinear harmonic scattering—a hallmark of

stable cavitation—was assessed via root mean square (RMS) power within 40 kHz spectral windows centered at harmonic frequencies (Fig.3.2 A). In pure water, harmonic power remained low and intensity-independent, reflecting the absence of cavitation nuclei. In contrast, MB suspensions exhibited intensity-dependent harmonic amplification (Fig.3.2 B), confirming that MBs efficiently convert ultrasound energy into localized mechanical stimuli at low intensities (0.11–0.38 MPa).

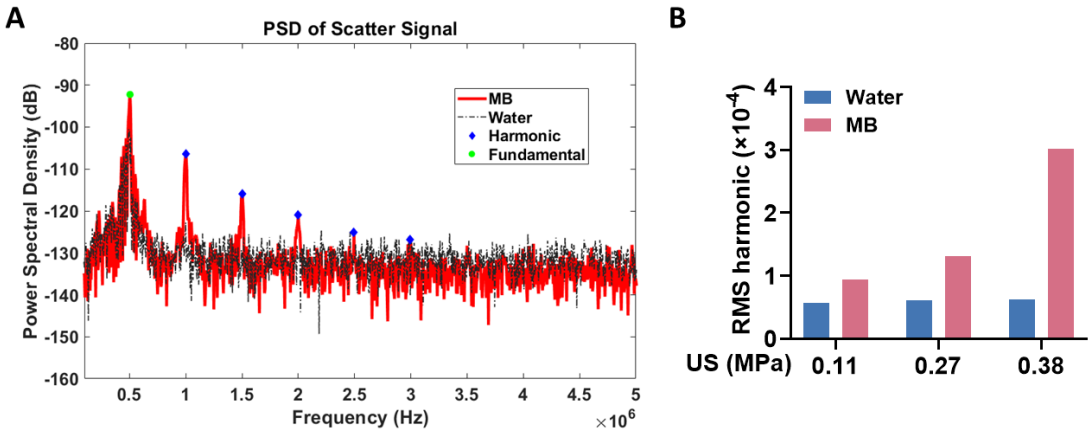

Figure 3.2. Characterization of MBs interaction with ultrasound.

(A) Frequency spectrum of backscattered signals from MB suspension during sonication (0.5 MHz, 50-cycle tone burst, 0.38 MPa peak negative pressure). Fundamental frequency (green dot) and harmonics (blue diamonds) are labeled. (B) RMS power of 2nd–8th harmonics in degassed water (black) versus MB suspension (red) across increasing acoustic pressures (0.11–0.38 MPa).

To evaluate the biosafety of MBs, RINm5F β-cells co-cultured with MBs for 72 hrs showed no reduction in proliferation activity (MTS assay; Fig.3.3 A), demonstrating excellent biocompatibility. This result validates the safety of MBs for *in vitro* and *in vivo* applications. In this study, MBs were simply mixed with RINm5F cells in the "MBs group", and PEG modification of the MB surface reduces the likelihood of endocytosis and membrane fusion.

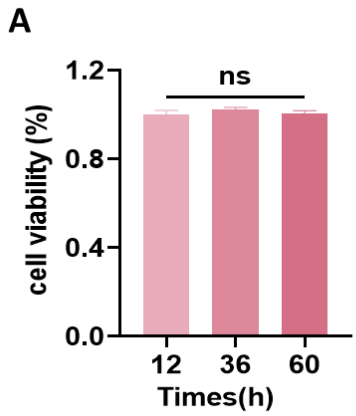

Figure 3.3. Biocompatibility of MBs.

(A) Cytocompatibility of MBs assessed by MTS assay. RINm5F cell viability (normalized to MBs-free controls) after 12–60 hrs exposure to MBs. *n* =3; mean ± SEM; *ns*: not significant by one-way ANOVA.

3.3.2 Ultrasound-induced Ca^{2+} influx and insulin release

To evaluate ultrasound-triggered β-cell activation, we performed live-cell Ca^{2+} imaging in RINm5F cells loaded with Fura-2 AM (Fig.3.4 A). Cells were exposed to ultrasound (0.5 MHz, 0.5 ms pulse width, 1 ms interval, 300 ms duration, 3 s repetition) in the presence of microbubbles (MBs; 0–1.65 × 10^9/mL) (Fig.3.4 B). At 0.14 MPa, ultrasound induced MB concentration-dependent Ca^{2+} influx, with saturation observed at 1.65 × 10^9 MBs/mL (Fig.3.4 C-E). We next assessed the acoustic pressure threshold for Ca^{2+} mobilization (0.07–0.38 MPa). Robust, dose-dependent Ca^{2+} responses occurred only in MBs-treated cells ($p < 0.001$ vs. MB-free controls at all pressures; Fig.3.4 F), confirming MBs are essential for ultrasound-mediated stimulation at low intensities.

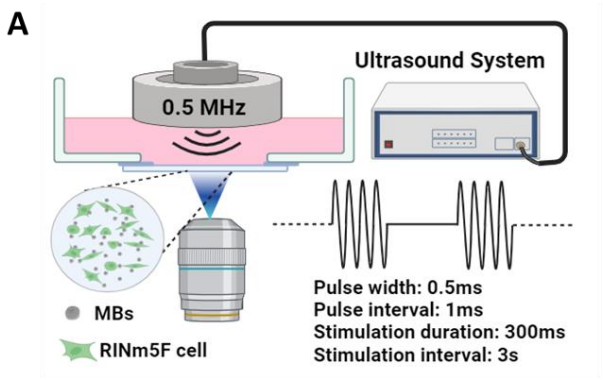
A
Ultrasound System
0.5 MHz
MBs
RINm5F cell
Pulse width: 0.5ms
Pulse interval: 1ms
Stimulation duration: 300ms
Stimulation interval: 3s

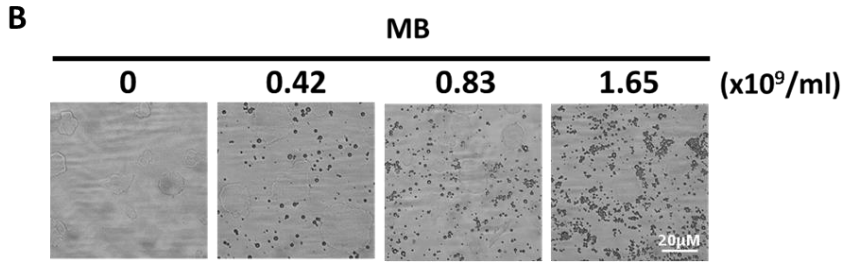
B
MB
0
0.42
0.83
1.65
(x10⁹/ml)
20μM

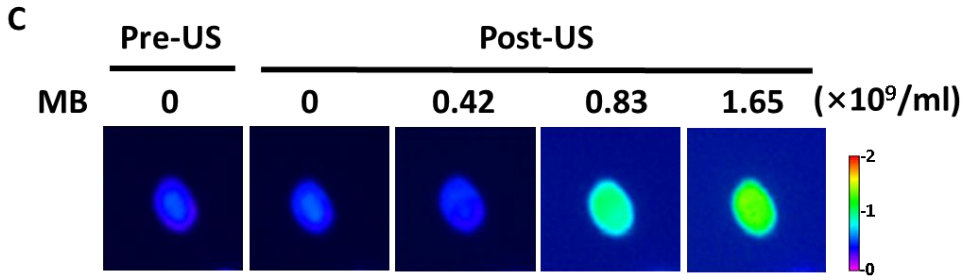
C
Pre-US
Post-US
MB
0
0
0.42
0.83
1.65
(×10⁹/ml)

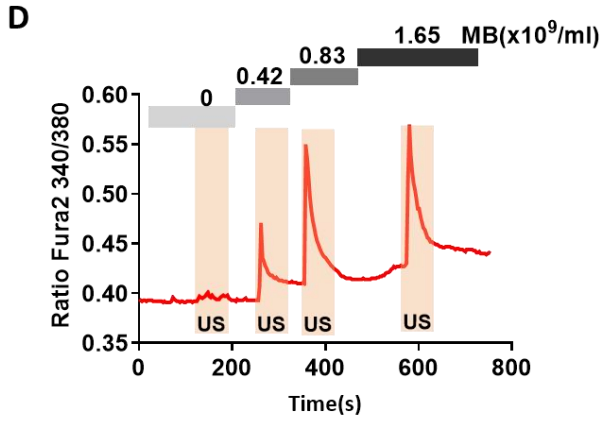
D
1.65 MB(x10⁹/ml)
0.83
0.42
0
Ratio Fura2 340/380
US
Time(s)

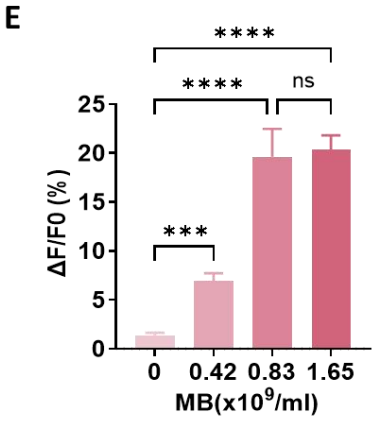
E
****
ns
***
ΔF/F0 (%)
MB(x10⁹/ml)

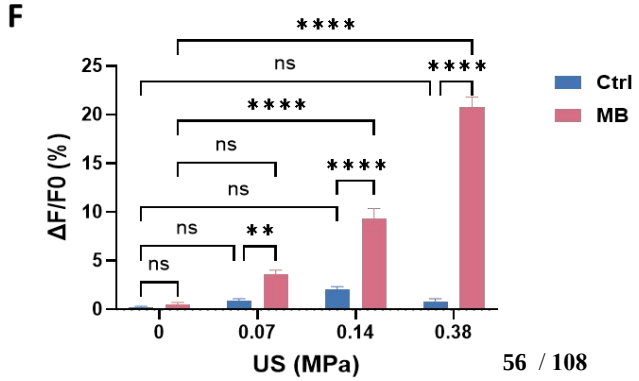
F
Ctrl
MB
ΔF/F0 (%)
US (MPa)

Figure 3.4. Microbubble-enhanced ultrasound stimulation triggers Ca^{2+} influx in RINm5F β-cells.

(A) Experimental setup for ultrasound stimulation (0.5 MHz, 0.5 ms pulse width, 1 ms interval, 300 ms duration, 3 s repetition) and live-cell Ca^{2+} imaging. MBs were suspended in culture medium above adherent RINm5F cells. (B) Schematic representation of different concentrations of microbubbles (0-1.65×10^9/mL) mixed with cells in the white field (scale bar: 20 μm). (C) Representative Fura-2 fluorescence images showing intracellular Ca^{2+} levels before and after ultrasound stimulation (0.14 MPa) with MBs (0-1.65×10^9/mL). (D) Time-course traces of Ca^{2+} measurement in the cells treated with different densities of microbubble under the same amplitude of ultrasound stimulation (0.14 MPa). (E) Quantification of Ca^{2+} response under 0.14 MPa ultrasound with increasing MB concentrations. n = 28-30 cells/group; mean ± SEM; ***p < 0.001, ****p < 0.0001, one-way ANOVA with Dunn's post-hoc tests. (F) Quantification of ultrasound intensity-dependent Ca^{2+} responses with/without MBs (1.65×10^9/mL). n = 10-55 cells/group; mean ± SEM; **p < 0.01, ****p < 0.0001, two-way ANOVA.

As Ca^{2+} influx triggers insulin exocytosis [42], we quantified released insulin via ELISA. Ultrasound + MBs elicited significant, intensity-dependent insulin release (p < 0.001 at 0.14 and 0.38 MPa), while no response occurred without MBs (Fig.3.5 A). This demonstrates that MBs-enhanced ultrasound selectively activates β-cells without off-target effects.

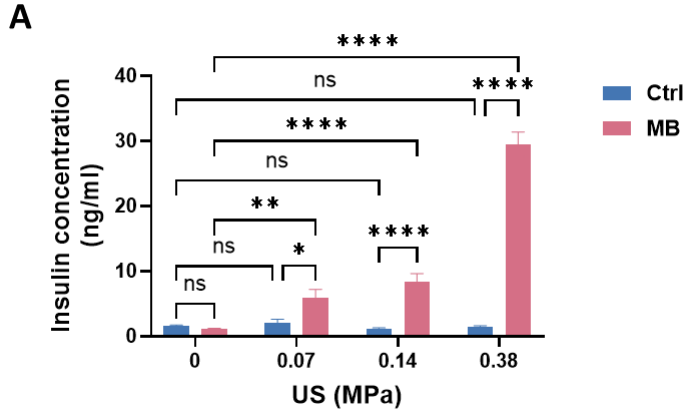

Figure 3.5. Microbubble-enhanced ultrasound stimulation triggers insulin release in RINm5F β-cells.

(A) Insulin release measured by ELISA 15 min post-stimulation. $n = 4$; mean ± SEM; *$p < 0.05$, **$p < 0.01$, ***$p < 0.001$, ****$p < 0.0001$, two-way ANOVA.

3.3.3 Microbubble-enhanced ultrasound stimulation promotes insulin release and improves glycemic control *in vivo*

To evaluate the therapeutic potential of MBs-enhanced ultrasound stimulation, we subcutaneously implanted RINm5F cells embedded in Matrigel into nude mice (Fig.3.6 A). Following a 6-hour fast, mice received the ultrasound treatment under isoflurane anaesthesia. Specifically, MBs were first administered to the cell transplantation site, followed by an intraperitoneal injection of glucose (2 g/kg). Ultrasound stimulation (0.38 MPa, 15 min duration, parameters consistent with prior protocols; see Fig.3.4 A) was immediately applied to the same region, with acoustic coupling gel minimizing signal attenuation (Fig.3.6 A).

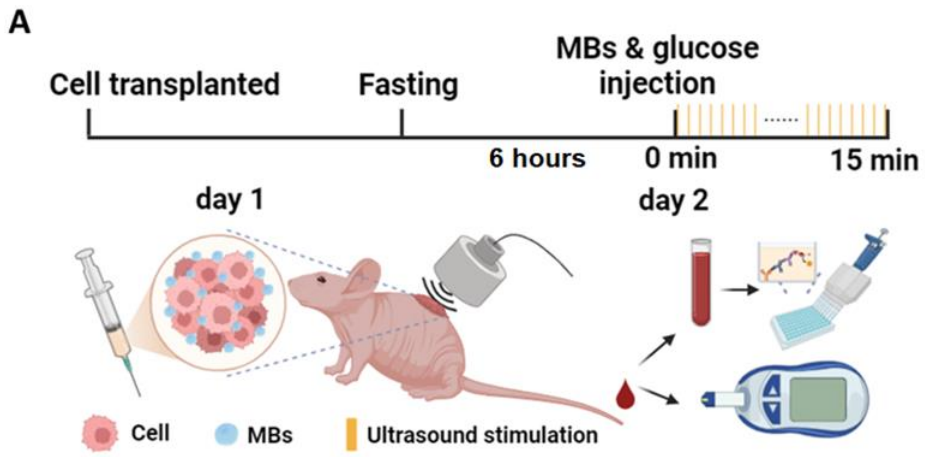

Figure 3.6. Schematic illustration of *in vivo* experiments.

(A) Experimental timeline and setup: RINm5F cells were implanted subcutaneously 24 hrs before the intraperitoneal glucose injection (2 g/kg). The MB+US group received microbubble injection followed by ultrasound stimulation (0.5 MHz, 0.38 MPa, 50% duty cycle, 300 ms pulse duration, 3 s interval) for 15 min post-glucose challenge. Blood was collected for glucose and insulin

measurements at 0 (before US) and 15 min (immediately after US).

As expected, glucose challenge rapidly elevated blood glucose levels in all groups (Fig.3.7 B). While control animals showed decreased insulin response (likely due to isoflurane effect [147, 148]), the MB+US group exhibited significantly higher insulin levels compared to controls ($p < 0.0001$; Fig.3.7 A). Ultrasound alone (US group) induced only marginal insulin elevation (Fig.3.7 A), underscoring the essential role of MBs in amplifying the bioeffects of ultrasound stimulation.

The enhanced insulin release in MB+US mice translated to superior glucose maintenance, with significantly lower blood glucose levels at 15 min post-challenge versus controls ($p < 0.001$; Fig.3.7 B). Notably, MBs remained stable throughout the experiment, with ultrasound imaging confirming persistent contrast signals 30 min post-injection (Fig.3.7 C), indicating sustained cavitation activity. These results demonstrate that MBs-localized ultrasound stimulation of transplanted β-cells can effectively augment glucose-dependent insulin release and improve glycemic control in vivo, offering a potential strategy for non-invasive diabetes management.

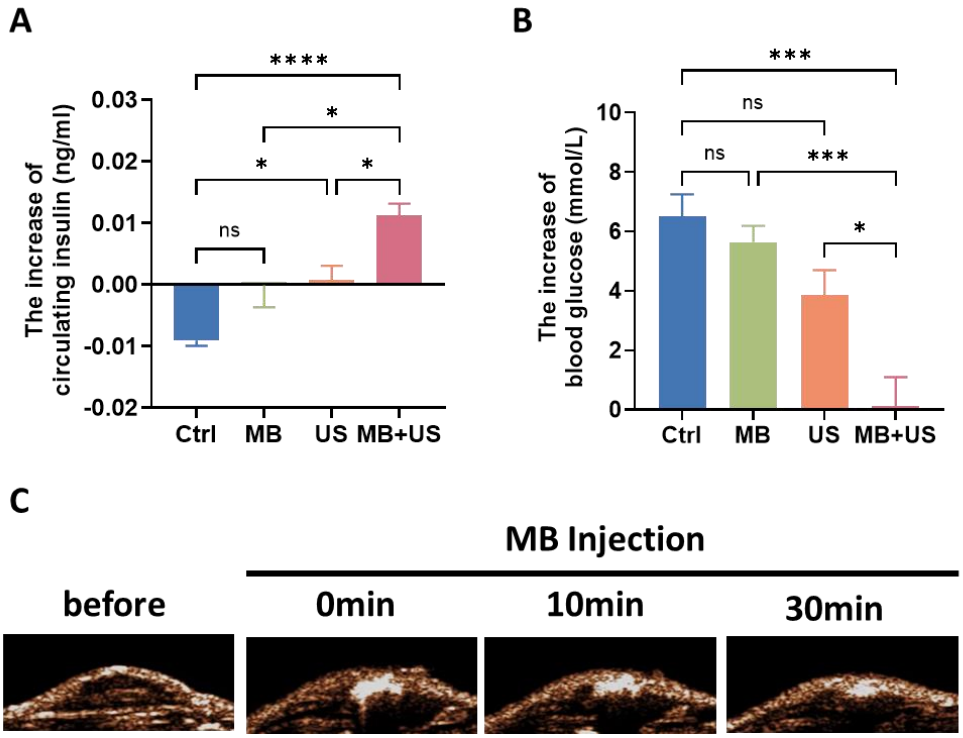

Figure 3.7. Microbubble-enhanced ultrasound stimulation promotes insulin release and improves glycemic control in mice.

(A) Plasma insulin levels normalized to baseline (t=0). The MB+US group showed significant enhancement vs. the Ctrl and US-only groups. n=5 each group; mean ± SEM; *p<0.05, ****p<0.0001, one-way ANOVA with post-hoc Tukey's test). (B) Blood glucose performance normalized to baseline (t=0). The MB+US group exhibited accelerated glucose clearance. n=5 each group; mean ± SEM; *p<0.05, ***p<0.001 vs. Ctrl at matched timepoint, one-way ANOVA with post-hoc Tukey's test). (C) Representative nonlinear contrast ultrasound images confirming stable MB distribution at implantation sites.

3.3.4 Mechanistic insights into microbubble-enhanced insulin release

Since Ca^{2+} influx directly triggers insulin exocytosis [42], we hypothesized that MBs-enhanced ultrasound activates mechanosensitive ion channels (Fig.3.8 A).

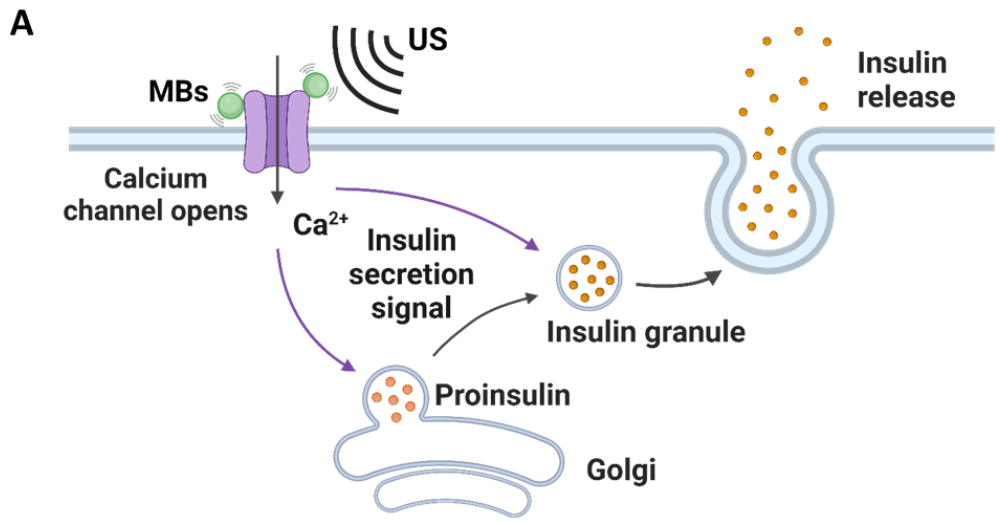

Figure 3.8. Schematic illustration of proposed mechanisms.

(A) Proposed mechanism: MBs-mediated ultrasound activates mechanosensitive channels to induce Ca^{2+} influx and insulin exocytosis.

qPCR confirmed robust expression of multiple mechanosensitive channels in RINm5F cells, with selective subtypes exhibiting particularly high abundance (Fig.3.9 A). To dissect the mechanism, we used gadolinium chloride ($GdCl_3$), a broad-spectrum mechanosensitive channel blocker [149]. At 0.14 MPa (parameters matching Fig.3.4 A), $GdCl_3$ abolished ultrasound-induced Ca^{2+} influx (Fig.3.9 B, C), indicating channel activation dominates. Consistent with Ca^{2+} data, $GdCl_3$ reduced insulin release by 75% under 0.14 MPa US+MB stimulation (Fig.3.9 D). The residual insulin release in $GdCl_3$-treated cells (statistically insignificant vs. controls) likely reflects a slight membrane perturbation. These results demonstrate that MBs-enhanced ultrasound primarily stimulates insulin release via mechanosensitive channel activation.

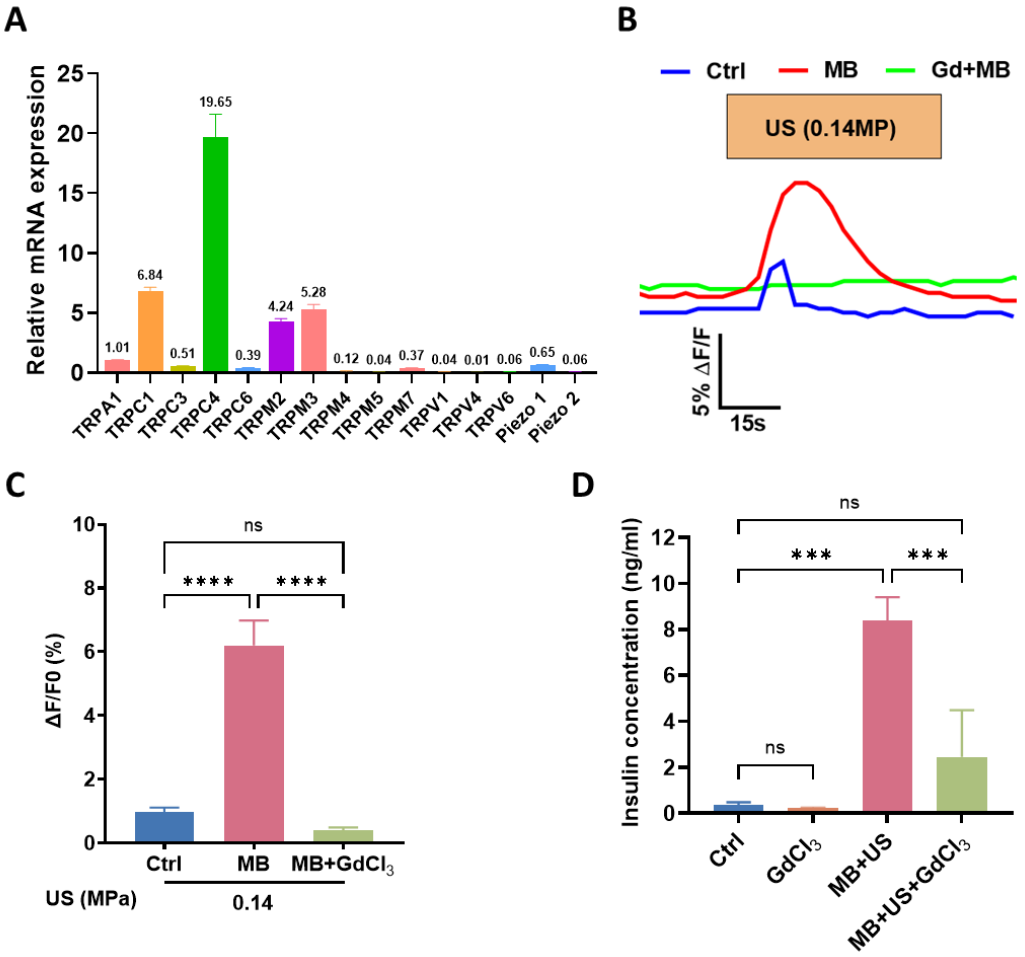

Figure 3.9. Mechanistic role of mechanosensitive ion channels in microbubble-enhanced ultrasound stimulation of insulin release.

(A) qPCR analysis of mechanosensitive channel expression in RINm5F cells. *n*=3; mean ± SEM. (B) Representative Fura-2 traces showing Ca^{2+} dynamics during 0.14 MPa ultrasound stimulation in control, MB only, and MB+$GdCl_3$ (50 µM) groups. (C) Quantified Ca^{2+} responses of (B). *n*=31-57 cells/group; mean ± SEM; ****p<0.0001, one-way ANOVA with post-hoc Tukey's test. (D) Insulin release after 0.14 MPa stimulation. *n*=3; mean ± SEM; ***p<0.001, one-way ANOVA with post-hoc Tukey's test.

3.3.5 Biosafety evaluation of microbubble-enhanced ultrasound stimulation

Given the potential for cavitation-induced cellular effects, we conducted

comprehensive biosafety assessments of our MBs-enhanced ultrasound approach. Initial *in vitro* studies using propidium iodide (PI) staining confirmed excellent cellular viability across all treatment groups, with no significant cell death observed following ultrasound stimulation at any intensity (Fig.3.10 A). Further investigation of transient membrane permeability revealed minimal reversible sonoporation, as evidenced by PI-positive rates below 0.5% at therapeutic intensities (0.07-0.14 MPa) and only marginally higher rates (~1.1%) at 0.38 MPa (Fig.3.10 B). These findings corroborate our mechanistic studies, demonstrating that insulin release at lower intensities primarily occurs through bio-safe mechanosensitive channel activation rather than membrane disruption.

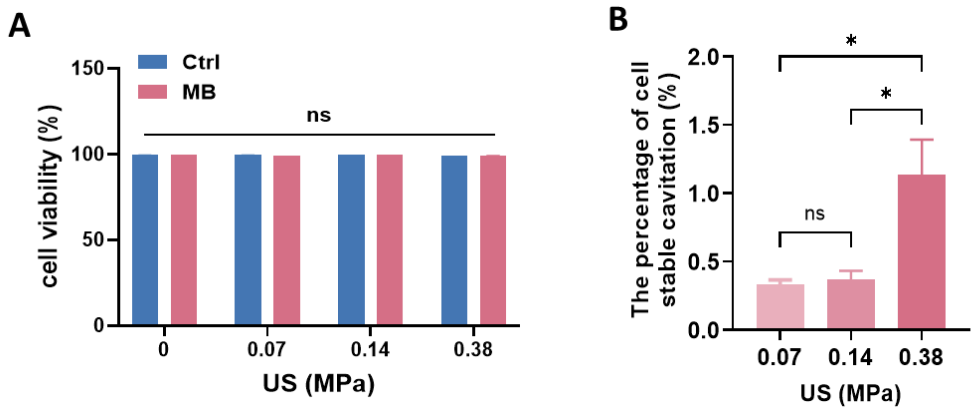

Figure 3.10. Biosafety assessment of microbubble-enhanced ultrasound stimulation *in vitro*.

(A) Cell viability following ultrasound treatments (conditions matching Fig.3.4 F, Fig.3.5 A), assessed by propidium iodide (PI) exclusion. n=3; ns: not significant by two-way ANOVA. (B) Sonoporation quantification via PI uptake during treatment. n=3; mean ± SEM; *p<0.05 vs control, one-way ANOVA with Tukey's test.

For *in vivo* safety validation, we examined transplanted tissues from treated mice through two complementary approaches. Cleaved caspase-3 immunofluorescence staining, a sensitive apoptosis marker, showed no detectable signals in either ultrasound-treated or MB+US groups, in contrast to clear positive signals in DMSO-

treated controls (Fig.3.11 A). Consistent with these results, hematoxylin and eosin (H&E) staining revealed preserved tissue architecture with no evidence of structural damage (Fig.3.11 B).

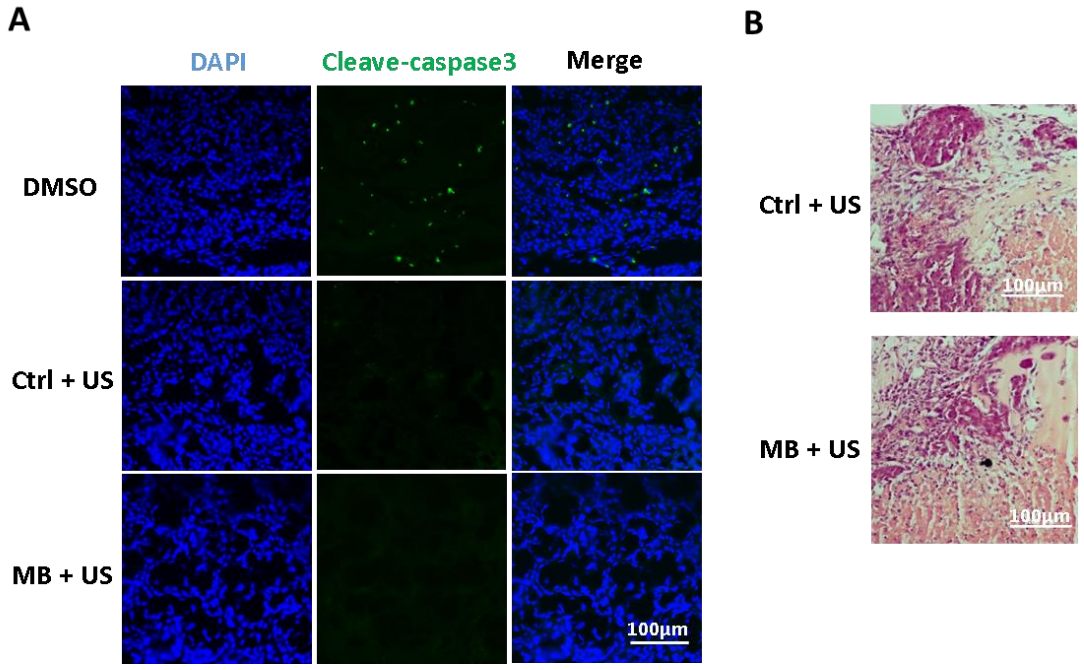

Figure 3.11. Biosafety assessment of microbubble-enhanced ultrasound stimulation *in vivo*.

(A) Cleaved caspase-3 immunofluorescence in transplanted tissues (DMSO: positive control; scale bar: 100 μm). (B) H&E staining of treated tissues showing preserved morphology (scale bar: 100 μm).

Collectively, these results establish the strong biosafety profile of MBs-enhanced ultrasound stimulation. The approach maintains cellular integrity at therapeutic intensities while achieving effective insulin release through controlled sonostimulation, with only minimal and reversible membrane effects observed at higher pressures. Both *in vitro* and *in vivo* assessments confirm the absence of significant cytotoxicity, apoptosis, or tissue damage, supporting the potential clinical translatability of this technique for diabetes management.

3.4 Conclusion

This study establishes the first proof-of-concept for blood glucose regulation through microbubble-assisted, β-cell-specific ultrasound stimulation in murine models. Our findings reveal that localized ultrasound application with microbubble mediation significantly enhances insulin release from transplanted RINm5F β-cells, effectively delaying glucose elevation in glucose-challenged animals. Through systematic optimization of ultrasound parameters and MB concentrations, we developed a dose-dependent insulin modulation paradigm while maintaining biosafety, as evidenced by reversible membrane sonoporation and absence of histopathological cellular damage. These results provide novel mechanistic insights into ultrasound-mediated glycemic control in mammals.

Chapter 4: Harnessing Sonogenetics for Non-Invasive Treatment of Type 2 Diabetes

4.1 Brief background and introduction

The previous study has demonstrated that targeted stimulation of pancreatic β-cells is crucial for ultimately regulating blood glucose levels in mice. However, the inherent limitations of microbubbles constrained their application in clinical settings and in vivo experiments. Sonogenetics presents another approach to amplify the localized effects of ultrasound. Moreover, it offers unparalleled cell-type specificity, making it a highly promising therapeutic approach for diabetes.

In this study, we developed a novel sonogenetic strategy to precisely modulate endogenous β-cells for glucose management. Our approach employs a pancreatic-tropic adeno-associated virus vector with an insulin promoter (AAV-INS-MscL) to achieve β-cell-specific expression of the bacterial mechanosensitive channel MscL. Following a single intraperitoneal AAV-INS-MscL administration, targeted ultrasound stimulation of the pancreas activated MscL-expressing β-cells in situ. In vitro studies confirmed MscL sensitizes β-cells to ultrasound, potentiating Ca^{2+} influx and insulin release. In vivo validation in T2DM mice demonstrated effective hyperglycemia reduction via triggered insulin release from endogenous β-cells, with high specificity (sparing α-cells) and a favorable safety profile. This paradigm enables long-term repeated non-invasive treatments post-single injection, demonstrating strong translational feasibility.

This work establishes the first sonogenetic platform for precise activation of endogenous β-cells to manage type 2 diabetes, uniquely bypassing the need for cell transplantation. By combining a minimally invasive AAV delivery with non-invasive ultrasound stimulation, our strategy offers a clinically tractable solution. We demonstrate that sonogenetic activation of endogenous β-cells provides a safe, effective, and non-invasive method for T2DM glycemic control, holding significant translational

promise for most T2D patients retaining functional β-cells.

4.2 Method

4.2.1 Animals

Male C57BL/6J mice at 6-8 weeks of age were used in this study. Animals were purchased from the Chinese University of Hong Kong and housed with controlled temperature (22±2°C), humidity (55±10%), and 12-h light/dark cycles in the Centralised Animal Facilities of the Hong Kong Polytechnic University. Animals had free access to standard laboratory chow and water. For the diabetic model, the establishment of the model and ultrasound treatment are described in Section 9. All animal procedures complied with ARRIVE guidelines and were approved by the Animal Subjects Ethics Sub-Committee (ASESC) of the Hong Kong Polytechnic University. Animal use and care were performed following the guidelines of the Department of Health – Animals (Control of Experiments) of the Hong Kong S.A.R. government.

4.2.2 Cell culture

Rodent pancreatic β-cell lines RINm5F or islets or primary β-cells were cultured in RPMI-1640 (Gibco, #11875093) supplemented with 10% (v/v) fetal bovine serum (FBS; Gibco, #A5209410), 1% (v/v) penicillin-streptomycin solution (Gibco #15140122) under standard conditions (37°C, 5% CO_2). For experiments, cells were seeded at optimized densities including, 8×10^3 cells/well in 96-well plates for viability assays, 1×10^5 cells in a 35mm confocal dish or a 35mm culture dish for imaging studies or patch clamp, followed by 24-hour adhesion prior to treatments.

4.2.3 Islet isolation and dispersion

Mice were killed by CO_2 inhalation and then performed islets isolation procedure, as referred to the established methods [150]. In short, pancreas from mice were inflated with 0.8 mg/mL collagenase XI (Sigma #C7657) in HBSS via the common bile duct.

Pancrease then removed and digested at 37 °C for 12 minutes and stopped by cold RPMI 1640 with 10% FBS. Then, purified by centrifugation at 290g for 30s for 3 times with cold HBSS. Islets were hand-picked under a stereomicroscope in RPMI 1640 with 10% FBS.

For single-cell dissociation, isolated islets were incubated in Enzyme Free Cell Dissociation Solution Hank's Based (Sigma #S-004-B) at 37°C for 10 mins. Gentle pipetting up and down until a single-cell suspension was achieved.

4.2.4 In vitro lentiviral transfection

RINm5F cells or primary islets were transfected with lentiviral vectors (pSlenti-EF1α-EGFP-Puro) encoding either the MscL gene or a control sequence at MOI = 10 in complete culture medium supplemented with 8 μg/mL Polybrene. After 24 hours, the viral supernatant was replaced with fresh medium. For RINm5F cells, GFP-positive cells were isolated by flow cytometry 72 hours post-transduction and maintained under 1 μg/mL puromycin selection to establish stable lines. For primary islets, successful transfection was indicated by GFP fluorescence. Only successfully transfected cells/islets were used in subsequent experiments.

4.2.5 Ultrasonic Stimulation

Ultrasound stimulation was delivered using an integrated ultrasound system equipped with a frequency 0.5MHz planar transducer (I7-0012-P-SU, Olympus). Stimulation parameters consisted of pulsed waveforms with a 50% duty cycle,1 kHz pulse repetition frequency, and under burst mode at 300 ms duration. The peak pressure of 0.35-0.87MPa was applied for *in vitro* experiments, while *in vivo* studies used a fixed 0.87 MPa. Acoustic coupling was achieved using degassed medical ultrasound transmission gel, with acoustic field distribution calibrated via a hydrophone. Sham controls underwent identical procedures, including gel application and transducer placement, but with the system powered off. Temperature was monitored to ensure $\leqslant 1^{\circ}$ C fluctuation during stimulation.

4.2.6 Agarose gel electrophoresis

Total RNA was isolated from 1×10^6 NC/MscL-RINm5F cells using a commercial RNA extraction kit (Takara #9767), followed by cDNA synthesis and PCR amplification according to the manufacturer's protocol (Takara #RR036A, #RR420A). Target genes were amplified using specific primers: MscL-G22S (Forward: 5′-GTCTCTTCACTGGTTGCCGA-3′; Reverse: 5′-TGCATCACAACAGCAGGGAT-3′) and rat-Gapdh (Forward: 5′-AGGTCGGTGTGAACGGATTT-3′; Reverse: 5′-AACTTGCCGTGGGTAGAGTC-3′). PCR products were combined with 6× DNA loading dye (Thermo Scientific #SM0243) alongside a 100 bp DNA ladder (Thermo Scientific #SM0243), then resolved on 2% molecular biology-grade agarose (Sigma #A9539) gels prepared in 1× TAE buffer containing 1× SYBR Safe DNA Gel Stain (Invitrogen #S33102). Electrophoresis was performed at 100 V for 30 min in 1× TAE running buffer, and then the gels were imaged under UV illumination using a ChemiDoc™ MP Imaging System (Bio-Rad).

4.2.7 Whole-cell patch clamp

Whole-cell patch clamp recordings were performed on NC/MscL-RINm5F cells prepared as previously described. Cells were continuously perfused with Margo-Ringer solution containing (in mM): 130 NaCl, 5 KCl, 1 $MgCl_2$, 2.5 $CaCl_2$, 20 HEPES, with D-mannitol added to achieve 285 mOsm/kg osmolarity (pH adjusted to 7.4). Borosilicate glass pipettes (resistance: 5-7 M) contained internal solution (in mM): 138 KCl, 10 NaCl, 1 $MgCl_2$, 10 HEPES, with D-mannitol added to 290 mOsm/kg (pH 7.2). Recordings were acquired at 22-24°C using an Axopatch 200B amplifier as well as a data acquisition system (DigiData 1322A, Axon Instruments). After establishing GΩ seals (>1 GΩ resistance) and achieving whole-cell configuration, membrane potentials were recorded in I=0 mode to determine resting potentials. Action potentials were elicited in current-clamp mode using a gap-free recording protocol.

4.2.8 Calcium imaging

Cells or islets were loaded with 3 μM Fura-2 AM (Invitrogen #F-1221) in Margo-Ringer solution containing (mM): NaCl 130, KCl 5, $MgCl_2$ 1, $CaCl_2$ 2.5, Glucose 10, HEPES 20 (pH 7.4) for 30 mins at 37°C in the dark, followed by 15-minute de-esterification in dye-free solution. Imaging was performed on an inverted fluorescence microscope (Nikon Eclipse Ti). The dish was then mounted on the stage of an inverted fluorescence microscope (Eclipse Ti-E, Nikon Instruments, Tokyo, Japan). Fura-2 measurements utilized dual-wavelength excitation (340 nm and 380 nm; 1 Hz switching frequency), and calcium dynamics were expressed as the ratio of emission intensities at 340 nm versus 380 nm.

4.2.9 Model mouse establishment, treatment, and evaluation

Mice were randomly assigned to two groups: one group received a standard diet (Control group), while the other group was fed a high-fat diet (HFD) for 6-8 weeks, followed by intraperitoneal injection of streptozotocin (STZ; 30 mg/kg, administered on three occasions) to establish the Type 2 Diabetes (T2D) group. After confirmation of successful T2D modeling, mice in the T2D group were further randomized into two subgroups. These subgroups received an intraperitoneal injection of either the NC (control) or MscL viral vector (5 × 10^11 vector genomes (vg) per mouse). Four weeks post-injection, mice underwent either ultrasound therapy or a sham procedure (ultrasound probe placement without activation) under anesthesia (isoflurane 1.5 to 2.0 % in O2). Blood glucose levels were measured immediately by a glucose test strip (Bayer Health Care LLC), and blood samples were collected for subsequent insulin quantification (described in 4.11).

4.2.10 Intraperitoneal glucose tolerance test (IPGTT)

Mice were fasted overnight (16 h) in temperature-controlled cages (23 ± 1°C) with ad libitum access to water. Following baseline tail-vein blood sampling (time 0), mice received intraperitoneal injections of 1 g/kg D-glucose dissolved in sterile 0.9% saline.

Blood glucose was measured at 0, 15, 60, 105, and 120 min post-injection via tail-vein sampling using a validated glucometer with glucose test strips (Bayer Health Care LLC). For insulin quantification, an additional 20 µL blood samples were collected at 0 and 15 min for the following ELISA (see 4.2.11).

4.2.11 Enzyme-linked immunosorbent assay (ELISA)

Insulin or glucagon levels in cell supernatants or serum were quantified using an Ultra Sensitive Mouse Insulin ELISA Kit (Crystal Chem #62100) or a Mouse Glucagon ELISA Kit (Crystal Chem #81518) according to the manufacturer's instructions. For *in vitro* experiments, islets were fasted in glucose-free RPMI 1640 medium (Gibco #11879020) for 4 hours at 37°C/5% CO_2 before treatment in complete culture medium (see Section 4.2). Islets of a similar size were used in each group. Supernatants were collected after 15mins stimulation, centrifuged at 200 × g for 5 min at 4°C, and stored at -80°C or immediately used. For *in vivo* experiments, serum was collected from mouse blood by centrifuge with 2000g at 4°C for 15 minutes. Concentrations were interpolated from a standard curve.

4.2.12 Immunofluorescence

RINm5F cells, primary pancreatic islets, or dissociated islet cells cultured in dishes fixed with freshly prepared 4% PFA in PBS for 15 minutes at room temperature, permeabilized and blocked in blocking buffer containing: 10% goat serum, 1% BSA, 0.2% Triton X-100 in PBS for 1 hour at room temperature. Primary antibodies—guinea pig anti-insulin (Abcam #ab195956, 1:200) and rabbit anti-Tag (Cell Signaling Technology #14793, 1:400)—were diluted in blocking buffer and incubated overnight at 4°C. After three PBS washes, samples were incubated for 1 h at room temperature with secondary antibodies: goat anti-guinea pig IgG-Alexa Fluor 647 (Abcam #ab150187, 1:1000) and goat anti-rabbit IgG-Alexa Fluor 647 (Invitrogen #A-21244, 1:1000), followed by nuclear counterstaining with 1 µg/mL DAPI (Invitrogen #D1306) for 10 min. Images were acquired using a microscope (Leica TCS SPE Confocal

Microscope).

4.2.13 MTS assay

RINm5F NC/MscL cells seeded in 96-well flat-bottom plates at 8×10^3 cells/well in 100 μL complete medium were treated as indicated. After cells adhered (overnight), 20 μL of MTS reagent (Abcam #ab197010) was added to each well. Plates were incubated at 37°C for 3 hrs in a humidified incubator, protected from light. Absorbance at 490 nm was measured using a microplate reader (Labexim Products LEDETECT 96 Microplate Reader) with a reference wavelength of 630 nm. Cell numbers were calculated by comparing to the initial value.

4.2.14 H&E staining

Pancreatic tissues were harvested from euthanized mice of each group. Tissues fixed in 4% PFA for 24 h at 4°C, dehydrated through graded ethanol series (70%, 80%, 90%, 95%, 100%), cleared in xylene, and embedded in paraffin. Serial sections (4-6 μm thickness) were cut using a rotary microtome, mounted on Superfrost Plus slides, and dried overnight at 37°C. Sections were deparaffinized in xylene, rehydrated through descending ethanol concentrations (100%→70%), and stained with hematoxylin and eosin (Solarbio #G1120) according to the manufacturer's instructions. After dehydration in ethanol and xylene clearing, the slides were mounted with resin adhesive. Histopathological assessment was performed by two blinded investigators using a light microscope (Nikon Eclipse Ni-E).

4.2.15 Statistical analysis

Data are presented as mean ± SEM. Analyses used GraphPad Prism. Normality was assessed via the Shapiro-Wilk normality test. Group comparisons employed an unpaired t-test (two groups) or ANOVA with Tukey's post hoc ($\geqslant$3 groups). $p < 0.05$ defined significance.

4.3 Results

4.3.1 Sonogenetic modulation of β-Cells enhances Ca^{2+} influx and insulin release

We first validated the sonogenetic capability of MscL overexpression in the pancreatic β-cell line RINm5F. Cells were transfected with control or MscL-packaged lentivirus, and expression levels were assessed three days post-transfection (Fig.4.1 A). GFP fluorescence confirmed successful transfection in both control and MscL groups (Fig.4.1 B). Immunofluorescence (indicated by tag, shown as red fluorescence) and agarose gel electrophoresis further demonstrated successful MscL expression at the protein and mRNA levels, respectively (Fig.4.1 B, C).

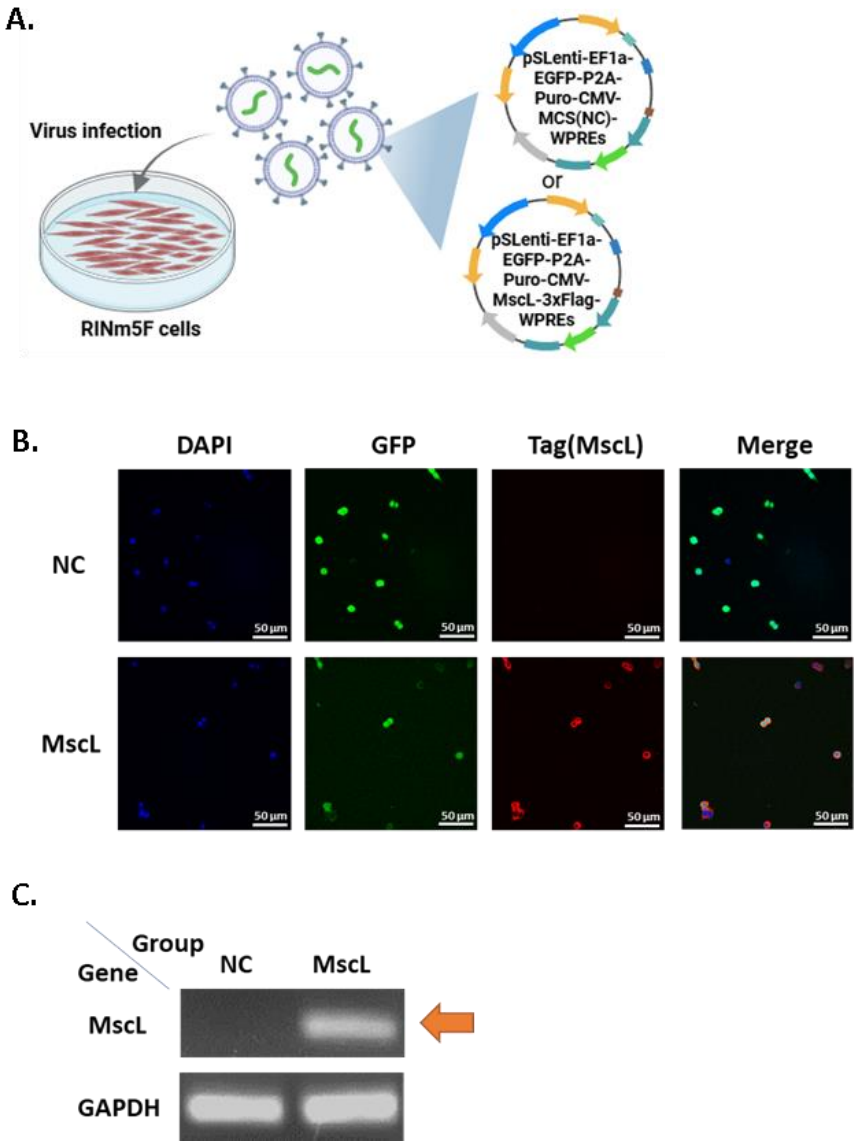

Figure 4.1 Transfection and expression of MscL on RINm5F cells.

(A) Schematic illustration of RINm5F cells transfection with NC/MscL lentivirus, and the virus constituents. (B) Representative fluorescence images of NC-RINm5F cells and MscL-RINm5F cells. GFP indicated the transfection efficiency. MscL expression was indicated by tag expression, which was shown as red fluorescence by immunofluorescence assay. (C) Agarose gel electrophoresis of the MscL gene, which extracted from NC-RINm5F cells and MscL-RINm5F cells. GAPDH as a reference gene.

To evaluate the mechanosensitive functionality of MscL, patch-clamp recordings were

performed under applied mechanical suction (Fig.4.2 A). Results revealed that MscL-expressing cells exhibited significantly larger inward currents compared to control cells under identical mechanical stimuli, with current magnitude increasing proportionally to the applied force (Fig.4.2 A, B). These findings confirmed the functional expression of MscL in RINm5F cells.

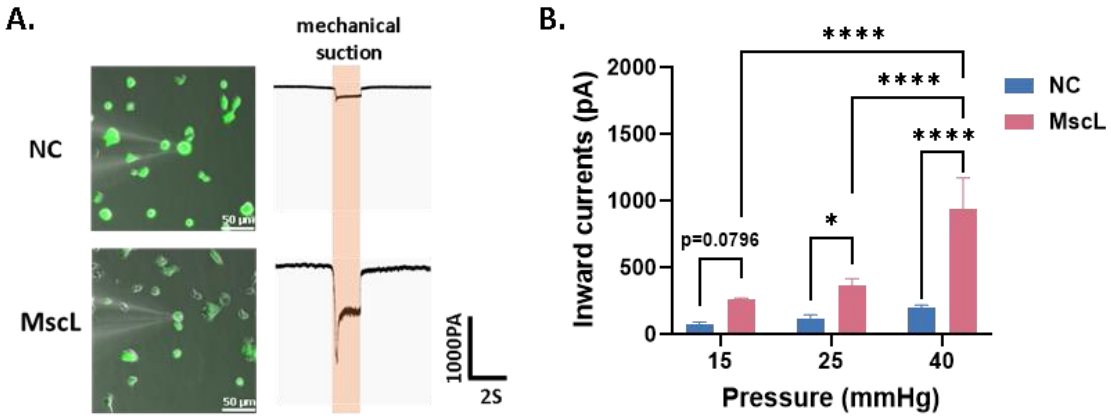

Figure 4.2 Functional validation of MscL of RINm5F cells.

(A) Representative images of patch clamp and representative curve of inward current of NC-RINm5F cells and MscL-RINm5F cells under mechanical suctions. (B) Inward currents of NC-RINm5F cells and MscL-RINm5F cells under mechanical suctions of 15, 25 and 40 mmHg pressure, respectively. From left to right column, n=6, 6, 6, 8, 3, 4. *P<0.05, ****P<0.0001, two-way ANOVA.

Subsequently, we examined the responsiveness of MscL-RINm5F cells to ultrasound stimulation (0.5 MHz, 0.5 ms pulse width, 1 ms interval, 300 ms duration, 3 s repetition) by Ca^{2+} imaging (Fig.4.3 A). As anticipated, ultrasound triggered a marked Ca^{2+} influx (elevated intracellular Ca^{2+} concentration) in MscL-RINm5F cells in a ultrasound dose-dependent manner, whereas control cells showed no such response (Fig.4.3 B, C). This confirms that the expression of MscL successfully enhances the sensitivity of RINm5F cells to ultrasound stimulation.

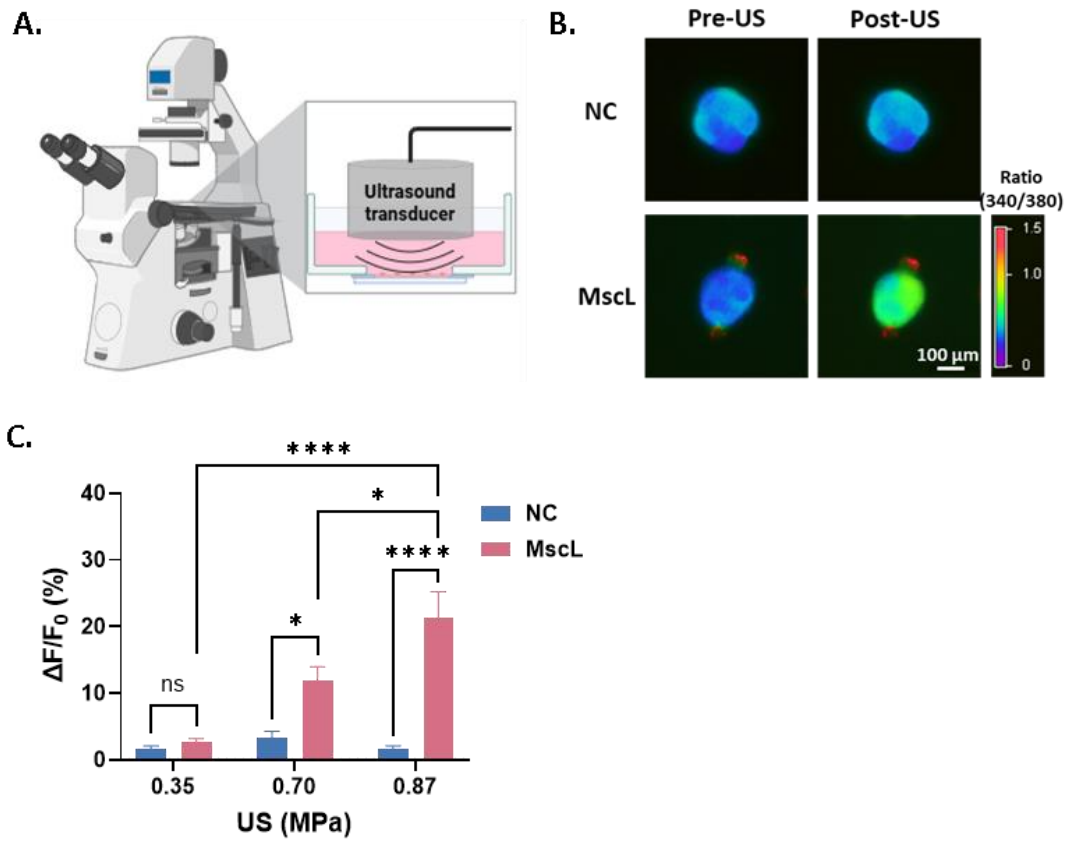

Figure 4.3 MscL overexpression of RINm5F cells enhances Ca^{2+} influx under ultrasound stimulation.

(A) Schematic illustration of experiment setup for ultrasound stimulation (0.5 MHz, 0.5 ms pulse width, 1 ms interval, 300 ms duration, 3 s repetition) and live-cell Ca^{2+} imaging. (B) Representative images of Ca^{2+} imaging of NC-RINm5F cells and MscL-RINm5F cells before and after ultrasound stimulation at 0.87MPa. Intracellular Ca^{2+} level was indicated by Fura-2 Ca^{2+} indicator, which represent as ratio of fluorescence intensities of 340nm/380nm. (C) Ca^{2+} response of cells to different ultrasound intensities. From left to right column, n=22, 23, 21, 24, 41, 40. *P<0.05, ****P<0.0001, two-way ANOVA.

Having validated the successful functional expression of MscL and enhanced Ca^{2+} influx in the MscL-expressing pancreatic β-cell line after ultrasound stimulation, insulin release was next investigated in mouse primary islets, which is correlated with increased intracellular Ca^{2+} [151]. Mouse primary islets were isolated and transfected

with control or MscL virus as previously done in RINm5F (Fig.4.4 A). The fluorescence images confirmed that the MscL transduction was successful, showing by the GFP fluorescence (Fig.4.4 B), and Ca^{2+} imaging confirmed that MscL enhanced ultrasound-induced Ca^{2+} influx in primary islets (Fig.4.4 C).

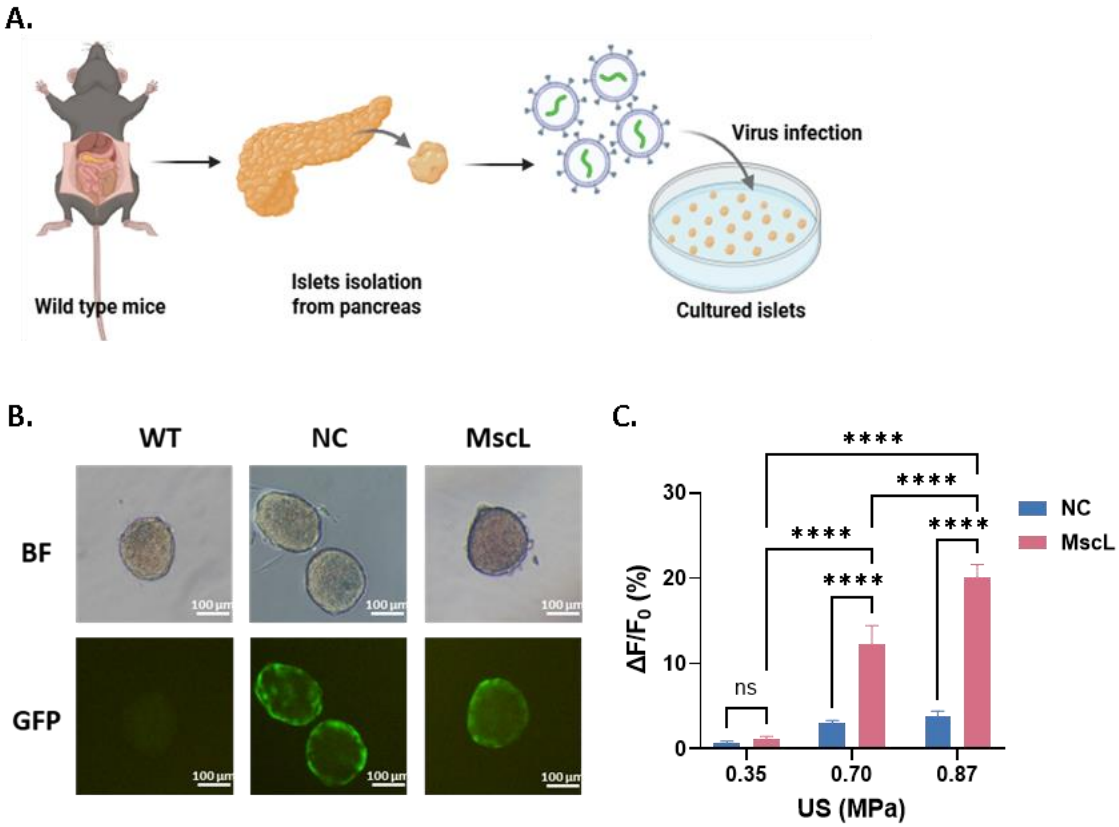

Figure 4.4 MscL overexpression of primary islet β-Cells enhances Ca^{2+} influx under ultrasound stimulation.

(A) Schematic illustration of primary islets isolation from mice and transfection with NC/MscL lentivirus. (B) Representative fluorescence images of WT-islets, NC-islets, and MscL-islets. GFP indicated the transfection efficiency. (C) Ca^{2+} response of primary islets to different ultrasound intensities. From left to right column, n=22, 35, 40, 47, 44, 83. ****P<0.0001, two-way ANOVA.

The calcium-dose dependent experiments confirmed that the amount of calcium influx is positively correlated to the insulin release (Fig.4.5 A). The ultrasound non-treated

group double confirmed that calcium influx and subsequent insulin release is only triggered by ultrasound stimulation (Fig.4.5 A). The insulin release assays demonstrated that MscL-islets released significantly more insulin into the culture medium following ultrasound stimulation compared to controls, while basal insulin release showed no difference between groups (Fig.4.5 B). And control islets showed no significant insulin release under these ultrasound intensities (Fig.4.5 B). These results validate that sonogenetic modulation of β-cells in the islets enhances ultrasound-triggered insulin release.

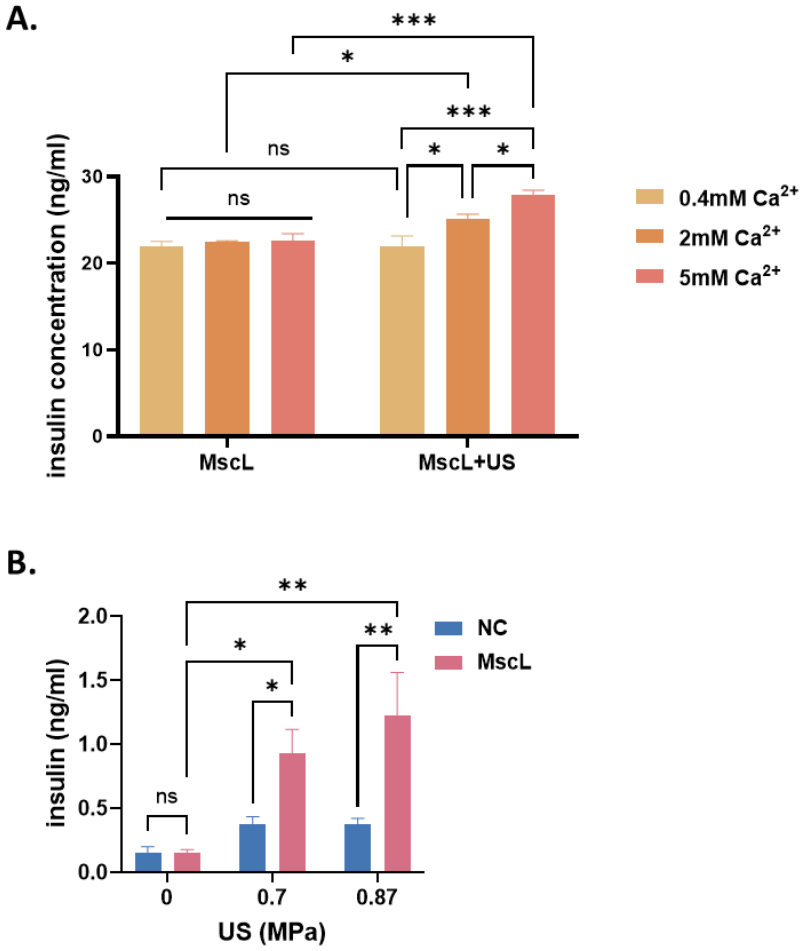

Figure 4.5 MscL overexpression of primary islet β-Cells enhances insulin release under ultrasound stimulation mediated by intracellular calcium increase.

(A) MscL-islets cultured in different calcium concentrations of medium with or without 0.7MPa ultrasound stimulation for 15mins. Insulin concentration was measured by insulin ELISA. *n*=3 in

each group. *P<0.05, ***P<0.001, two-way ANOVA. (B) Insulin release of islets to vary ultrasound intensities after 15mins ultrasound stimulation. Insulin concentration in culture medium were measured by ELISA. From left to right column, n=5, 5, 6, 7, 7, 7. *P<0.05, **P<0.01, two-way ANOVA. Data are shown as mean±s.e.m.

4.3.2 Effectiveness of sonogenetics to regulate insulin and blood glucose in T2D mice

We have achieved ultrasound-stimulated insulin release specifically in MscL-expressing cells, with minimal perturbation of non-MscL-expressing cells. We hypothesized that this specific increase in insulin release could ameliorate hyperglycemia in diabetic mice. Consequently, a series of experiments were designed to evaluate the therapeutic potential of this approach for T2D diabetes (Fig.4.6 A). T2D mouse models were first established using a combination of high-fat diet feeding and streptozotocin (STZ) administration (Fig.4.6 A). Successful induction of the T2D phenotype was confirmed by monitoring body weight and random blood glucose levels (Fig.4.6 B, C). Subsequently, highly effective pancreatic targeting AAV8 serotype vectors carrying the NC/MscL gene construct under a β-cell-specific promoter were administered to T2D mice via intraperitoneal injection (Fig.4.6 A). MscL expression, exceeding 40% efficiency (data not shown), was confirmed to be localized specifically to pancreatic β-cells four weeks post-injection, with no detectable expression in other cell types (Fig.4.6 D). This demonstrated effective viral targeting and successful cell-type-specific transgene expression.

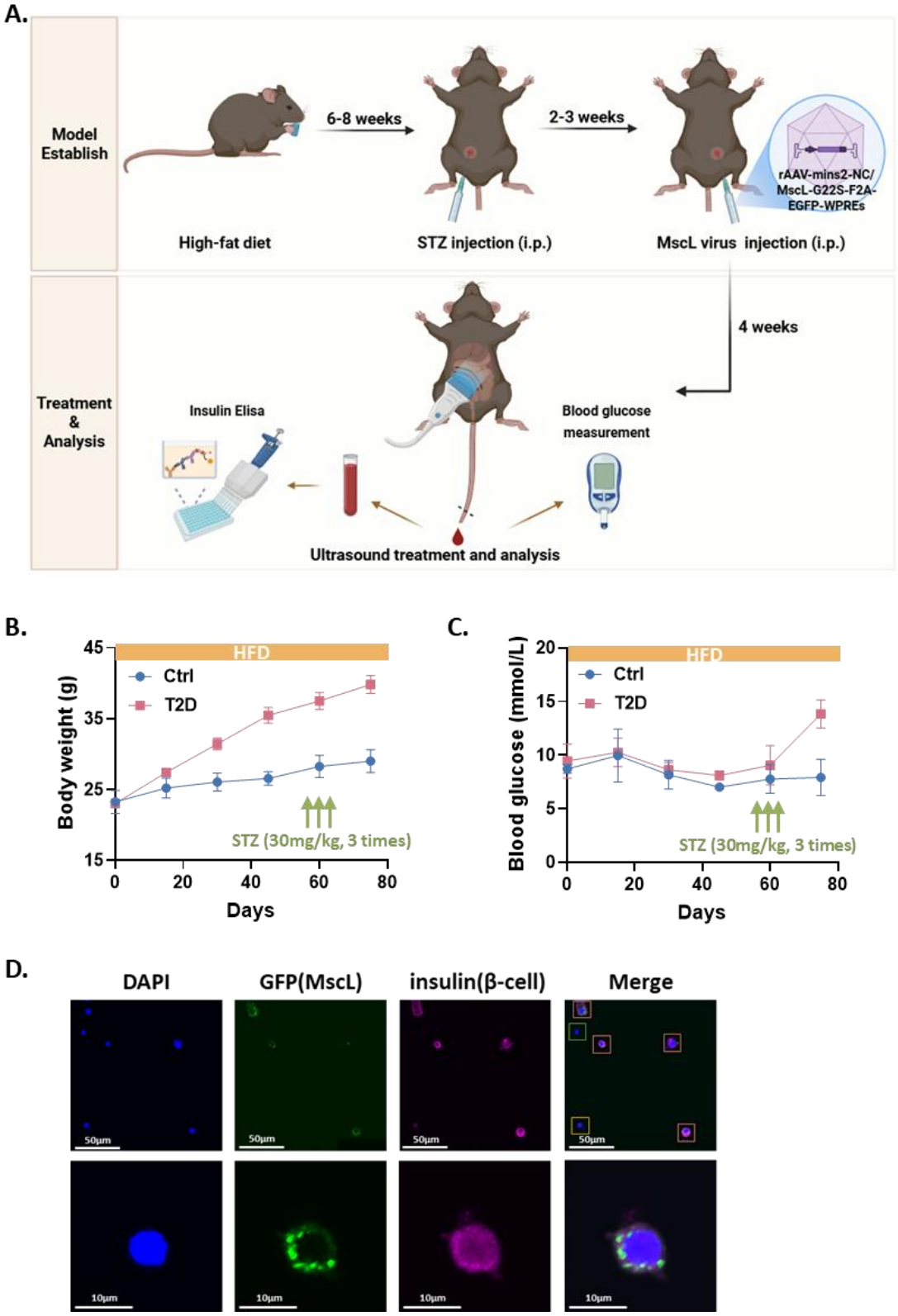

Figure 4.6 NC/MscL T2D mice model establishment and validation.

(A) Schematic illustration of the procedure of mouse model establishment and experiments. The control group received a standard diet. The T2D group received a high-fat diet (HFD) for 6-8 weeks,

followed by intraperitoneal injection of STZ (30 mg/kg, 3 times). Successfully modeled T2D mice were then re-randomized to receive intraperitoneal injections of either NC or MscL viral vectors (5×10^{11} vg/mouse). Four weeks post-injection, mice underwent ultrasound therapy or sham procedure (setup placement, no activation), the treatment effect was evaluated by blood glucose measurement and insulin detection. Mouse body weight (B) and random blood glucose (C) of control mice and T2D model mice during the model establishment. (D) Representative images of MscL expression (indicated by GFP fluorescence) and co-localization with β-cells (indicated by insulin marker, shown as red fluorescence). Islets were isolated from T2D mice and dispersed into single cells. Bottom: Enlarged images of single cells. In the merged picture (top right), green boxes indicate non-β-cells, yellow boxes indicate β-cells without MscL expression, and orange boxes indicate β-cells with MscL expression.

Prior to ultrasound therapy, the pancreas was localized using an ultrasound imaging system, which was then replaced with the therapeutic ultrasound system (Fig.4.7 A). Accounting for energy attenuation during *in vivo* ultrasound delivery, an acoustic pressure of 0.87 MPa was applied to ensure efficacy according to the previous investigation; all other parameters remained consistent with prior studies. Ultrasound treatment was administered for 15 minutes (Fig.4.7 B). Immediate blood glucose levels were measured, and small blood samples were collected for insulin quantification both immediately before and after treatment (Fig.4.7 B). All mice were maintained under isoflurane anesthesia throughout the procedures. Consistent with *in vitro* findings, the MscL+US group exhibited a significant increase in serum insulin levels post-sonication compared to other groups (which showed decreased insulin due to isoflurane anesthesia) (Fig.4.7 C, D). More importantly, a significant reduction in immediate blood glucose levels was observed in the MscL+US group after ultrasound treatment, in contrast to other groups (which exhibited increased glucose levels under isoflurane anesthesia) (Fig.4.7 E, F). In summary, these *in vivo* experiments demonstrate that our developed sonogenetic approach significantly reduces immediate blood glucose levels in T2D

mice by enhancing targeted insulin release.

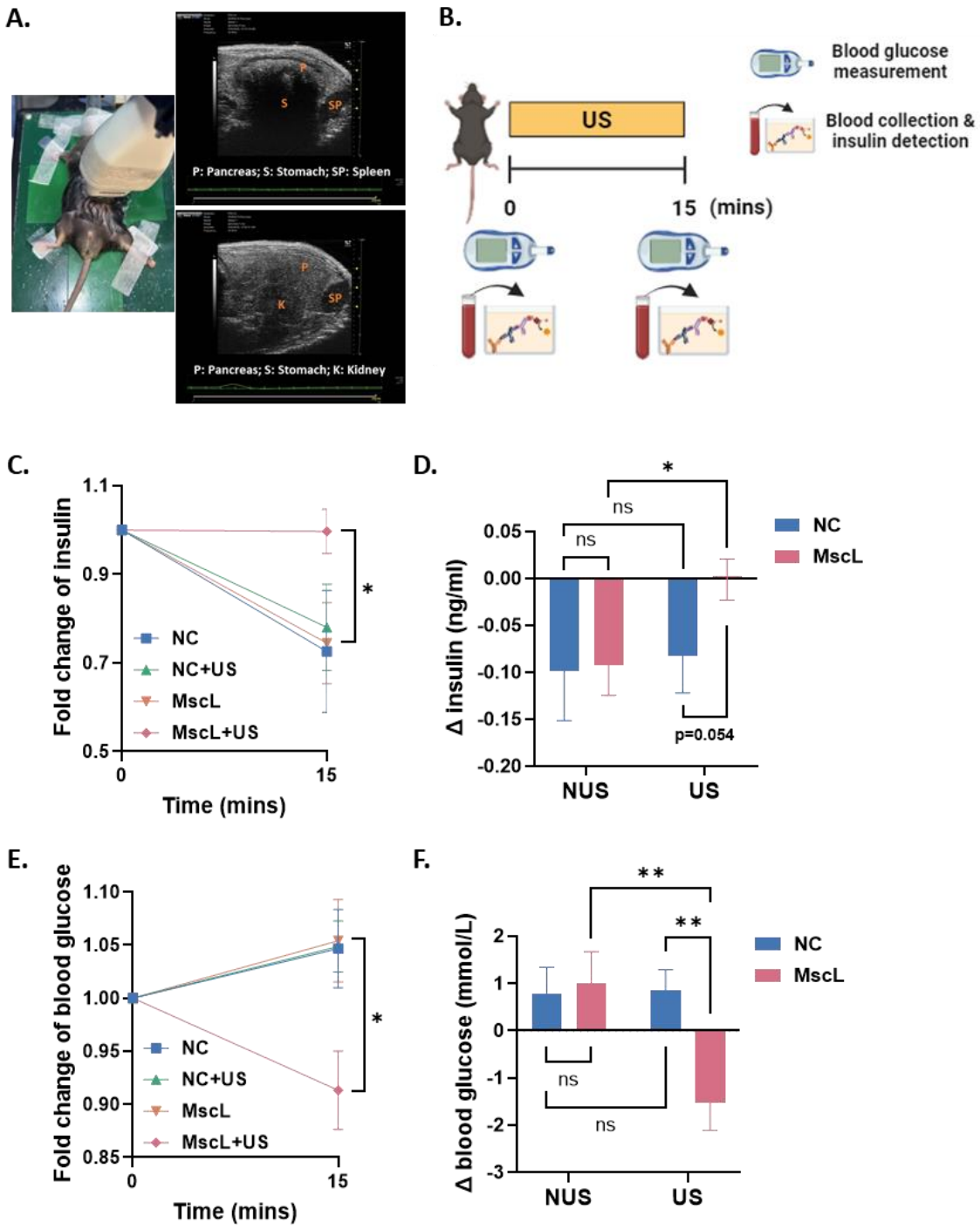

Figure 4.7 Sonogenetics increased the insulin release and decreased the transient blood glucose in the T2D mouse model.

(A) Localization of the pancreatic position in mice. Left: Representative photograph of the pancreatic localization procedure in a mouse. The mouse was maintained under isoflurane

anesthesia, with heart rate monitored via limb leads connected to a platform electrode system. Right: Representative ultrasound images. (B) Schematic illustration of the procedure of the ultrasound treatment. (C) Insulin fold change from 0 (pre-treatment) to 15mins (post-treatment) in each group. Insulin concentration was detected by ELISA, and then normalized to 0 min point. n=6 in NC and NC+US group, n=5 in MscL and MscL+US group. *P<0.05 (MscL+US to MscL), unpaired t test. (D) The increased insulin concentration after treatment in each group was calculated by subtracting the 0 min value from 15 min value. n=6 in NC and NC+US group, n=5 in MscL and MscL+US group. *P<0.05, unpaired t test. (E) Blood glucose fold change from 0 (pre-treatment) to 15 minutes (post-treatment) in each group. Blood glucose was measured by a blood glucose meter, and then normalized to 0 min point. n=6 in NC and NC+US group, n=5 in MscL and MscL+US group. *P<0.05 (MscL+US to MscL), unpaired t test. (F) The increased blood glucose after treatment in each group was calculated by subtracting the 0 min value from 15 min value. n=6 in NC and NC+US group, n=5 in MscL and MscL+US group. **P<0.01, two-way ANOVA. Data are shown as mean±s.e.m.

4.3.3 Sonogenetic treatment significantly improves the symptoms of T2D mice

Impaired glucose tolerance represents a key characteristic of type 2 diabetes. To evaluate whether the developed method alleviates glucose tolerance impairment in the T2D mouse model, intraperitoneal glucose tolerance test (IPGTT) experiments were conducted as follows (Fig.4.8 A). Mice were fasted overnight prior to experimentation. On the following day, procedures were performed under isoflurane anesthesia. At the start of the experiment, an intraperitoneal glucose solution (1 g/kg) was administered, immediately followed by ultrasound stimulation using a 15min ON-30min OFF regimen (all US parameters are consistent with Fig.4.7) for a total duration of 2 hours (Fig.4.8 A). Blood glucose was measured at 0 min (pre-glucose injection), 15 min, 60 min, 105 min, and 120 min using a blood glucose meter (Fig.4.8 A). Due to limitations in mouse blood volume, blood samples for insulin measurement were collected only at 0 min (pre-injection) and 15 min to assess insulin release before and after ultrasound

stimulation (Fig.4.8 A). Consistent with prior findings, MscL+US treatment significantly increased circulating insulin levels (Fig.4.8 B, C). Correspondingly, blood glucose profiles revealed a markedly lower increase in the MscL+US group compared to other T2D mice (Fig.4.8 D). The end-point blood glucose increased from 120min point to 0 min in the MscL+US group was significantly less than other groups (Fig.4.8 E). Further analysis of glucose tolerance by the area under the curve (AUC), which is one of the standard clinical metrics employed to assess diabetic status, demonstrated significant therapeutic efficacy for the MscL+US group (Fig.4.8 F).

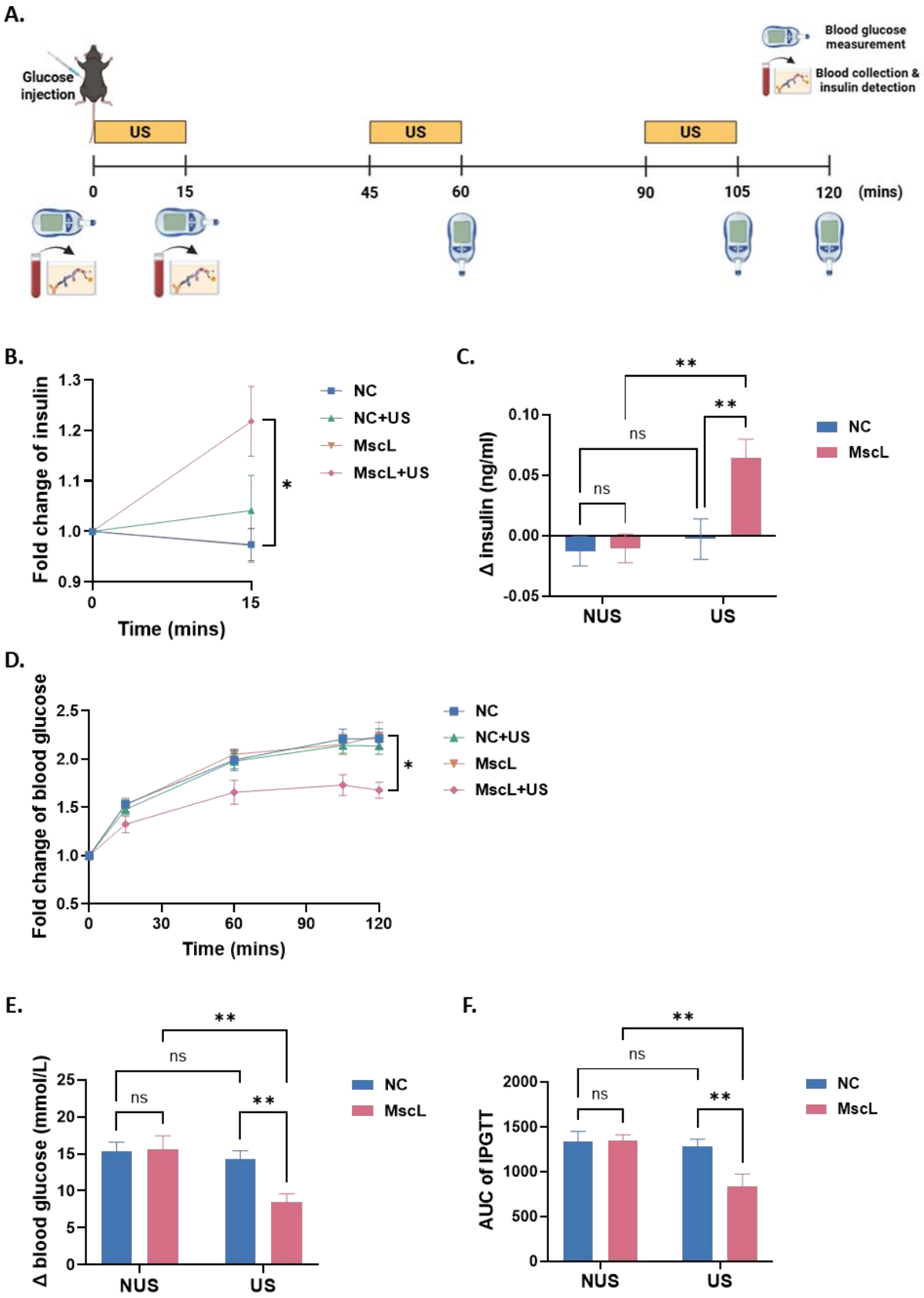
A.
Glucose injection
US
US
US
Blood glucose measurement
Blood collection & insulin detection
0
15
45
60
90
105
120
(mins)
B.
Fold change of insulin
1.3
1.2
1.1
1.0
0.9
0
15
Time (mins)
NC
NC+US
MscL
MscL+US
*
C.
Δ Insulin (ng/ml)
0.10
0.05
0.00
-0.05
**
**
ns
ns
NUS
US
NC
MscL
D.
Fold change of blood glucose
2.5
2.0
1.5
1.0
0.5
0
30
60
90
120
Time (mins)
NC
NC+US
MscL
MscL+US
*
E.
Δ blood glucose (mmol/L)
25
20
15
10
5
0
**
ns
ns
**
NUS
US
NC
MscL
F.
AUC of IPGTT
2000
1500
1000
500
0
**
ns
ns
**
NUS
US
NC
MscL

Figure 4.8 MscL+US treatment alleviates IPGTT performance on T2D mice via specific increased insulin release.

(A) Schematic illustration of the procedure of the ultrasound treatment and the IPGTT test. (B) Insulin fold change from 0 (pre-treatment) to 15 minutes (post-treatment) in each group. Insulin concentration was detected by ELISA, and then normalized to 0 min point. *n*=6 in NC and NC+US group, *n*=5 in MscL and MscL+US group. **P*<0.05 (MscL+US to MscL), unpaired t test. (C) The increased insulin concentration after treatment in each group was calculated by subtracting the 0 min value from 15 min value. *n*=6 in NC and NC+US group, *n*=5 in MscL and MscL+US group. ***P*<0.01, two-way ANOVA. (D) Normalized blood glucose curve during the IPGTT test in each group. Blood glucose was measured by a blood glucose meter, and then normalized to 0 min point. *n*=6 in NC and NC+US group, *n*=5 in MscL and MscL+US group. **P*<0.05 at 60min, 105min, and 120min point (MscL+US to MscL), unpaired t test. (E) The increased blood glucose at the end-point 120min in each group was calculated by subtracting the 0 min value from the 120 min value. *n*=6 in NC and NC+US group, *n*=5 in MscL and MscL+US group. ***P*<0.01, two-way ANOVA. (F) The AUC of the original IPGTT test curve. The baseline is the blood glucose value at 0 min point in each curve. *n*=6 in NC and NC+US group, *n*=5 in MscL and MscL+US group. ***P*<0.01, two-way ANOVA. Data are shown as mean±s.e.m.

Notably, compared to sham-operated healthy (non-diabetic) mice, the MscL+US treatment group exhibited over 60% restoration in insulin release levels, and IPGTT performance also showed a restoration of nearly half (Fig.4.9 A-E). This indicated the therapeutic potential of MscL+US for T2D.

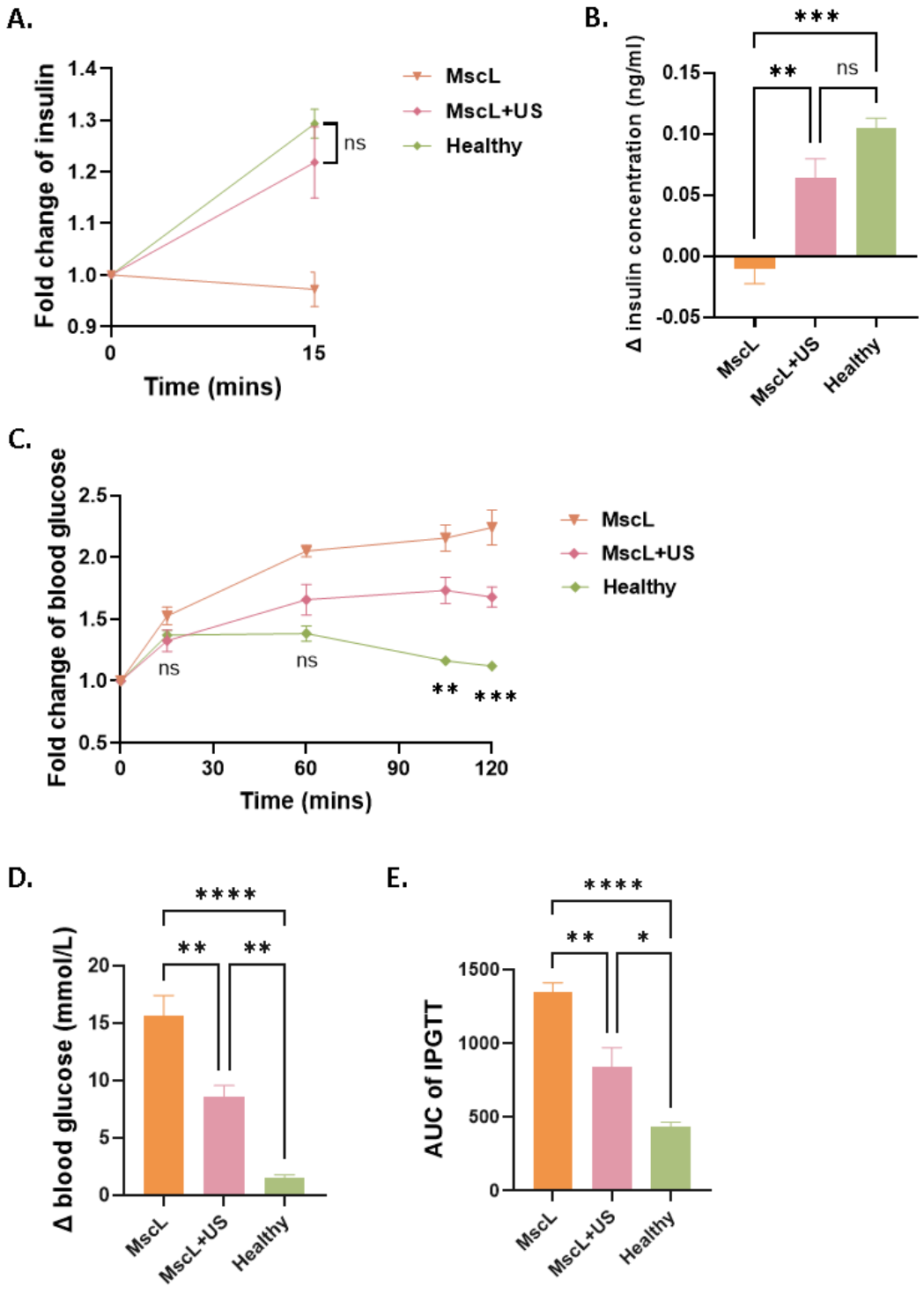

Figure 4.9 Compare IPGTT performance of MscL+US group with sham-operated healthy (non-diabetic) mice.

(A) Insulin fold change from 0 (pre-treatment) to 15mins (post-treatment) in each group. Insulin concentration was detected by ELISA, and then normalized to 0 min point. *n*=5 in MscL and

MscL+US group, *n*=4 in healthy group. *ns,* not significant (MscL+US vs Healthy) by an unpaired t-test. (B) The increased insulin concentration after treatment in each group was calculated by subtracting the 0 min value from 15 min value. *n*=5 in MscL and MscL+US group, *n*=4 in healthy group. ***P*<0.01, ****P*<0.001, one-way ANOVA. (C) Normalized blood glucose curve during the IPGTT test in each group. Blood glucose was measured by a blood glucose meter, and then normalized to 0 min point. *n*=5 in MscL and MscL+US group, *n*=4 in healthy group. *ns*, not significant at 15- and 60-minute points, ***P*<0.01 at 105-min point, ****P*<0.001 at 120-min point (MscL+US vs Healthy), by an unpaired t-test. (D) The increased blood glucose at the end-point 120min in each group was calculated by subtracting the 0 min value from the 120 min value. *n*=5 in MscL and MscL+US group, *n*=4 in healthy group. ***P*<0.01, *****P*<0.0001, one-way ANOVA. (E) The AUC of the original IPGTT test curve. The baseline is the blood glucose value at 0 min point in each curve. *n*=5 in MscL and MscL+US group, *n*=4 in healthy group. **P*<0.05, ***P*<0.01, *****P*<0.0001, one-way ANOVA. Data are shown as mean±s.e.m.

Additionally, a minor increase in insulin release was observed in the NC+US group (non-statistically significant), while no obvious change in blood glucose levels was observed (Fig.4.7 C-F, Fig.4.8 B-F). This finding is consistent with previous reports and further underscores the critical role of specifically enhancing β-cell insulin release for glycemic regulation.

Then, islets were isolated from T2D-MscL/NC mice post-*in vivo* experiments for further validation (Fig.4.10 A). These islets were subjected to 0.7 MPa (due to lesser attenuation *in vitro*) ultrasound for 15 mins, and supernatant was collected for measurement of both insulin and glucagon (the two major islet hormones) in the same supernatant sample (Fig.4.10 A). Results demonstrated that 0.7 MPa ultrasound stimulation significantly increased insulin release from MscL-islets without affecting glucagon release (Fig.4.10 B, C). This suggests that β-cell-specific modification with MscL enables ultrasound-triggered, spatially selective modulation of insulin release at defined pressures, without perturbing glucagon release from adjacent α-cells within the

islet.

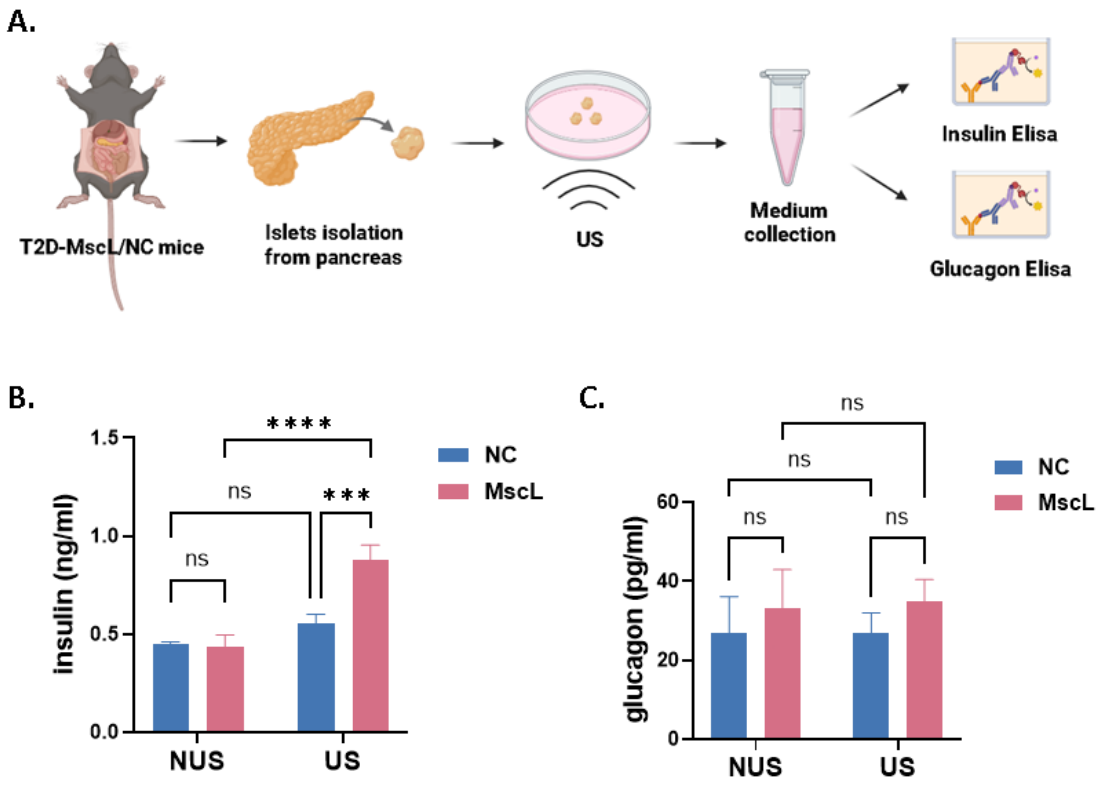

Figure 4.10 Validation of MscL expression in β-Cells selectively enhances insulin release without affecting glucagon release upon ultrasound stimulation of pancreatic islets.

(A) Schematic illustration of*ex vivo* experiment. Insulin (B) and glucagon (C) concentrations in the medium after US treatment/sham operation for 15mins was measured by ELISA. n=5 in each group. ***P<0.001, ****P<0.0001, two-way ANOVA. Data are shown as mean±s.e.m.

4.3.4 Biosafety examination of sonogenetic T2D treatment method

This sonogenetics-based therapy for type 2 diabetes demonstrates significant potential for future clinical translation. Consequently, evaluating the safety profile of this approach is essential, including the safety of MscL overexpression in cells and the safety of ultrasound stimulation. We evaluated the safety of the sonogenetics method both *in vitro* and *in vivo*. First, in *in vitro* experiments, the proliferative activity of cells following MscL transfection was assessed by MTS assay. The results indicated that the

proliferative activity of MscL-cells was unaffected compared to NC-cells (Fig.4.11 A). Also, no significant differences were observed in the resting membrane potential between the two cell groups (Fig.4.11 B). Analysis of intracellular insulin stores via immunofluorescence revealed no significant difference in insulin content between the groups (Fig.4.11 C, D). It demonstrated that MscL overexpression does not impair insulin synthesis and storage in β-cells. In *in vivo* experiment, pancreatic tissue from mice administered the MscL virus exhibited no morphological differences compared to NC-mice (Fig.4.11 E). Random and fasting blood glucose levels in MscL-expressing mice were also comparable to those in NC-mice (Fig.4.11 F, G). This suggested that MscL expression in murine pancreatic β-cells did not compromise their function.

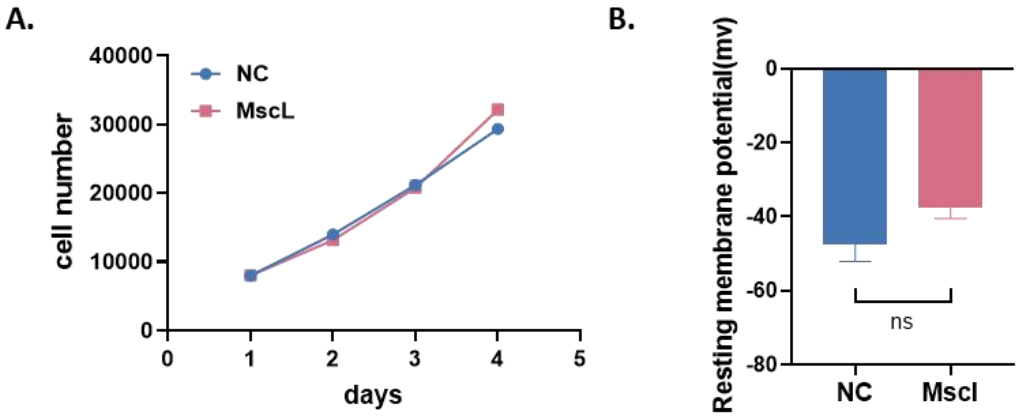
A.
40000
30000
20000
10000
0
cell number
NC
MscL
0
1
2
3
4
5
days
B.
Resting membrane potential(mv)
0
-20
-40
-60
-80
ns
NC
Mscl

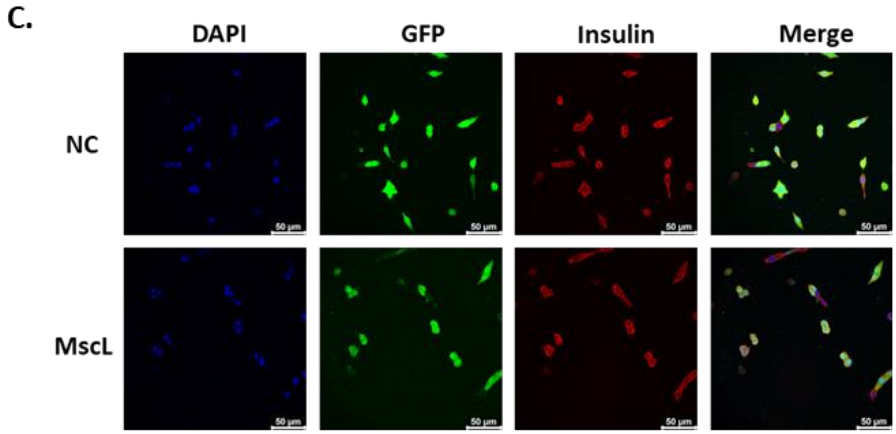
C.
DAPI
GFP
Insulin
Merge
NC
MscL

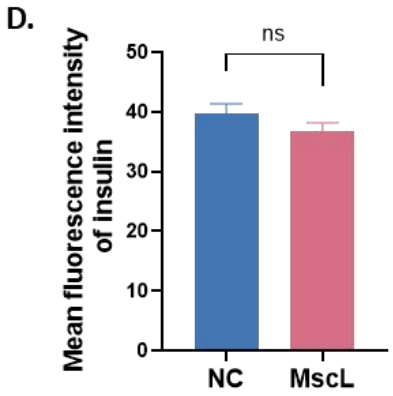
D.
Mean fluorescence intensity of insulin
ns
50
40
30
20
10
0
NC
MscL

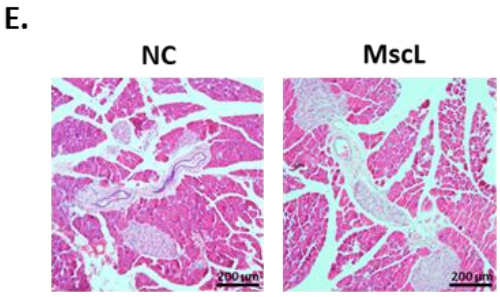
E.
NC
MscL

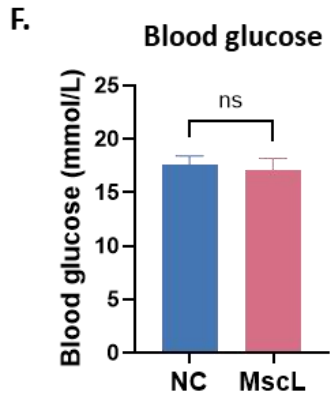
F.
Blood glucose
Blood glucose (mmol/L)
ns
25
20
15
10
5
0
NC
MscL

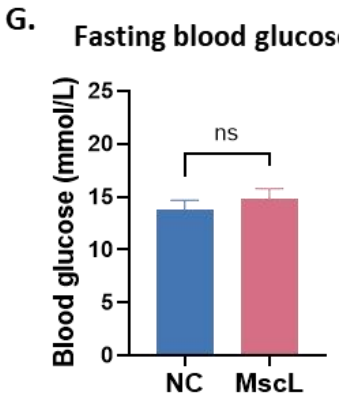
G.
Fasting blood glucose
Blood glucose (mmol/L)
ns
25
20
15
10
5
0
NC
MscL

Figure 4.11 Safety evaluation of MscL expression.

(A) Cell proliferation of NC-RINm5F and MscL-RINm5F cells in four consecutive days. Cell number was measured by the MTS assay. *n*=3 in each group. (B) Resting membrane potential of NC-RINm5F cells and MscL-RINm5F cells. *n*=4 in each group. ns, no significant in unpaired t-test. (C) Representative images of insulin (shown as red fluorescence) in NC-RINm5F cells and MscL-RINm5F cells by immunofluorescence. (D) Quantification of the mean fluorescence intensity of insulin in (C). *n*=10 in each group. ns, no significant in unpaired t-test. (E) Representative images of hematoxylin and eosin (H&E) staining of the pancreas from NC-mice and MscL-mice. Random blood glucose (F) and fasting blood glucose (G) in NC-mice and MscL-mice. *n*=8-10 in NC group, *n*=6-10 in MscL group. ns, no significant in unpaired t-test.

Beyond confirming that MscL expression has no adverse effects on β-cell viability or function, the impact of ultrasound treatment was also examined. *In vitro*, apoptosis in islet cells following ultrasound stimulation was assessed using immunofluorescence, indicated by cleaved-caspase 3. Results showed no significant apoptosis, regardless of ultrasound exposure (Fig.4.12 A). In the mouse model, animals exhibited normal behavior for several days post-ultrasound treatment (data not shown). Body weight measured on day 5 post-treatment showed no change compared to pre-treatment values (Fig.4.12 B). Finally, morphological examination of the pancreatic tissue revealed no apparent damage after ultrasound treatment (Fig.4.12 C). Collectively, these data indicate that the ultrasound protocol employed in this study is well-tolerated and exhibits a favorable biosafety profile.

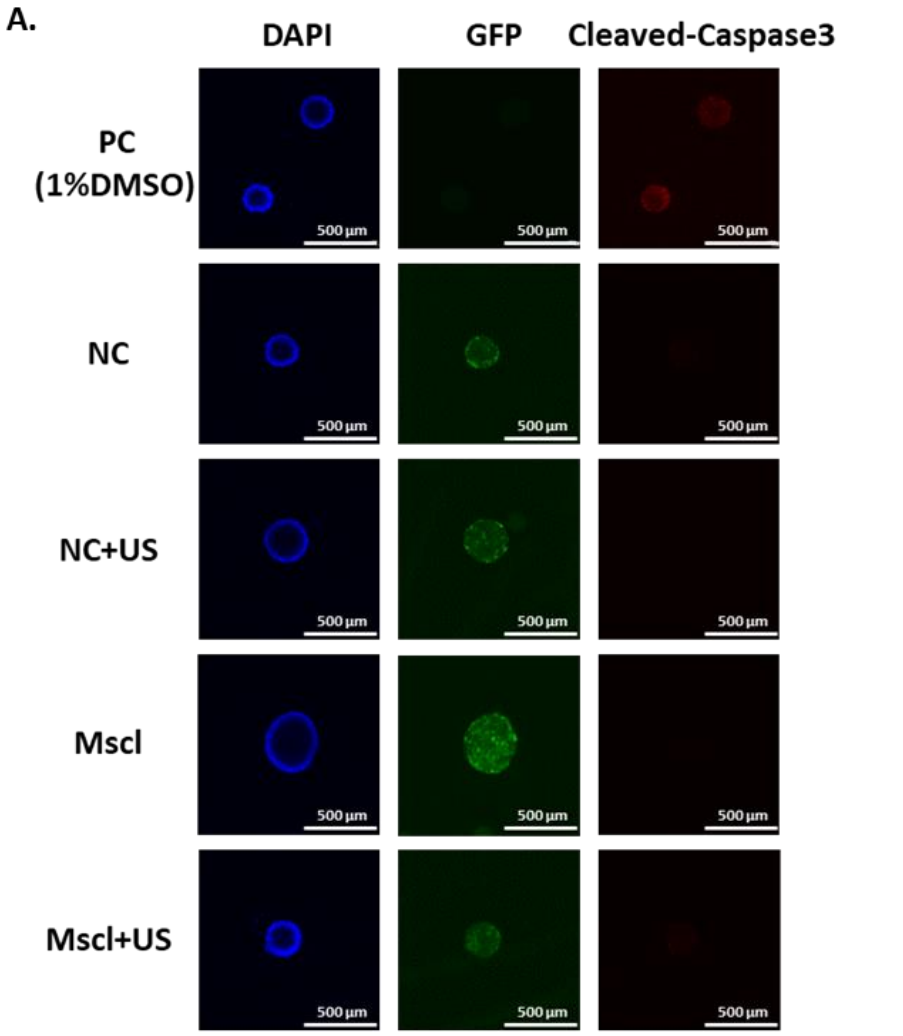
A.
DAPI
GFP
Cleaved-Caspase3
PC
(1%DMSO)
NC
NC+US
Mscl
Mscl+US
500 μm

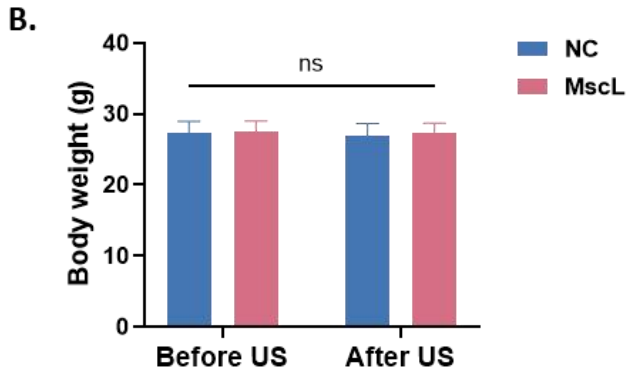
B.
Body weight (g)
40
30
20
10
0
ns
NC
MscL
Before US
After US

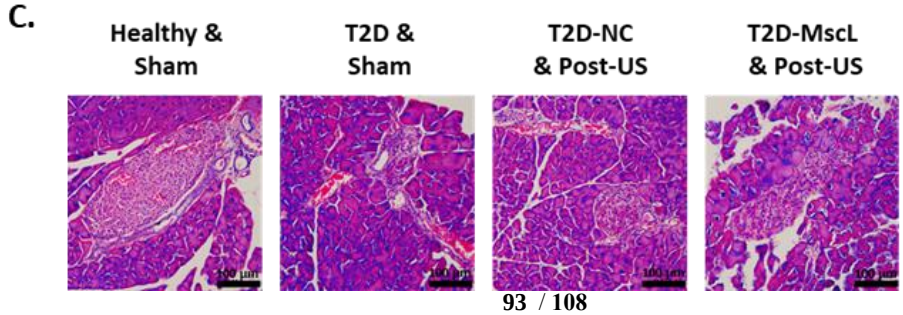
C.
Healthy &
Sham
T2D &
Sham
T2D-NC
& Post-US
T2D-MscL
& Post-US

Figure 4.12 Safety evaluation of sonogenetics treatment.

(A) Representative images of apoptosis of islets after sham/ultrasound stimulations at 0.7MPa for 15mins in each group, indicated by cleaved-caspase 3 marker (the right column). 1%DMSO added in WT islets was used as a positive control (the top row). (B) Body weight of NC-mice and MscL-mice before and after 5 days of US treatment. n=4 in each group. ns, no significant difference in two-way ANOVA. (C) Representative images of H&E staining of the pancreas in each group. Data are shown as mean±s.e.m.

4.4 Conclusion

This study presents the application of sonogenetics-based spatiotemporally precise control of insulin release and ultimately glycemic modulation in type 2 diabetic mice. Our *in vitro* experiments demonstrated that MscL overexpression significantly sensitizes the β cells to ultrasound stimulation, thereby potentiating Ca^{2+} influx and subsequent insulin release in β-cells. This holds particular relevance for type 2 diabetes management, as patients typically exhibit impaired glucose-dependent insulin secretion. *In vivo* validation confirmed that specific stimulation of β-cells effectively controlled hyperglycemia in diabetic mice through enhanced insulin release, while maintaining normal activity patterns in neighboring endocrine cells (e.g., glucagon-secreting α-cells). Besides, this approach demonstrated a satisfactory safety profile. In conclusion, this strategy provides a novel, non-invasive, and clinically viable therapeutic option for type 2 diabetes.

Chapter 5: Discussion and future perspectives

Existing evidence supports ultrasound-modulated insulin release in pancreatic β-cells [12-14], laying the foundation and hope for ultrasound-based diabetes therapy. Nonetheless, the development of specific therapeutic methods and significant efficacy in the diabetic mouse model remains to be demonstrated. Prior investigations have primarily employed non-specific pancreatic ultrasound stimulation. Crucially, the pancreas contains multiple endocrine cell populations - including insulin-antagonizing glucagon-secreting islet α-cells and acinar cells (constituting the pancreatic cellular majority) - that reside in intimate spatial association with islet β-cells [43, 44]. This anatomical proximity renders conventional ultrasound approaches incapable of cellular discrimination, potentially inducing counterproductive α-cell activation that obscures glucose-regulatory outcomes. This suggests that β-cell-specific targeting represents the critical determinant for achieving precise ultrasound-mediated glycemic control.

The pivotal advancement of the first MBs-based study lies in demonstrating that ultrasound-targeted β-cell activation not only enhances insulin release but also effectively mitigates acute hyperglycemic spikes in vivo [Refer to Chapter 3]. This achievement validates the feasibility of selective β-cell modulation for glucose management and provides direct experimental evidence supporting the potential of ultrasound-based strategies for future diabetes intervention [Refer to Chapter 3]. However, this study used a transplantation and MBs-based idealized model, the inherent limitations of MBs (e.g., instability and challenges in systemic delivery) constrained its *in vivo* investigation and further clinical translation. Thus, another strategy which could circumvent the MBs to locally enhance the ultrasound effect was investigated. Most importantly, sonogenetics has better cell-specific ability. By utilizing the sonogenetics-based treatment, we achieved truly non-invasive diabetes management in the T2D mice model, this is the first study that using autologous islet cells for the direct ultrasound treatment of diabetes [Refer to Chapter 4].

Gene therapy and cell transplantation have garnered significant research attention and

development in current diabetes treatment [30, 152]. Significantly, physical control technologies have been used to regulate gene expression systems in a controlled manner [100]. Pioneering studies have explored physical cues - such as light [68], magnetism [153], temperature [154, 155], mechanical force [156], and electricity [157] - triggered insulin expression or release from transplanted engineered cells for diabetes treatment. In such approaches, genetically modified cells are transplanted to the mice to respond to the physical cues to produce insulin, thereby enabling glycemic regulation. Although complex gene editing and transplantation may be necessary for type 1 diabetes management, more type 2 diabetes patients, which proportion of around 90% retain functional β-cells, possess the capacity to be directly activated by ultrasound to stimulate insulin release due to their physiological properties [12]. Our study aims to develop a new strategy for non-invasive triggering of on-demand insulin release through endogenous pancreatic islet cells for T2D patients, eliminating the need for exogenous cell transplantation while maintaining precise spatiotemporal control over glucose homeostasis. This provides a simpler, safer, and more convenient therapeutic alternative for certain diabetic patient populations.

To better evaluate the clinical therapeutic potential, we also compare our sonogenetics approach with the non-diabetic mice (healthy mice) [Refer to Chapter 4]. Encouragingly, MscL+US-treated T2D mice restored more than half of their insulin secretion capacity compared to batch-matched T2D control mice and non-diabetic mice. This aligns with expectations, as our established T2D mouse model mimics partial islet destruction (via STZ injection), resulting in reduced islet number and compromised function compared to healthy mice. Consequently, the inability to fully restore insulin secretion to healthy mouse levels is reasonable. In the IPGTT experiment, although the MscL+US group initially showed blood glucose suppression due to transient insulin release, the results still exhibited characteristics of insulin resistance (i.e., the curve failed to decline rapidly in later stages, and blood glucose at 2 hours did not return to near-baseline levels). This is because our T2D model also mimics insulin resistance (induced by long-term high-fat diet feeding), which cannot be overcome by increased

insulin alone. For this issue, subsequent therapeutic applications could incorporate insulin-sensitizing agents in a combination therapy regimen. Additionally, we propose that a more prolonged ultrasound treatment protocol (up to several months) may further ameliorate insulin resistance in the T2D mouse model, representing another potentially effective therapeutic approach.

Although our sonogenetics method involves a single intraperitoneal injection, this minimally invasive procedure is clinically well-tolerated and routine. First, it represents a systemic delivery method which does not require complex localized targeting and can be seamlessly replaced by standard intravenous or intramuscular injections—leveraging its simplicity, low risk, and established clinical adoption. Second, the AAV vector enables sustained transgene expression for months to years following a single administration, permitting long-term repeated non- invasive ultrasound treatments. Its non-integrating nature also ensures safety while maintaining durable expression.

In both of two studies, anesthesia was necessary in murine models due to the uncontrollable behavior in conscious rodent models hinders the progress of the treatment, thus the observed results inevitable incorporate anesthesia-induced effects, including isoflurane-associated hyperglycemia and suppressed insulin secretion [147] (despite standardized anesthesia protocols being implemented across all subjects in this study to maintain single-variable conditions and minimize confounding impacts) [Refer to Chapter 3 and Chapter 4]. While this methodological consideration poses no challenges for future human clinical applications, subsequent investigations employing conscious-state models may be essential to better simulate therapeutic efficacy in clinical settings.

The development of wearable ultrasound patch technologies may provide an optimal solution [158]. Most importantly, the integration of patch-based ultrasound systems could further enhance practicality by enabling ambulatory glucose management, effectively eliminating the need for hospital-based treatments and allowing seamless integration into daily glycemic control regimens [159]. The approach developed in this

project together with the wearable ultrasound patch technologies will be similar to insulin pump therapy, yet distinguishes itself through non-invasive administration and sustained available duration, thereby addressing the patient discomfort and compliance issues associated with percutaneous needle insertion and the inconvenience of the frequent exogenous insulin replenishment.

Further research and development efforts remain imperative to optimize these methodologies. For example, developing ultrasound-amplifying materials with enhanced *in vivo* stability and efficient β-cell targeting by systemic delivery. Second, the selection of optimal ion channel targets. Although this study employed MscL to validate the methodology of sonogenetics, the efficacy of alternative mechanosensitive calcium ion channels - such as the Piezo protein family and transient receptor potential (TRP) channel family - requires comparative evaluation in this context to identify optimal candidates. Finally, the correlation between acoustic parameters and the quantity of insulin release also necessitates further investigation for personalized dosage guidance. These represent critical research priorities for advancing these technologies toward practical implementation.

Nevertheless, this thesis demonstrated exciting effectiveness and considerable clinical value of these approaches for type 2 diabetes therapies, establishing a novel framework for non-pharmacological diabetes management.

Reference

1. Association, A.D., *Diagnosis and classification of diabetes mellitus.* Diabetes care, 2013. **36**(Supplement_1): p. S67-S74.
2. Cho, N.H., et al., *IDF Diabetes Atlas: Global estimates of diabetes prevalence for 2017 and projections for 2045.* Diabetes research and clinical practice, 2018. **138**: p. 271-281.
3. Gregg, E.W., N. Sattar, and M.K. Ali, *The changing face of diabetes complications.* The lancet Diabetes & endocrinology, 2016. **4**(6): p. 537-547.
4. Petersmann, A., et al., *Definition, classification and diagnosis of diabetes mellitus.* Experimental and Clinical Endocrinology & Diabetes, 2019. **127**(S 01): p. S1-S7.
5. *9. Pharmacologic approaches to glycemic treatment: standards of care in diabetes—2024.* Diabetes Care, 2024. **47**(Supplement_1): p. S158-S178.
6. Sorli, C. and M.K. Heile, *Identifying and meeting the challenges of insulin therapy in type 2 diabetes.* Journal of multidisciplinary healthcare, 2014: p. 267-282.
7. Silver, B., et al., *EADSG guidelines: insulin therapy in diabetes.* Diabetes therapy, 2018. **9**(2): p. 449-492.
8. Morino, S., et al., *Mild electrical stimulation with heat shock ameliorates insulin resistance via enhanced insulin signaling.* PloS one, 2008. **3**(12): p. e4068.
9. Ponomareva, S., et al., *Magnetic particles for triggering insulin release in INS-1E cells subjected to a rotating magnetic field.* Nanoscale, 2022. **14**(36): p. 13274-13283.
10. Reinbothe, T.M., et al., *Optogenetic control of insulin secretion in intact pancreatic islets with β-cell-specific expression of Channelrhodopsin-2.* Islets, 2014. **6**(1): p. e28095.
11. Hou, X., L. Liu, and L. Sun, *Precise modulation of cell activity using sono-responsive nano-transducers.* Biomaterials, 2025. **314**: p. 122857.
12. Castellanos, I.S., et al., *Ultrasound stimulation of insulin release from pancreatic beta cells as a potential novel treatment for type 2 diabetes.* Ultrasound in medicine & biology, 2017. **43**(6): p. 1210-1222.
13. Singh, T., et al., *Therapeutic ultrasound-induced insulin release in vivo.* Ultrasound in Medicine & Biology, 2020. **46**(3): p. 639-648.
14. Suarez-Castellanos, I., et al., *Effect of therapeutic ultrasound on the release of insulin, glucagon, and alpha-amylase from ex vivo pancreatic models.* Journal of Ultrasound in Medicine, 2021. **40**(12): p. 2709-2719.
15. Ibsen, S., et al., *Sonogenetics is a non-invasive approach to activating neurons in Caenorhabditis elegans.* Nature communications, 2015. **6**(1): p. 8264.
16. Liu, T., et al., *Sonogenetics: recent advances and future directions.* Brain stimulation, 2022. **15**(5): p. 1308-1317.
17. Tang, J., et al., *Recent advancement of sonogenetics: a promising noninvasive cellular manipulation by ultrasound.* Genes & Diseases, 2024. **11**(5): p. 101112.
18. Perozo, E., et al., *Open channel structure of MscL and the gating mechanism of*

mechanosensitive channels. Nature, 2002. **418**(6901): p. 942-948.
19. Sukharev, S.I., et al., *A large-conductance mechanosensitive channel in E. coli encoded by mscL alone.* Nature, 1994. **368**(6468): p. 265-268.
20. Ye, J., et al., *Ultrasonic control of neural activity through activation of the mechanosensitive channel MscL.* Nano letters, 2018. **18**(7): p. 4148-4155.
21. Qiu, Z., et al., *Targeted neurostimulation in mouse brains with non-invasive ultrasound*. Cell reports, 2020. **32**(7).
22. Xian, Q., et al., *Modulation of deep neural circuits with sonogenetics.* Proceedings of the National Academy of Sciences, 2023. **120**(22): p. e2220575120.
23. Kharroubi, A.T. and H.M. Darwish, *Diabetes mellitus: The epidemic of the century.* World journal of diabetes, 2015. **6**(6): p. 850.
24. Pleus, S., et al., *Definition, classification, diagnosis and differential diagnosis of diabetes mellitus: update 2023*. Experimental and Clinical Endocrinology & Diabetes, 2024. **132**(03): p. 112-124.
25. Ta, S., *Diagnosis and classification of diabetes mellitus*. Diabetes care, 2014. **37**(1): p. 81-90.
26. Wilkin, T., *The accelerator hypothesis: a review of the evidence for insulin resistance as the basis for type I as well as type II diabetes*. International Journal of obesity, 2009. **33**(7): p. 716-726.
27. Vermeulen, I., et al., *Contribution of antibodies against IA-2β and zinc transporter 8 to classification of diabetes diagnosed under 40 years of age.* Diabetes care, 2011. **34**(8): p. 1760-1765.
28. *Introduction and methodology: Standards of Care in Diabetes—2024*. 2024, American Diabetes Association. p. S1-S4.
29. *16. Diabetes care in the hospital: standards of care in diabetes—2024.* Diabetes Care, 2024. **47**(Supplement_1): p. S295-S306.
30. Tan, S.Y., et al., *Type 1 and 2 diabetes mellitus: A review on current treatment approach and gene therapy as potential intervention.* Diabetes & metabolic syndrome: clinical research & reviews, 2019. **13**(1): p. 364-372.
31. Jaap, A., *Liraglutide and cardiovascular outcomes in type 2 diabetes.* New England Journal of Medicine, 2016. **375**(4): p. 311-322.
32. Zinman, B., et al., *Empagliflozin, cardiovascular outcomes, and mortality in type 2 diabetes.* New england journal of medicine, 2015. **373**(22): p. 2117-2128.
33. Rendell, M.S., N.B. Glazer, and Z. Ye, *Combination therapy with pioglitazone plus metformin or sulfonylurea in patients with type 2 diabetes: influence of prior antidiabetic drug regimen.* Journal of Diabetes and its Complications, 2003. **17**(4): p. 211-217.
34. Aghazadeh, Y. and M.C. Nostro, *Cell therapy for type 1 diabetes: current and future strategies.* Current diabetes reports, 2017. **17**(6): p. 37.
35. Xiao, X. and G.K. Gittes, *Concise review: new insights into the role of macrophages in β-cell proliferation.* Stem cells translational medicine, 2015. **4**(6): p. 655-658.
36. Zang, L., et al., *Mesenchymal stem cell therapy in type 2 diabetes mellitus.* Diabetology & metabolic syndrome, 2017. **9**(1): p. 36.

37. Zang, L., et al., *Efficacy and safety of umbilical cord-derived mesenchymal stem cells in Chinese adults with type 2 diabetes: a single-center, double-blinded, randomized, placebo-controlled phase II trial.* Stem Cell Research & Therapy, 2022. **13**(1): p. 180.
38. Callejas, D., et al., *Treatment of diabetes and long-term survival after insulin and glucokinase gene therapy.* Diabetes, 2013. **62**(5): p. 1718-1729.
39. Jaén, M.L., et al., *Long-term efficacy and safety of insulin and glucokinase gene therapy for diabetes: 8-year follow-up in dogs.* Molecular Therapy Methods & Clinical Development, 2017. **6**: p. 1-7.
40. Han, J., et al., *Remission of diabetes by insulin gene therapy using a hepatocyte-specific and glucose-responsive synthetic promoter.* Molecular Therapy, 2011. **19**(3): p. 470-478.
41. Yoon, J.-W. and H.-S. Jun, *Recent advances in insulin gene therapy for type 1 diabetes*. Trends in molecular medicine, 2002. **8**(2): p. 62-68.
42. Kerper, N., S. Ashe, and M. Hebrok, *Pancreatic β-cell development and regeneration.* Cold Spring Harbor perspectives in biology, 2022. **14**(5): p. a040741.
43. Lacy, P.E., *The pancreatic beta cell: structure and function.* New England Journal of Medicine, 1967. **276**(4): p. 187-195.
44. Da Silva Xavier, G., *The cells of the islets of Langerhans.* Journal of clinical medicine, 2018. **7**(3): p. 54.
45. Benabid, A.-L., et al., *Combined (thalamotomy and stimulation) stereotactic surgery of the VIM thalamic nucleus for bilateral Parkinson disease.* Stereotactic and functional neurosurgery, 1987. **50**(1-6): p. 344-346.
46. Shealy, C.N., J.T. Mortimer, and J.B. Reswick, *Electrical inhibition of pain by stimulation of the dorsal columns: preliminary clinical report.* Anesthesia & Analgesia, 1967. **46**(4): p. 489-491.
47. Benabid, A.L., et al., *Long-term suppression of tremor by chronic stimulation of the ventral intermediate thalamic nucleus.* The Lancet, 1991. **337**(8738): p. 403-406.
48. Deer, T.R., et al., *A systematic literature review of spine neurostimulation therapies for the treatment of pain.* Pain medicine, 2020. **21**(7): p. 1421-1432.
49. Lefaucheur, J.-P., et al., *Evidence-based guidelines on the therapeutic use of transcranial direct current stimulation (tDCS).* Clinical neurophysiology, 2017. **128**(1): p. 56-92.
50. Peckham, P.H. and J.S. Knutson, *Functional electrical stimulation for neuromuscular applications.* Annu. Rev. Biomed. Eng., 2005. **7**(1): p. 327-360.
51. Miyamoto, T., et al., *Effect of percutaneous electrical muscle stimulation on postprandial hyperglycemia in type 2 diabetes*. Diabetes research and clinical practice, 2012. **96**(3): p. 306-312.
52. Sanchez, M.J., et al., *Effects of neuromuscular electrical stimulation on glycemic control: a systematic review and meta-analysis.* Frontiers in Endocrinology, 2023. **14**: p. 1222532.
53. Rubinowicz-Zasada, M., et al., *The combined effect of neuromuscular electrical*

stimulation and insulin therapy on Glycated hemoglobin concentrations, lipid profiles and hemodynamic parameters in patients with Type-2-diabetes and hemiplegia related to ischemic stroke: a pilot study. International Journal of Environmental Research and Public Health, 2021. **18**(7): p. 3433.

54. Lebovitz, H.E., *Interventional treatment of obesity and diabetes: an interim report on gastric electrical stimulation.* Reviews in Endocrine and Metabolic Disorders, 2016. **17**(1): p. 73-80.
55. Li, S., et al., *Chronic intestinal electrical stimulation improves glucose intolerance and insulin resistance in diet-induced obesity rats.* Obesity, 2017. **25**(6): p. 1061-1068.
56. Yin, J., et al., *Vagal nerve stimulation for glycemic control in a rodent model of type 2 diabetes.* Obesity surgery, 2019. **29**(9): p. 2869-2877.
57. Payne, S.C., et al., *Differential effects of vagus nerve stimulation strategies on glycemia and pancreatic secretions.* Physiological Reports, 2020. **8**(11): p. e14479.
58. Kufaishi, H., et al., *Possible Glycemic Effects of Vagus Nerve Stimulation Evaluated by Continuous Glucose Monitoring in People with Diabetes and Autonomic Neuropathy: A Randomized, Sham-Controlled Trial.* Diabetes Technology & Therapeutics, 2025. **27**(1): p. 52-59.
59. Guyot, M., et al., *Pancreatic nerve electrostimulation inhibits recent-onset autoimmune diabetes.* Nature biotechnology, 2019. **37**(12): p. 1446-1451.
60. Luo, Y.-C., et al., *An integrated systematic approach for investigating microcurrent electrical nerve stimulation (MENS) efficacy in STZ-induced diabetes mellitus.* Life Sciences, 2021. **279**: p. 119650.
61. Hamblin, M.R., *Mechanisms and applications of the anti-inflammatory effects of photobiomodulation.* AIMS biophysics, 2017. **4**(3): p. 337.
62. Chen, A.C., et al., *Low-level laser therapy activates NF-kB via generation of reactive oxygen species in mouse embryonic fibroblasts.* PloS one, 2011. **6**(7): p. e22453.
63. Brouwer, A., et al., *Effects of light therapy on mood and insulin sensitivity in patients with type 2 diabetes and depression: results from a randomized placebo-controlled trial.* Diabetes Care, 2019. **42**(4): p. 529-538.
64. Salehpour, F., et al., *Therapeutic potential of intranasal photobiomodulation therapy for neurological and neuropsychiatric disorders: a narrative review.* Reviews in the Neurosciences, 2020. **31**(3): p. 269-286.
65. Maharwal, N., R. Shrivastava, and S.K. Majumder, *Insight into Optogenetics for Diabetes Management.* ACS Synthetic Biology, 2025. **14**(5): p. 1324-1335.
66. Deng, X., et al., *Optogenetic therapeutic strategies for diabetes mellitus.* Journal of Diabetes, 2024. **16**(6): p. e13557.
67. Kushibiki, T., et al., *Optogenetic control of insulin secretion by pancreatic β-cells in vitro and in vivo.* Gene therapy, 2015. **22**(7): p. 553-559.
68. Mansouri, M., et al., *Smart-watch-programmed green-light-operated percutaneous control of therapeutic transgenes.* Nature communications, 2021. **12**(1): p. 3388.

69. Rössger, K., G. Charpin-El-Hamri, and M. Fussenegger, *A closed-loop synthetic gene circuit for the treatment of diet-induced obesity in mice.* Nature communications, 2013. **4**(1): p. 2825.
70. Carter, C.S., et al., *Exposure to static magnetic and electric fields treats type 2 diabetes.* Cell metabolism, 2020. **32**(4): p. 561-574. e7.
71. Pascual-Leone, A., V. Walsh, and J. Rothwell, *Transcranial magnetic stimulation in cognitive neuroscience–virtual lesion, chronometry, and functional connectivity.* Current opinion in neurobiology, 2000. **10**(2): p. 232-237.
72. Lefaucheur, J.-P., et al., *Evidence-based guidelines on the therapeutic use of repetitive transcranial magnetic stimulation (rTMS).* Clinical neurophysiology, 2014. **125**(11): p. 2150-2206.
73. Kistenmacher, A., et al., *Persistent blood glucose reduction upon repeated transcranial electric stimulation in men.* Brain Stimulation, 2017. **10**(4): p. 780-786.
74. Wardzinski, E.K., et al., *Double transcranial direct current stimulation of the brain increases cerebral energy levels and systemic glucose tolerance in men.* Journal of Neuroendocrinology, 2019. **31**(4): p. e12688.
75. Yu, B., et al., *A static magnetic field improves iron metabolism and prevents high-fat-diet/streptozocin-induced diabetes.* The Innovation, 2021. **2**(1).
76. Chen, X., et al., *Repetitive transcranial magnetic stimulation elicits weight loss and improved insulin sensitivity in type 2 diabetic rats.* Animal Models and Experimental Medicine, 2025. **8**(4): p. 739-749.
77. Hildebrandt, B., et al., *The cellular and molecular basis of hyperthermia.* Critical reviews in oncology/hematology, 2002. **43**(1): p. 33-56.
78. Gupte, A.A., et al., *Heat treatment improves glucose tolerance and prevents skeletal muscle insulin resistance in rats fed a high-fat diet.* Diabetes, 2009. **58**(3): p. 567-578.
79. Kondo, T., et al., *Hyperthermia with mild electrical stimulation protects pancreatic β-cells from cell stresses and apoptosis.* Diabetes, 2012. **61**(4): p. 838-847.
80. Kondo, T., et al., *Activation of heat shock response to treat obese subjects with type 2 diabetes: a prospective, frequency-escalating, randomized, open-label, triple-arm trial.* Scientific reports, 2016. **6**(1): p. 35690.
81. Kondo, T., et al., *Mild electrical stimulation with heat shock reduces visceral adiposity and improves metabolic abnormalities in subjects with metabolic syndrome or type 2 diabetes: randomized crossover trials.* EBioMedicine, 2014. **1**(1): p. 80-89.
82. Hooper, P.L., *Hot-tub therapy for type 2 diabetes mellitus*. New England Journal of Medicine, 1999. **341**(12): p. 924-925.
83. James, T.J., et al., *The effect of repeated hot water immersion on insulin sensitivity, heat shock protein 70, and inflammation in individuals with type 2 diabetes mellitus.* American Journal of Physiology-Endocrinology and Metabolism, 2023. **325**(6): p. E755-E763.
84. Pettit-Mee, R.J., *The Role of Heat Shock Protein 72 in Endothelial Insulin Resistance in Type 2 Diabetes: Using Passive Heat Therapy to Improve Endothelial*

Insulin Responsiveness. 2022, University of Missouri-Columbia.
85. Gerazova-Efremova, K., S. Dinevska-Kjovkarovska, and B. Miova, *Heat-shock protein 70–mediated heat preconditioning attenuates hepatic carbohydrate and oxidative disturbances in rats with type 1 diabetes.* Canadian Journal of Diabetes, 2019. **43**(5): p. 345-353.
86. Zhang, D., et al., *Multi-frequency therapeutic ultrasound: A review.* Ultrasonics sonochemistry, 2023. **100**: p. 106608.
87. Liang, W., et al., *Low-intensity pulsed ultrasound: a physical stimulus with immunomodulatory and anti-inflammatory potential.* Annals of Biomedical Engineering, 2024. **52**(8): p. 1955-1981.
88. Bachu, V.S., et al., *High-intensity focused ultrasound: a review of mechanisms and clinical applications.* Annals of biomedical engineering, 2021. **49**(9): p. 1975-1991.
89. Han, B., et al., *The advance of ultrasound-enabled diagnostics and therapeutics.* Journal of Controlled Release, 2024. **375**: p. 1-19.
90. Bader, K.B., et al., *Overview of therapeutic ultrasound applications and safety considerations: 2024 update.* Journal of Ultrasound in Medicine, 2025. **44**(3): p. 381-433.
91. Leinenga, G., et al., *Ultrasound treatment of neurological diseases—current and emerging applications.* Nature Reviews Neurology, 2016. **12**(3): p. 161-174.
92. Jiang, X., et al., *A review of low-intensity pulsed ultrasound for therapeutic applications.* IEEE Transactions on Biomedical Engineering, 2018. **66**(10): p. 2704-2718.
93. Li, J., et al., *Ultrasound-mediated diagnostic imaging and advanced treatment with multifunctional micro/nanobubbles.* Cancer letters, 2020. **475**: p. 92-98.
94. Zhang, C., et al., *Functional micro/nanobubbles for ultrasound medicine and visualizable guidance.* Science China Chemistry, 2021. **64**(6): p. 899-914.
95. Lu, S., et al., *Mechanistic insights and therapeutic delivery through micro/nanobubble-assisted ultrasound.* Pharmaceutics, 2022. **14**(3): p. 480.
96. Qin, Y., et al., *Ultrasound nanotheranostics: Toward precision medicine.* Journal of Controlled Release, 2023. **353**: p. 105-124.
97. Yang, Y., et al., *Mechanisms underlying sonoporation: Interaction between microbubbles and cells.* Ultrasonics Sonochemistry, 2020. **67**: p. 105096.
98. Zhu, M., et al., *Sonogenetics in the treatment of chronic diseases: a new method for cell regulation.* Advanced Science, 2024. **11**(48): p. 2407373.
99. Wu, P., et al., *The principles and promising future of sonogenetics for precision medicine.* Theranostics, 2024. **14**(12): p. 4806.
100. Huang, J. and M. Fussenegger, *Programming mammalian cell behaviors by physical cues.* Trends in Biotechnology, 2025. **43**(1): p. 16-42.
101. Hahmann, J., et al., *Sonogenetics for monitoring and modulating biomolecular function by ultrasound.* Angewandte Chemie International Edition, 2024. **63**(13): p. e202317112.
102. Fan, C.-H., et al., *Sonogenetic-based neuromodulation for the amelioration of Parkinson's disease.* Nano letters, 2021. **21**(14): p. 5967-5976.

103. Ndode-Ekane, X.E., et al., *MRI-Guided Electrode Implantation for Chronic Intracerebral Recordings in a Rat Model of Post– Traumatic Epilepsy—Challenges and Gains.* Biomedicines, 2022. **10**(9): p. 2295.
104. Singh, A., et al., *Enhanced tumor cell killing by ultrasound after microtubule depolymerization.* Bioengineering & Translational Medicine, 2021. **6**(3): p. e10233.
105. Song, Y., et al., *Mechanosensitive channel Piezo1 induces cell apoptosis in pancreatic cancer by ultrasound with microbubbles.* Iscience, 2022. **25**(2).
106. Wang, T., et al., *A logic AND-gated sonogene nanosystem for precisely regulating the apoptosis of tumor cells.* ACS Applied Materials & Interfaces, 2020. **12**(51): p. 56692-56700.
107. Wu, Y., et al., *Control of the activity of CAR-T cells within tumours via focused ultrasound.* Nature biomedical engineering, 2021. **5**(11): p. 1336-1347.
108. Pan, Y., et al., *Mechanogenetics for the remote and noninvasive control of cancer immunotherapy.* Proceedings of the national academy of sciences, 2018. **115**(5): p. 992-997.
109. Provansal, M., et al., *Vision restoration by optogenetic therapy and developments toward sonogenetic therapy.* Translational vision science & technology, 2022. **11**(1): p. 18-18.
110. Cadoni, S., et al., *Ectopic expression of a mechanosensitive channel confers spatiotemporal resolution to ultrasound stimulations of neurons for visual restoration.* Nature Nanotechnology, 2023. **18**(6): p. 667-676.
111. Costa, V., et al., *Osteogenic commitment and differentiation of human mesenchymal stem cells by low-intensity pulsed ultrasound stimulation.* Journal of Cellular Physiology, 2018. **233**(2): p. 1558-1573.
112. Li, F., et al., *Ultrasound irradiation combined with hepatocyte growth factor accelerate the hepatic differentiation of human bone marrow mesenchymal stem cells.* Ultrasound in Medicine & Biology, 2018. **44**(5): p. 1044-1052.
113. Xu, P., et al., *Low-intensity pulsed ultrasound-mediated stimulation of hematopoietic stem/progenitor cell viability, proliferation and differentiation in vitro.* Biotechnology letters, 2012. **34**(10): p. 1965-1973.
114. Moghaddam, Z.H., M. Mokhtari-Dizaji, and M. Movahedin, *Effect of acoustic cavitation on mouse spermatogonial stem cells: colonization and viability.* Journal of Ultrasound in Medicine, 2021. **40**(5): p. 999-1010.
115. Lv, Y., et al., *Effects of low-intensity pulsed ultrasound on cell viability, proliferation and neural differentiation of induced pluripotent stem cells-derived neural crest stem cells.* Biotechnology letters, 2013. **35**(12): p. 2201-2212.
116. Song, B.-W., et al., *A combinational therapy of articular cartilage defects: rapid and effective regeneration by using low-intensity focused ultrasound after adipose tissue-derived stem cell transplantation.* Tissue Engineering and Regenerative Medicine, 2020. **17**(3): p. 313-322.
117. Ylä-Herttuala, S., *Endgame: glybera finally recommended for approval as the first gene therapy drug in the European union.* Molecular Therapy, 2012. **20**(10): p. 1831-1832.

118. Li, C. and R.J. Samulski, *Engineering adeno-associated virus vectors for gene therapy.* Nature Reviews Genetics, 2020. **21**(4): p. 255-272.
119. Xie, Q., et al., *The atomic structure of adeno-associated virus (AAV-2), a vector for human gene therapy.* Proceedings of the National Academy of Sciences, 2002. **99**(16): p. 10405-10410.
120. Dong, J.-Y., P.-D. Fan, and R.A. Frizzell, *Quantitative analysis of the packaging capacity of recombinant adeno-associated virus.* Human gene therapy, 1996. **7**(17): p. 2101-2112.
121. Huang, Y.-S., et al., *Sonogenetic modulation of cellular activities using an engineered auditory-sensing protein.* Nano letters, 2019. **20**(2): p. 1089-1100.
122. Duque, M., et al., *Sonogenetic control of mammalian cells using exogenous Transient Receptor Potential A1 channels.* Nature communications, 2022. **13**(1): p. 600.
123. Dunbar, C.E., et al., *Gene therapy comes of age.* Science, 2018. **359**(6372): p. eaan4672.
124. Di Pasquale, E., et al., *Lentiviral vectors and cardiovascular diseases: a genetic tool for manipulating cardiomyocyte differentiation and function.* Gene therapy, 2012. **19**(6): p. 642-648.
125. Thompson, A.A., et al., *Gene therapy in patients with transfusion-dependent β-thalassemia.* New England Journal of Medicine, 2018. **378**(16): p. 1479-1493.
126. Howe, S.J., et al., *Insertional mutagenesis combined with acquired somatic mutations causes leukemogenesis following gene therapy of SCID-X1 patients.* The Journal of clinical investigation, 2008. **118**(9).
127. Hacein-Bey-Abina, S., et al., *LMO2-associated clonal T cell proliferation in two patients after gene therapy for SCID-X1.* science, 2003. **302**(5644): p. 415-419.
128. Xu, Y., et al., *Surface modification of lipid-based nanoparticles.* ACS nano, 2022. **16**(5): p. 7168-7196.
129. Matougui, N., et al., *Lipid-based nanoformulations for peptide delivery.* International journal of pharmaceutics, 2016. **502**(1-2): p. 80-97.
130. Dave, V., et al., *Lipid-polymer hybrid nanoparticles: Synthesis strategies and biomedical applications.* Journal of microbiological methods, 2019. **160**: p. 130-142.
131. Cheng, M.H.Y., et al., *Induction of bleb structures in lipid nanoparticle formulations of mRNA leads to improved transfection potency.* Advanced Materials, 2023. **35**(31): p. 2303370.
132. Battaglia, L. and M. Gallarate, *Lipid nanoparticles: state of the art, new preparation methods and challenges in drug delivery.* Expert opinion on drug delivery, 2012. **9**(5): p. 497-508.
133. Zylberberg, C., et al., *Engineering liposomal nanoparticles for targeted gene therapy.* Gene therapy, 2017. **24**(8): p. 441-452.
134. Peng, J., et al., *Intratumoral fate of functional nanoparticles in response to microenvironment factor: Implications on cancer diagnosis and therapy.* Advanced Drug Delivery Reviews, 2019. **143**: p. 37-67.

135. Wu, C.-Y., et al., *Targeted delivery of engineered auditory sensing protein for ultrasound neuromodulation in the brain.* Theranostics, 2020. **10**(8): p. 3546.
136. Jiang, T., et al., *Dual-functional liposomes based on pH-responsive cell-penetrating peptide and hyaluronic acid for tumor-targeted anticancer drug delivery.* Biomaterials, 2012. **33**(36): p. 9246-9258.
137. Fischer, D., et al., *In vitro cytotoxicity testing of polycations: influence of polymer structure on cell viability and hemolysis.* Biomaterials, 2003. **24**(7): p. 1121-1131.
138. Wu, Z., A. Asokan, and R.J. Samulski, *Adeno-associated virus serotypes: vector toolkit for human gene therapy.* Molecular therapy, 2006. **14**(3): p. 316-327.
139. Wang, D., P.W. Tai, and G. Gao, *Adeno-associated virus vector as a platform for gene therapy delivery.* Nature reviews Drug discovery, 2019. **18**(5): p. 358-378.
140. Naso, M.F., et al., *Adeno-associated virus (AAV) as a vector for gene therapy.* BioDrugs, 2017. **31**(4): p. 317-334.
141. Cheng, H., et al., *Efficient and persistent transduction of exocrine and endocrine pancreas by adeno-associated virus type 8.* Journal of biomedical science, 2007. **14**(5): p. 585-594.
142. Wang, Z., et al., *Widespread and stable pancreatic gene transfer by adeno-associated virus vectors via different routes.* Diabetes, 2006. **55**(4): p. 875-884.
143. Akache, B., et al., *The 37/67-kilodalton laminin receptor is a receptor for adeno-associated virus serotypes 8, 2, 3, and 9.* Journal of virology, 2006. **80**(19): p. 9831-9836.
144. Wang, Y.-C., et al., *Pancreas-directed AAV8-hSPINK1 gene therapy safely and effectively protects against pancreatitis in mice.* Gut, 2024. **73**(7): p. 1142-1155.
145. Guan, G., et al., *NFAT5 exacerbates β-cell ferroptosis by suppressing the transcription of PRDX2 in obese type 2 diabetes mellitus.* Cellular and Molecular Life Sciences, 2025. **82**(1): p. 64.
146. Ramzy, A., et al., *AAV8 Ins1-Cre can produce efficient β-cell recombination but requires consideration of off-target effects.* Scientific Reports, 2020. **10**(1): p. 10518.
147. Tanaka, K., et al., *Mechanisms of impaired glucose tolerance and insulin secretion during isoflurane anesthesia.* Anesthesiology, 2009. **111**(5): p. 1044-1051.
148. Zuurbier, C.J., et al., *Optimizing anesthetic regimen for surgery in mice through minimization of hemodynamic, metabolic, and inflammatory perturbations.* Experimental Biology and Medicine, 2014. **239**(6): p. 737-746.
149. Ermakov, Y.A., et al., *Gadolinium ions block mechanosensitive channels by altering the packing and lateral pressure of anionic lipids.* Biophysical journal, 2010. **98**(6): p. 1018-1027.
150. Li, D.-S., et al., *A protocol for islet isolation from mouse pancreas.* Nature protocols, 2009. **4**(11): p. 1649-1652.
151. Trexler, A.J. and J.W. Taraska, *Regulation of insulin exocytosis by calcium-dependent protein kinase C in beta cells.* Cell Calcium, 2017. **67**: p. 1-10.
152. Bornstein, S.R., J.F. Wright, and C. Steenblock, *The promising potential of gene therapy for diabetes mellitus.* Nature Reviews Endocrinology, 2024. **20**(11): p.

627-628.
153. Stanley, S.A., et al., *Remote regulation of glucose homeostasis in mice using genetically encoded nanoparticles.* Nature medicine, 2015. **21**(1): p. 92-98.
154. Stefanov, B.A., et al., *Genetically encoded protein thermometer enables precise electrothermal control of transgene expression.* Advanced Science, 2021. **8**(21): p. 2101813.
155. Bai, P., et al., *A fully human transgene switch to regulate therapeutic protein production by cooling sensation.* Nature medicine, 2019. **25**(8): p. 1266-1273.
156. Zhao, H., et al., *Tuning of cellular insulin release by music for real-time diabetes control.* The Lancet Diabetes & Endocrinology, 2023. **11**(9): p. 637-640.
157. Krawczyk, K., et al., *Electrogenetic cellular insulin release for real-time glycemic control in type 1 diabetic mice.* Science, 2020. **368**(6494): p. 993-1001.
158. Fang, M., et al., *Wearable Ultrasound Technology in Health Monitoring and Therapy: Technological Innovations, Differentiated Applications, and Future Directions.* ACS sensors, 2025.
159. Yang, Y., et al., *Wearable ultrasound regulation of blood glucose levels in type 2 diabetic db/db mice.* Ultrasonics, 2025: p. 107739.